UNIVERSITY OF CAPE COAST

MODELLING AND ASSESSING THE TRENDS IN WAVE CLIMATE OVER THE PAST FOUR DECADES IN THE COAST OF GULF OF GUINEA

ADEOLA MICHAEL DAHUNSI

2021

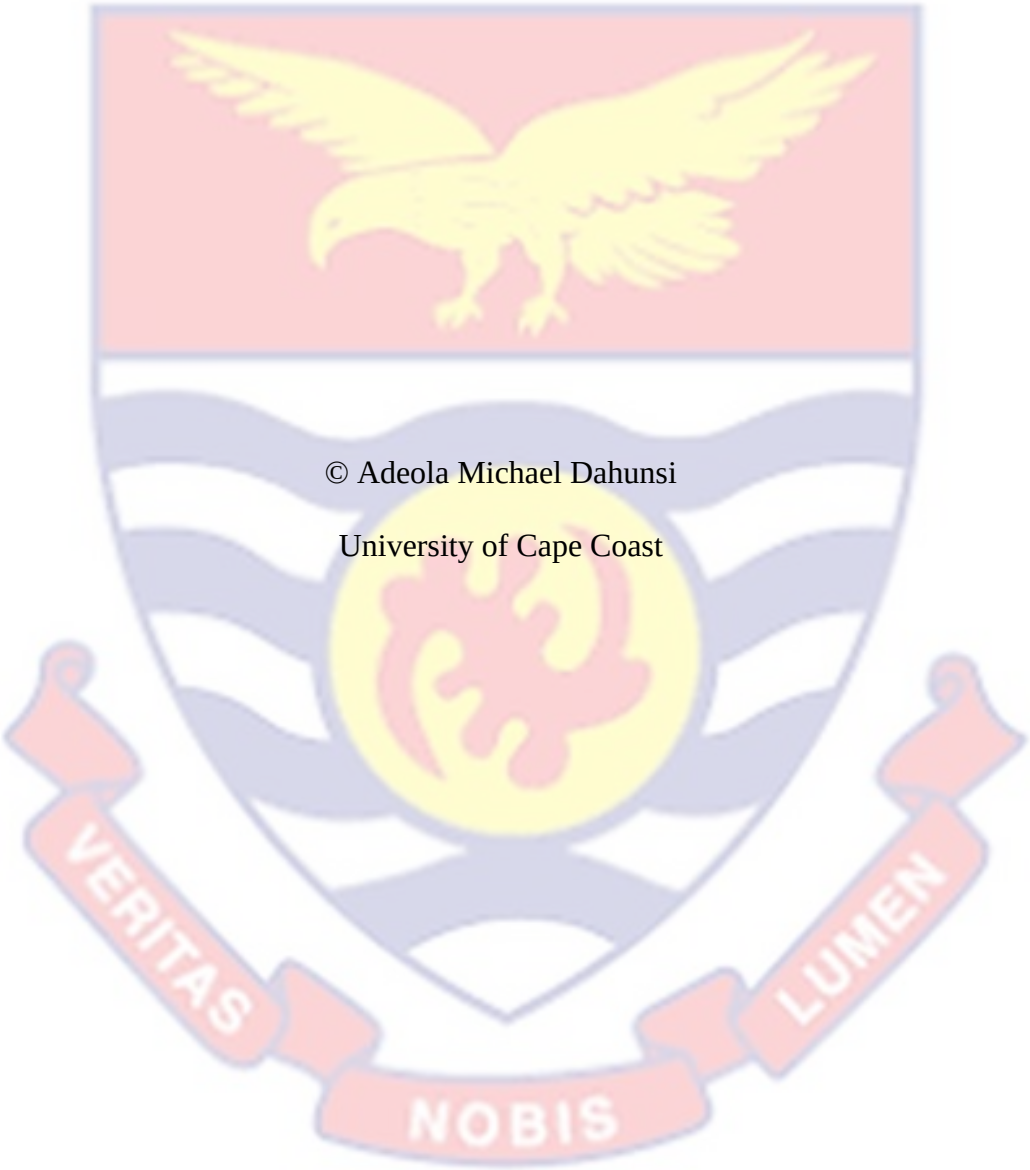

UNIVERSITY OF CAPE COAST

MODELLING AND ASSESSING THE TRENDS IN WAVE CLIMATE OVER THE PAST FOUR DECADES IN THE COAST OF GULF OF GUINEA

BY

ADEOLA MICHAEL DAHUNSI

Thesis submitted to the Department of Fisheries and Aquatics Sciences, School of Biological Sciences, College of Agriculture and Natural Sciences University of Cape Coast, in partial fulfilment of the requirements for award of Master of Philosophy degree in Oceanography and Limnology

NOVEMBER, 2021

DECLARATION

Candidate's Declaration

I hereby declare that this thesis is the result of my own original research and that no part of it has been presented for another degree in this university or elsewhere.

Candidate's Signature…… Date……..

Name: ……Adeola Michael Dahunsi……

Supervisors' Declaration

We hereby declare that the preparation and presentation of the thesis were supervised in accordance with the guidelines on supervision of thesis laid down by the University of Cape Coast.

Principal Supervisor's Signature…….. Date……...

Name: ……Prof. Moses Jojo Eghan……...

Co-Supervisor's Signature…… Date……..

Name: ……Dr. Osinowo Adekunle Ayodotun.……

ABSTRACT

The focus of this study is the assessment of the past wave conditions in the Gulf of Guinea region of the West African coast to get a better understanding of the trends the waves have been following over the past four decades. The third-generation spectral wave model, WAVEWATCH III (WW3), was used to hindcast the wave climate between 1st January, 1980 – 31st December, 2019, which provided data on significant wave height (*Hs*), mean wave period (*Tm*), mean wave direction and mean wind speed (U10). Validation results confirmed that WW3 is an efficient model for simulating wave condition as it agrees well with observation and other datasets like ERA5 (European Centre for Medium-Range Weather Forecasts - ECMWF Reanalysis 5th Generation). The trend analyses done showed that the *Hs* with average values of 1.0836 m, 0.9312 m and 1.1913 m on annual, winter and summer bases increased at rates of 2.6×10^{-3} m, 1.6×10^{-3} m and 3.4×10^{-3} m per year, respectively. For *Tm*, average values of 5.3897 s, 5.3876 s and 5.3911 s for annual, winter and summer changed at rates of 6.1353×10^{-4} s, -1.7×10^{-3} s and 2.3×10^{-3} s per year, respectively. Mean values of 4.7001 m/s. 4.2344 m/s and 5.0292 m/s were estimated for U10 on annual, winter and summer bases increasing at rates of 3.5×10^{-3} m/s, 4.2×10^{-3} m/s and 3.1×10^{-3} m/s per year, respectively. The wave direction is also observed to be predominantly S-SW mostly originating from the southwestern Atlantic Ocean. The statistical projections done for various return period showed that this increase will continue into the future with higher risks to coastal and offshore structures by the end of the century in 2100.

KEY WORDS

Wind Wave

Ocean Swell

Wind Sea

Wave Climate

Significant Wave Height

Mean Wave Period

Mean Wave Direction

WAVEWATCH III

ERA5

Gulf of Guinea

Return Period

Gumbel Distribution

ACKNOWLEDGEMENTS

I like to acknowledge my Principal Supervisor, Prof. Moses Jojo Eghan of Department of Physics, University of Cape Coast, Ghana and my Co-supervisor, Dr. Adekunle Osinowo of the Department of Marine Science and Technology, Federal University of Technology, Akure, Nigeria for the supportive supervision and mentorship during this research. I acknowledge the sponsorship and support of the World Bank, the Government of Ghana, the University of Cape Coast (UCC), the Department of Fisheries and Aquatic Sciences (DFAS-UCC), and the Centre for Coastal Management (CCM-UCC) through the Africa Centre of Excellence in Coastal Resilience (ACECoR) Project.

I appreciate the support of my colleagues including Andoh Kwaku Amponsah (Ghana), Blessing Ebi Ogonodi (Nigeria), Emmanuel Sandy Ofosu (Ghana), Francis Nuamah (Ghana), Fred Kwaku Ahiati (Ghana), John Ekow Amoah (Ghana), Kwami Agbetossou (Togo), Martin Opoku (Ghana), Charles Abimbola Faseyi (Nigeria), Temitope Adejoke Adewale (Nigeria), Mary Opeyemi Soetan (Nigeria), Houangninan Emmanuel Calèbe Midinoudewa (Benin) and Abdou Matinou Ogbon (Benin).

I thank my family and friends for the help throughout the journey before and during the research.

DEDICATION

To my Poor Dad, Mr. Boyede Paul Dahunsi and my Rich Dad, Late Chief Zacchaeus Olabusoye Dahunsi for giving me the foundation on which I build.

TABLE OF CONTENTS

LIST OF TABLES

LIST OF FIGURES

LIST OF ABBREVIATIONS

ACECoR - Africa Centre of Excellence in Coastal Resilience Project

ANOVA – Analysis of Variance

ANSI - American National Standards Institute

ASCII - American Standard Code for Information Interchange

BC - Benguela Current

CC - Climate Change

CCM - Centre for Coastal Management

CFL - Courant–Friedrichs–Lewy

CMEMS - Copernicus Marine Environment Monitoring Service

CRMSD – Centred Root Mean Square Difference

DFAS - Department of Fisheries and Aquatic Sciences

Dm - Mean Wave Direction

Hs - Significant Wave Height

ECMWF - European Centre for Medium-Range Weather Forecasts

EMC - Environmental Modelling Center

ENSO - *El Nino* Southern Oscillation

ERA5 - ECMWF Reanalysis 5th Generation

FORTRAN - Formula Translation

GC - Guinea Current

GDP – Gross Domestic Product

GSHHS - Global Self - consistent Hierarchical High - resolution Shoreline

GoG – Gulf of Guinea

IPCC - Intergovernmental Panel on Climate Change

ITCZ - Inter-tropical Convergence Zone

JONSWAP - Joint North Sea Wave Project

MATLAB – Matrix Laboratory

MBE - Mean Bias Error

MFWAM - Meteo France WAve Model

MMAB - Marine Modelling and Analysis Branch

MPI - Message Passing Interface

NAO - North Atlantic Oscillation

NASA - National Aeronautics and Space Administration

NCAR - National Center for Atmospheric Research

NCEI - National Centres for Environmental Information

NCEP - National Centers for Environmental Prediction

NDBC - National Data Buoy Centre

NECC - North Equatorial Counter Current

NetCDF - Network Common Data Form

NGDC - National Geophysical Data Center

NOAA - National Oceanic and Atmospheric Administration

NPO - North Pacific Oscillation

OpenMP - Open Multi-Processing

RCP - Representative Concentration Pathway

RMSE - Root Mean Square Error

SAM - Southern Annular Mode

SD – Standard Deviation

SLR - Sea Level Rise

SOI - Southern Oscillation Index

SST - Sea Surface Temperature

SWAN - Simulating WAves Nearshore

Tm - Mean Wave Period

U10 - Mean Wind Speed

UCC - University of Cape Coast

WAM - Wave Modelling

WAMDI - Wave Model Development and Implementation

WP - Wave Power

WW3 - WAVEWATCH III

WW3DG - WAVEWATCH III Development Group

CHAPTER ONE

INTRODUCTION

Coastal areas have very dynamic environment due to the continuous influences from land, atmosphere, ocean as well as human activities. Coastal areas continue to experience changes from all these multifaceted interactions (Giardino et al., 2018). The coastal area is known to provide diverse ecosystem services (Alves et al., 2020) which are all under threat from stressors being faced by this dynamic environment. One of these stressors is the impacts of climate change (Pachauri et al., 2014). Wave is the major source of energy in the coastal area and owing to its persistency causes damages seen in the form of storm surges and coastal erosion. Wind-driven waves are bound to change in the face of climate change since the wind climate is expected to change too (Almar et al., 2015; Anthony et al., 2019; Sadio et al., 2017). This potential for increase in extreme wave conditions therefore warrants the need to assess the trend in the wave climate over the past recent decades to enable reliable projections of what the future holds for wave conditions in the Gulf of Guinea region.

Background

The ocean is recognized as a key player in the determination of earth's climate because it covers about 70.8 % of the entire surface of the earth and holds approximately 97% of the water on Earth (Garrison, 2012; Snelgrove, 1999). As expected, the surrounding coastal areas attract a lot of people due to the vast resources it holds, which encourages activities such as fishing, water transportation,

trade and tourism. Most big cities of the world and West Africa such as Accra, Lagos, Lomé, Cotonou etc. are located on the coast. McGranahan et al. (2007) reported that more than 10 % of the human population of the earth live within contour line of 10 m above the mean sea-level. Despite this level of importance in provision of shelter, it has been projected that the coastal areas will experience a change in mean sea level of about 50 cm by the end of 2100 century (Parry et al., 2007). This prediction means there will be increase in the exposure risk of coastal inhabitants to hazards such as flooding.

The West African coastal area, which is the coastal part of Gulf of Guinea (GoG) is housing around 31% of the region's population and there is an expectation of increase in the future (Croitoru et al., 2019). According to the 2019 World Bank report, growth in population as a result of urbanization in these coastal regions is at a rate of 4 % per annum, which is nearly double the world average. The coastal area also provides shelters for 56 % of the GDP of West Africa (Croitoru et al., 2019). It has been extensively reported that the coastal area of GoG holds various essential natural resources and ecosystems that present priceless environmental services (Faye, 2010).

Coasts are dynamic systems because they continually experience changes due to their constant interactions with terrestrial, oceanic, atmospheric as well as anthropogenic activities. Therefore, coasts are subjected to various morpho-dynamic adjustments of form and process at varying spatial and temporal scales due to geomorphological and oceanographical influences (Cowell et al., 2003). The coastal area is known to be affected by external influences from terrestrial sources

such as deforestation and hydrological modifications as well as marine sources like waves (swells), tsunamis and ocean currents like Guinea currents. Globally, the coast is exposed to the problem of erosion, which affects about 70 % of the Earth's sandy beaches, which are also sites for various recreation purposes (Bird, 1985; Giardino et al., 2015). Some likely drivers of the severity of this erosion have been linked to the issue of Sea Level Rise (SLR) as a result of what is referred to as temperature driven expansion of the global ocean, ice melting in the polar region and changed precipitation patterns. Other factors include change in wind climate due to climate change and anthropogenic contributions (Zhang et al., 2004).

Various evidences of SLR in form of coastal flooding, salt water intrusion, coastal erosion etc. from different parts of the World have been recorded in literatures. According to Climate Change models run under the various Representative Concentration Pathway (RCP), a global increase of about 0.18-0.59 m is predicted to be experienced before the end of the century (2100) (Field et al., 2014; Pachauri et al., 2014). The effect of SLR that have been documented in literatures include shoreline changes, coastal flooding, changed tidal range, changed sediment distribution pattern, salt water intrusion into groundwater aquifers and disruption of ecosystems (Alves et al., 2020). The frequency of these various Climate Change (CC) impacts has led to changes in wind/storm conditions, which have also resulted in changed wave climate.

Despite the continued increase of the sea-level, if the action of wave along the coast is not considered, there will likely be no erosion but just flooding. This is because it is the action of wave on the sediments as they continuously break on the

beach that loosens the sediments and is responsible for carrying these freed sediments offshore, thereby causing erosion. These transport may come in the form of receding ebb, generated rip-current or via longshore current (Fredsøe and Deigaard, 1992).

The Guinea current, which is the predominant current in the GoG region, flows from west to east offshore. Its average speed has a seasonal variation from 0.5 m/s in winter (dry season) to 1.0 m/s in summer (wet season). The current speed peaks at 0.75 m/s during winter and 1.5 m/s during summer. As the Guinea current moves eastward, it turns out to be weaker (Allersma and Tilmans, 1993). The tide in this coast is reported to have a mean tidal range of about 1.0 m with a uniform phase of semi-diurnal tide. The wind condition is mostly dominated by a continuous monsoon from the south-west altered by the land and sea breezes within the region close to the coast (Almar et al., 2015).

Waves are generally considered to be propagating dynamic disturbances transferring energy from one point to another in a medium without causing significant permanent displacement of the medium itself (Ostdiek and Bord, 2012). In other words, the particles of the medium only oscillate about a relatively constant axis. In Physics, waves are said to have at least two field quantities in the wave medium, which in the case of ocean waves can be space and time. Though there are wave types that do not make use of a medium for their propagations e.g., electromagnetic waves, others like sound waves, heat waves and water waves do require a medium to travel through.

Surface wave, which is mostly wind driven is predominant in most water bodies, occurs at varying spatial and temporal scales as shown in Figure 1 (Munk, 1951). These include capillary waves, gravity waves, surges, tsunamis, and tides, which may have periods ranging from seconds to hours as shown in Figure 2. The energy impacted by these various waves also differs according to their properties. The force which generates ocean surface waves differs, of which the prevalent ones include atmospheric pressure exerted on the surface through winds, Ocean surface tension, earthquakes, Coriolis force as a result of the rotation of the Earth, Earth's gravity as well as gravity from other planetary, non-planetary and celestial bodies like the Sun and Moon (Figure 2).

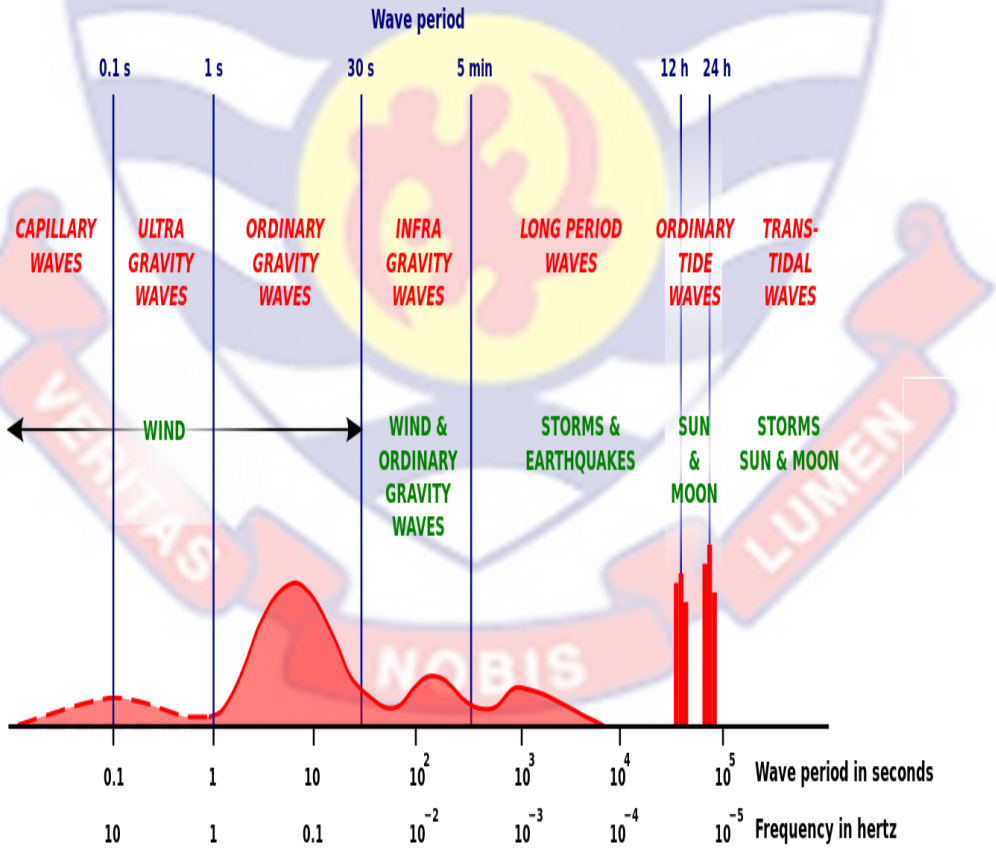

Figure 1: Magnitude of waves with different wave energy at various scales (Adapted from (Munk, 1951).

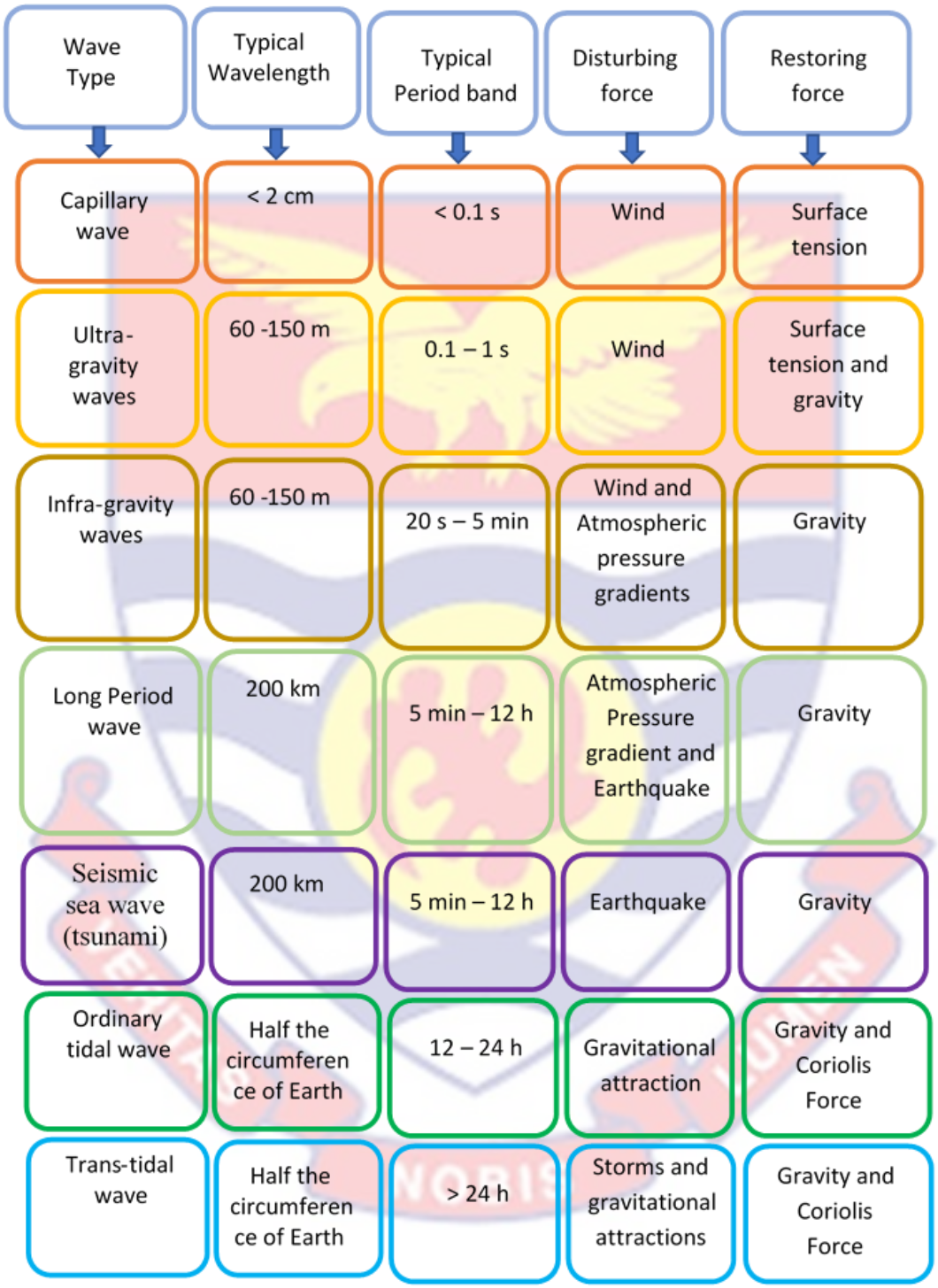

Figure 2: Types and properties of ocean waves (Adapted from https://en.wikipedia.org/wiki/Wind_wave).

The properties of the generated waves (such as wave celerity, wave-height, wave period etc.) depend on the disturbing forces (Bouws et al., 1998; Massel, 2017). In other words, a wind generated wave will propagate at a celerity similar to the wind speed that acted on a disturbed water. Likewise, the magnitude of all earthquake will determine the severity of the accompanying tsunami. Wind generated waves and tides are more frequent than others like tsunamis and they are more regular and hence predictable (Casale, 2004; Margottini, 2004).

Knowledge about wave climate is very important for various practical applications in ocean and coastal science. Examples of such applications are in navigation, coastal morpho-dynamics studies and ocean wave research. Others include planning and implementation of marine and coastal engineering operations and structures both offshore and onshore (Hisaki, 2018). These days, data from observation such as in-situ measurements and remote sensing have increased the confidence by which the changes in wave properties such as wave heights, periods, and directions can be described. This is more informative when data is available to aid the averaging over a long period of time since these changes might not be detectable in short time. These variabilities in wave climate will likely lead to changes in other coastal geomorphological features such as shoreline orientation and shape. Some other likely impacts of changing wave conditions are equilibrium and disturbance of coastal ecosystems (Hoegh-Guldberg and Bruno, 2010), changes in nearshore coastal processes (Chowdhury and Behera, 2017; Zacharioudaki and Reeve, 2011) and variation in air-sea interchange, which is a major player in determining the global climate system (Cavaleri et al., 2012).

Serious erosions have been reported in the West African coast in the last few decades. For example, there were reports of severe erosion events along some parts of the continental shelf of Ivory Coast in 2007 and 2011. This led to the damage of several buildings and eroded around 12 m of the coastline. These severe occurrences were witnessed mostly between the months of August and September (Toualy et al., 2015).

Wave heights show trends on long-terms but are equally influenced by changes in wind direction, waves type, temperature and wind speed. Gulev and Grigorieva, (2004) found out that persisting changes in the heights of wind generated waves are strongly related to some oceanic phenomena. These phenomena include North Atlantic Oscillation (NAO), North Pacific Oscillation (NPO) and *El Nino* Southern Oscillation (ENSO) (Figure 3). Trends pattern in severe wave height include inter-annual changes in the occurrence (frequency) and strength (intensity) of extreme wave events. Numerous studies making use of reanalysed data from wave models have been extracted to study the trends in wave climate.

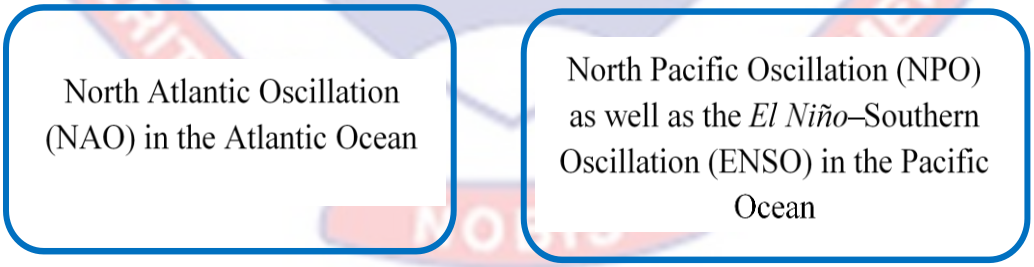

Figure 3: Major meteorological ocean phenomena that influence the wave conditions.

Mendes et al. (2007) observed two bands of cyclone tracks in the Southern Atlantic, one in north-east Argentina and the other north of the Antarctic Peninsula close to the Weddell Sea. They noticed an impact of the Southern Annular Mode (SAM) in the areas around extra-tropical cyclones close to 40 °S and 55 °S. Though it has been established for several years that swells generated from the South-Western Atlantic Ocean travel to the Gulf of Guinea (Figure 4), it is yet to be understood which of these bands have the most dominating influence on wave in the coasts of the Gulf of Guinea (Sitarz, 1960, Mendes et al., 2007).

Reanalysis using NCEP–NCAR Fyfe (2003) indicates that there has been a shift towards the poles of the storm track in the last decades. This might be the reason why there is a reduction in the occurrence of cyclones in the Sub-Antarctic Ocean and a small upsurge in the occurrence of cyclones in the Antarctic Ocean. The analysis of Hemer et al. (2010) showed that there is statistically insufficient correlation between the wave height of Atlantic Ocean and the Southern Oscillation Index (SOI). However, the ENSO of the Pacific Ocean showed a strong correlation (Hemer et al., 2010).

The prevailing mode of interannual changes in the equatorial Atlantic behave in a similar way with ENSO, sharing the inter-annual rotation of warming and cooling of sea surface temperature (SST) in the eastern arm of the basin located around 0–30° W and linked with variation in the trade winds. A warmer SST anomaly is connected with weak trade winds in the equatorial Atlantic basin. On the other hand, a cool SST anomaly is linked with stronger easterly winds. These winds in the northern part of GoG are mostly from the southwest. Variations of this

wind, especially the St. Helen anticyclone, can cause 15-day wind surges, which can reach the northern part of GoG (Coëtlogon et al., 2010).

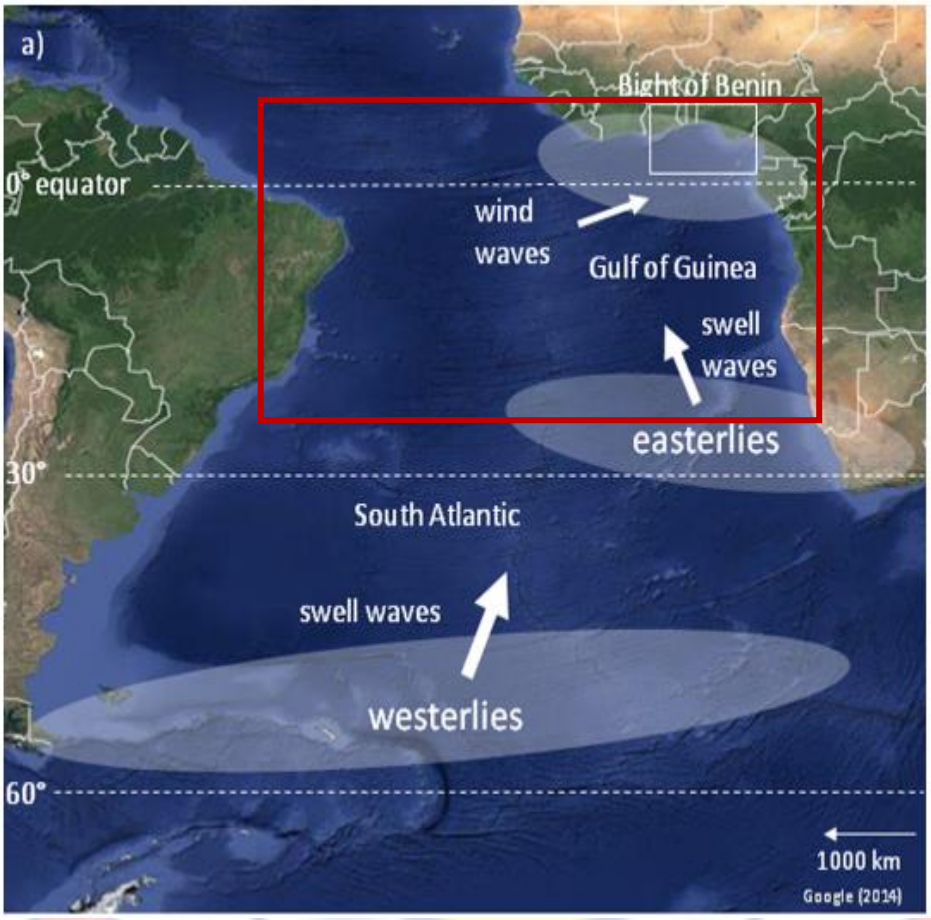

Figure 4: The Mid Atlantic (red box) including Gulf of Guinea coast showing the swell source in the South Atlantic Ocean (Almar et al., 2015).

Changes in the climate of regional waves, in terms of its wave height, wave period and wave direction, usually occur in response to variations in atmospheric circulation. This may be as a result of change in climate, which makes it a topic of interest from different angles particularly in a dynamic environment like the coastal area. A significant change in the wave climate as a result of change in climate will in turn affect various features of the coast. The affected features include the coastal

morphology, the position (location of the shoreline) and orientation (direction of the shoreline) of the coast and the effectiveness of coastal structures (Ndour et al., 2018; Ondoa et al., 2016).

Wave climate is a definition of the patterns of wave height, wave period and wave direction estimated as an average over a particular period of time for a location (Herbich and Walters, 1987, Wiegel, 2013). As a result of its importance in the estimation of the trends of the wave in a particular region, wave climate has been simulated using numerical ocean models to run hindcast and forecast for provision of sufficient information on it. This is sometimes done alongside modelling of ocean current and sediment transport through coupling (Ranasinghe, 2016). These models help to solve unresolvable coastal problems by providing data on temporal and spatial scales, which is impossible or too expensive to be physically surveyed or observed. Models also help in the prediction of coastal dynamics for coastal and offshore engineering works. Also, ocean hydrodynamic models have been of help in effective and accurate transfer of information about swells (offshore) waves to coastal areas where their impacts are of concern to coastal managers and inhabitants (Ranasinghe, 2016).

Though the impacts of wave activities are seen offshore as well as on the coast, its offshore effects may not be as destructive as on the coast except for extreme cases, which may affect ships and offshore structures like oil rigs, buoys and other drifting or stationary platforms. These stationary platforms are most impacted due to the fact that the water molecules remain relatively unmoved with the waves but transfer the energy from one molecule to another in a relatively

spherical or orbital manner. This means that drifting objects only oscillate in an upward and downward motion when the wave transfers energy through their paths but stationary platforms are continuously hit with the energy which affects them overtime and gradually loosen them. This is similar to the interaction between the approaching wave and the coast. As offshore waves move into shallow water, they tend to convert their kinetic energy into potential energy, which leads to increased wave heights, giving them the capability to impact even higher upland as they break (Garrison, 2009).

As a result of their high energy, waves play major roles in determining shoreline because they dictate the amount of sediment that is removed or deposited, thereby causing erosion and accretion, respectively. Some of the factors that determine the erosional or depositional rates at a particular coast include the relative tidal range, which is defined as the ratio between the predominant significant wave height and predominant tidal range. The tidal range is the area of the coast exposed to wave activities from time to time and it is usually the difference between the high and the low tide line. Other factors that determine the amount of sediment removed or added are SLR, sediment type, sediment grain size, direction of shoreline orientation to the direction of current and wave coming to the coast (measured in degree-angle), beach gradient/slope and most especially wave climate, which determines the energy of the incoming waves. Therefore, if a coast is known to have a relatively high tidal range, it will be expected that waves come in more inland, especially during high tides whereas a beach with a steep gradient will most likely have plunging type of wave breaking, which loosens the sediment more.

Based on orientation, a beach with an orientation parallel to incoming waves will experience less erosion compared to others (Mangor et al., 2004).

Since it is projected that there will be changes in atmospheric climate including wind patterns, it is therefore expected that wave climate being atmospheric driven will likely experience this atmospheric climate change driven variation. This change is expected on global as well as regional scales in the atmosphere and ocean. When wave climate studies are caried out on global scale, it mostly gives hints about the general trends of the wave parameters but is not able to give a detailed and high-resolution spatial trend in regional wave climate. For effective management measures to be put in place, accurate measurements of regional wave climate have to be done to properly represent the situation in the region (Chowdhury et al., 2019; Chowdhury and Behera, 2019). Among the many potential impacts of CC on the coasts, the one that has received the most attention is the coastal recession as a result of sea-level rise (SLR), while relatively less attention has been given to the other potential impacts of coastal CC. Various publications have pointed out that other CC impacts may in fact outweigh the SLR impact on the coasts (Ranasinghe and Stive, 2009, Ranasinghe, 2016). One such potentially serious CC impact that has not been sufficiently studied is the coastal response to CC induced variations in offshore wave characteristics.

Statement of the Problems

Despite its importance in the determination of the potential effects of climate change (CC) on the wave climate around the coast of West Africa, not

sufficient research has been conducted to study the trends in the wave climate in GoG region of the mid-Atlantic. This has been linked to the shortage of needed data since this region has sparse distribution of ocean observing systems like buoys. This study is designed to add to knowledge on effects of CC in this region by using the few available data as foundation to increase data availability and ocean predictability in this region.

The future offshore (swell) wave climate has been predicted to experience changes in response to global warming, which will likely affect the winds and storm, which drives the generation of these wave. This predicted variation has been projected to lead to increase in the severity of coastal problems such as flooding and erosion in West Africa. Waves are major drivers of coastal processes and hence, a change in their climate will definitely modify coastal phenomena such as sediment transport. The change may cause a shift in wave direction, which will likely modify the transport of sediment in the surfing area and cause a significant change of coastline. This change may cause disturbance in the sediment balance thereby unsettling the system leading to the modification of the sediment transport induced by the waves.

Consequently, coastline will be eroded more even in places where erosion has not been reported in the past. Changes in wave climate also has the potential of impacting coastal structures such as coastal defence systems, fish landing sites, oil rigs, seaport structures etc (Figure 5). Hence, the study of the past trends and likely pattern of change in wave climate offshore is fundamentally important and necessary. This will serve as foundation for obtaining the future condition of the

waves which will make it easier for coastal planners and managers to better prepare for the impact of changing wave conditions on the coastal area of West Africa.

Severe waves can have damaging consequences on coasts, for example, through events like coastal erosion, which may likely lead to breakdown of marine infrastructures. Therefore, there is extensive interest in the monitoring of these happenings especially in the perspective of CC and for improving the understanding of CC contributions to the episode of extreme wave conditions (Vanem, 2015).

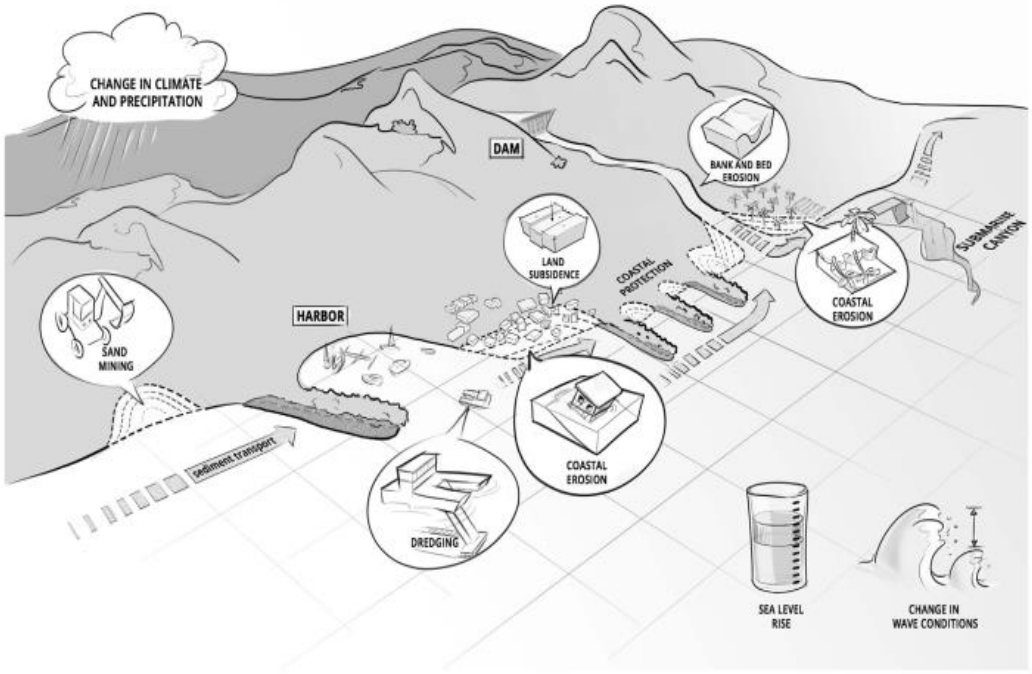

Figure 5: Key factors that affect the coastal areas and resulting in morphological alterations (Giardino et al., 2018).

The mean values of a long temporal span of wave heights are valuable in assessing the presence of a trend across an interval of long period. This trends in significant wave height, combined with an assessment of the events of intense waves at a particular periodic reoccurrence, gives a good grasp of wave conditions

at coastal areas. Nevertheless, outcomes of studies are determined by the source and type of data used as well as the statistical analysis carried out (Mathiesen et al., 1994).

Aim of the Study

The general objective of this study was to model and assess the trends in past wave climate in the GoG. This past trend was used to determine the likely potential future trends of the wave climate resulting from CC in this region.

Specific Objectives of the Study

The specific objectives of this study were:

1. To hind cast ocean wave parameters such as wave height, wave period and wave direction, using wind-wave spectral model for a period spanning from 1980-2019.
2. To validate model generated data using available in-situ (buoy) data.
3. To check the trends in the wave conditions on a monthly, annual, seasonal and decadal basis.
4. To check for possible Pacific-Atlantic inter-basin teleconnection by assessing the effect of the ENSO and the Atlantic Mode on the wave climate in GoG.
5. To assess the effect of coastal structures on trends in extreme wave events during the years considered.

Significance of the Study

It has been recommended in various studies in GoG region of West Africa that management plans are more effective when done on regional scale rather than

local or national. Alves et al. (2020) in their recent study of coastal erosion and flooding risks as well as applicable management measures in West Africa region reported that despite numerous measures that have been applied at various locations, they have not yielded maximum results because they are mostly done at the local scale. Therefore, it was recommended that coastal management be done at regional scale as that is more economical and effective. The regional scale coastal management approach involves countries in the region pulling resources together for the implementation of coastal management projects. This will reduce the likelihood of knock-on effects of a coastal management project in one country on a neighbouring country. For this reason, research that looks at the effects of wave on regional scale is pertinent because it will be major source of data and information for future studies and management plans.

The purpose of this study was to provide wave data on a spatio-temporal scale that allows studies and predictability of wave events in the GoG. The data obtained from the modelling of wave climate in this study can be a basis for other coastal and oceanic studies in the region. Studies such as large-scale transport rates of coastal sediments for the coast of West Africa will benefit from the data generated from this study. Assessment of the effect of climate change on future rates of coastal sediment transport using the average projected wave conditions will rely on the data from the hindcast in this study. This will make the result of this work serve as foundation for future studies by providing much needed data in the West Africa region (Giardino et al., 2018).

Delimitation

This study focused on the trend of wave conditions in the Gulf of Guinea and the possible projected waves conditions in this region. In this study, the wave climate was defined as the average condition of the three (3) bulk wave parameters significant wave height, mean wave period and mean wave direction in the Gulf of Guinea. The study also included the average condition of the wind speed between the study period of 1980 to 2019. Other parameters such as wavelength and peak period were not assessed in this study. The study covered the part of the Gulf of Guinea between longitude 10^{o}N-10^{o}S and latitudes 15^{o}E-15^{o}W which includes countries beyond West Africa.

Limitation

Even though this study was successfully carried out and the model results were well validated, some difficulties were faced during the research. These challenges include the inability to carry out further validation closer to the coast of West Africa using in-situ data. This was because of the unavailability of buoy (in-situ) data close to the coast around the GoG needed for that purpose. The National Data Buoy Centre (NDBC) which is the source of in-situ wave data globally does not have record of past nor present wave data for the GoG because available buoys in the region do not measure wave parameters. This gap was filled by validating data generated in this study against other previously existing wave model datasets. The results of this model intercomparison showed good agreement which increased the confidence of the data closer to the coast. The future projection for wave climate

carried out in this study was statistically done which makes it largely dependent on the historical data used for the projection. Dynamical approach using wave models could have possibly represent the future changes better but it was beyond the scope of the time-slice defined in this study.

Organization of Thesis

The first chapter gives the introduction of the study including the background of the research, statement of the problem and the main and specific objectives of the study. Chapter one also includes the justification of the research, the delimitation as well as the limitations. In Chapter Two, the review of literature needed for this study is presented including the information about Ocean wave models. The methods used for this study including the information on study area, the modelling approach, the model validation and data analysis methods are presented in Chapter Three. The Chapter Four of this thesis presents the results of the analysis carried out in the study. Chapter Five covers the summary of results, conclusions and recommendations made for the research.

Chapter Summary

The motivation behind this study has been presented in this chapter including the objectives as well as the justifications which are the benefits of the study to the coastal nations in Gulf of Guinea, West Africa.

CHAPTER TWO

LITERATURE REVIEW

A review of the previous literatures related to this study is presented in this chapter. A recap of the various types of wind generated waves and their dynamics as well as the applicable analysis and prediction methods in their study is covered. An overview of the history and general fundamental equations of numerical wind wave models with their assumptions, processes and scales are established in this chapter. A short description of the model to be used in this study, WAVEWATCH III, is presented. This chapter also includes a section on Climate Change and its impacts on the coastal areas.

The Gulf of Guinea (GoG)

The GoG is a very valuable region especially because of the oil and gas reserves (Osinowo et al., 2018). For about three decades, crude oil has been the chief natural resource of the GoG region. Economically, this accounts for more than 7% of foreign exchanges by the major oil-producing countries like Gabon, Nigeria, Congo-Brazzaville and Angola in the region. According to Germain and Armengol, 1999, this represents more than one-third of the gross domestic product (GDP) of this region. This economic situation is more likely to continue due to huge hydrocarbon potential.

Studies have shown that the continental shelf of GoG is narrow mostly not wider than 20–25 km around the coasts of countries such as Côte d'Ivoire, Togo and Benin. This is a little wider in places such as Cape Three Points and the Volta

Delta ranging from 20–80 km wide. A submarine canyon locally referred to as **Trou Sans Fond** has been reported off the Canal de Vridi in Côte d'Ivoire (Giardino et al., 2018). In general, the coastal area of GoG is low-lying, though there are relatively steep coasts in some places. The GoG has several rocky as well as pocket beaches especially at the western-most part (Allersma and Tilmans, 1993).

The waves that reach the coast of West Africa have two major sources of formation: the wind waves or seas that are formed by the relatively not strong local monsoon and the swell waves that originate far offshore from storms in the south-western part of the Atlantic Ocean. The variation of the wave properties on a seasonal basis is not strong in this region. The highest value of 1.6 m for wave height is recorded during the southern winter. This value is even lower for wind waves (seas) with average values of 0.4 m and 215^{o} for wave height and wave direction, respectively.

In a study over the Bight of Benin in the GoG, Almar et al., 2015 observed that between 1979 and 2012, the mean values of wave height, peak wave period and wave direction are respectively 1.36 m, 9.4 s and 189° SSW. During Southern winter, the annual mean wave height is lesser and around 0.4 m, while the direction is further tilted to the west (215°). On a seasonal basis, the northward parts of GoG show maximum amplitudes of significant wave height of approximately 2.0 m, which occurs during Northern summer (Toualy et al., 2015). Osinowo et al. (2018) in a study assessing wave energy over the mid-Atlantic including the Gulf of Guinea making use of a 37-year numerical hindcast data found that the Gulf of

Guinea region is a low wave energy region though this energy is relatively high in the summer which is the raining season in this region.

Wind-Wave Dynamics

The roles of both waves and winds are very significant in driving various coastal, oceanic and atmospheric processes. From Figure 1 and 2 in Chapter One, ocean surface waves in their various forms of Infra-gravity waves, Capillary waves, Long Period/Seismic Sea wave (Seiches, Tsunami), Ultra-Gravity waves, Gravity waves, Ordinary Tidal waves and Trans-tidal waves have different spatial and temporal scales ranging from centimetres to kilometres and from seconds to hours (Bouws et al., 1998), respectively. Wind generated waves, which are the predominant ones, also vary in size and celerity, which is determined by the features of the winds causing the waves. In other words, the properties of the wind such as its speed, duration and fetch (i.e., the length of the water surface on which the wind acts) determines the features of the waves it will generate too.

Wind Seas are waves generated locally that are of short wavelength, more chaotic and travel slower than the surface wind driving them. As Wind Seas travel away from the area of generation, they are sorted into more uniform and regular wave trains that are referred to as Swell. They are less chaotic compared to the Seas. Swells are matured, self-sustaining waves and they can travel far away from the area of generation before breaking at a distance coast (Ardhuin et al., 2009). Studies have shown that both Wind Seas and Swells constitute the means for more than half

of the energy transferred by Ocean surface waves; more than those of tsunamis, tides, storm surges etc. (Alves, 2006).

In the tropical region of the Earth, swells are known to be the dominant wave type determining the wave climate in the region. This is problematic for wave prediction in the sense that Swells are not locally generated and hence, do not provide information on the efficiency/energy of the local wind conditions (Ardhuin et al., 2009). This is further explained by the low correlation between local wind speed and wave climate in the West African coast found in the study by Young et al. (2011). This correlation improves during stormy period, which intensifies the conditions of local winds (Young et al., 2011).

Two sources have been linked to generation of the Swells seen in Tropical Atlantic Ocean: The North Atlantic Ocean region and the South Atlantic Ocean close to the Antarctic region. Wave with the highest wavelengths in the Atlantic Ocean are experienced in West Africa and Western Europe. The Swells experienced in the West Africa coast have been linked to storms generated in South Western Atlantic Ocean close to the Antarctic region (Ardhuin et al., 2009).

Owing to the fact that swell waves carry highest percentage of wave energy in the surface of the ocean, they always attract most attention in wave study because of their impacts on coastal and offshore infrastructures. In recent times, attention has been drawn to the study of swell including its generation, propagation and breaking (Alves, 2006; Ardhuin et al., 2009), its contribution to air-sea interaction. Studies have shown that the rate of decay of swell wave is connected to a reverse

momentum flux process, which happens as the swell interacts with the air boundary above the ocean surface (Semedo et al., 2009, 2011; Sullivan et al., 2008).

Wave Analysis and Prediction

Most countries of the world have dedicated oceanographic and meteorological bodies for the observation, monitoring, prediction and analysis of Meteocean parameters including Ocean wave. This is to provide the needed data and information for coastal and marine activities such as offshore oil drilling, ship navigation, coastal engineering works, early warning services etc. This wave data analysis can be done either on a short-term or long-term basis depending on the reason for analysis or applications (Kamphuis, 2020). The short-term wave data analysis involves analysing just waves of the same storm event i.e., just a single wave train, whereas the long-term wave data analysis is carried out on a statistical basis spanning several years. As expected, the data need of these two methods of wave analysis will differ. Whereas the short-term wave data analysis requires short duration which may range from 0.5 - 20 mins, the long-term wave data analysis requires data covering some hours to some decades (Bouws et al., 1998).

Due to the complexity in resolving all the processes simultaneously taking place in the Ocean at the same time, some assumptions are made to make it possible to approximate these processes to be able to make scientific sense out of them (Kamphuis, 2020). These assumptions include treating waves as stationary process and assuming that Swells propagate linearly following the Earth's Great Circles.

These make it possible to approximate them using the linear wave theory (Alves, 2006).

The application of data related to extreme wave climate in areas such as installations of coastal structures, aquaculture, hydro-energy generation, building and operation of ships and offshore structures makes the information about these extreme conditions very valuable. These needed information include the return period of met-ocean parameters like significant wave height which was defined by Munk (1944) as the average of the highest one-third of all encountered waves in a particular period. The forecast values of these parameters in certain return periods is also a very key information for climate change related studies (Vanem, 2015). It is a major knowledge for proper risk management and planning of proper mitigation and adaptation measures. These return periods have been estimated using different approaches in literatures in the past, which come with their varying levels of uncertainties in predicting extreme climatic parameters for the present and future use. Some of these methods are initial distribution approach, the peak over threshold approach, the block maxima approach, and the average conditional exceedance rate method (Vanem, 2015).

Numerical Wind-Wave Models

Numerical modelling of ocean waves is a very vital part of Oceanography since it is impossible to install instruments for in-situ observations like buoys over a vast expanse of the Ocean due to the high cost of installation and maintenance. Ocean models are based on mathematical depiction of physical processes. Based

on the approach used in solving the fundamental hydrodynamic equations, numerical wave models can be subdivided into two types. These include the Deterministic Models, which are also referred to as being phase-resolving because they rely on approximation of the equations. They can be implemented both in shallow and intermediate water. They have the ability to provide high spatio-temporal frequency description of the sea surface elevation. The second type are the Spectral models, which are also seen as being phase-averaged because they give statistical description of the wave parameters spatio-temporally. They do this at the intersection of the grids, which are used to divide the study area into smaller areas for computation. They give the time-to-time statistical distribution of wave energy in terms of frequency, elevation and direction from one grid to another (Dastgheib et al., 2016; Thammasittirong et al., 2014).

The efforts of several scientists to simulate ocean conditions have been dated to span several years. These include attempt by Sverdrup and Munk as far back as 1947, who developed a method to forecast ocean conditions to aid vessels landing on the shore. This approach finds a relationship between the prevailing speed of the wind and oscillations of the sea surface (Schwartz, 2006). Wave spectral relation was derived in 1953 by Nueman to relate significant wave height and wave period (Goda, 2010). Pierson in 1957, pioneered a method of using Fourier Series of superimposed waves composed of varying wavelengths and phases to solve the wave energy spectrum statistically.

Spectral models have evolved over the years from first-generation models to second-generation and to the latest third generation models (Bouws et al., 1998).

The first-generation models are the earliest models that were built in the 1960s and they have the capability to model the growth and dissipation of wave energy. They make use of 2D spectrum of frequency and direction. The shortcoming of this generation of model is that they were not able to resolve non-linear interactions between different wave frequencies. This was because non-linear interactions were implicitly defined in the form of wind and energy input on the assumption that waves stop growing when they reach a predefined saturation level (Phillips, 1957).

In the early 1970s, proposition by (Barnett, 1968; Ewing, 1971), which follows every single wave component as it develops was applied in physical models. This gave a better understanding of the importance of the role of non-linear wave-wave interactions in wind wave development. This led to the expansion of focus on wave growth experiments to study the effect of non-linear wave-wave interactions as well as the wind input (Hasselmann et al., 1973; Mitsuyasu, 1969). This knowledge benefitted the development of Joint North Sea Wave Project - JONSWAP Spectrum by (Hasselmann et al., 1973).

The invention of the JONSWAP spectrum and the improved interpretation of the underlying physical processes of wind waves piloted the introduction of the parametric models, which are also referred to as the second-generation models (Cavaleri and Rizzoli, 1981; Hasselmann et al., 1976). The second generation of wave models were improvements on the First-generation models, which started using parameterizations to approximate the non-linear wave interactions because the actual computation of these interaction requires high computing powers. They made use of the JONSWAP spectrum derived spectral shape and parameterized

non-linear wave-wave interactions (Hasselmann et al., 1973). The deficiency in the second-generation models is that the limitation placed on the spectral shape leads to inconsistencies in degree of freedom and non-linear parameterizations (Group, 1985).

The third-generation of Spectral models were introduced in the 1980s, kick-starting the comprehensive description of physical processing, which govern wave propagation. This generation of models made fewer assumptions compared to previous generations (AIT et al., 2014; Dastgheib et al., 2016; Ranasinghe, 2016; Ranasinghe et al., 2013). The characteristics of the third-generation models include:

a. The freedom to develop without an **a priori limit** on the shape of the wave spectrum. The conformity to Physics of the spectrum is assured by the balance between the source and sink terms.

b. There is explicit computation of the non-linear wave-wave interaction denoted as S_{nl} which is defined in such a way that it has equal value for degrees of freedom like the discrete representation of the spectrum.

c. The means of estimating the source and sink terms are well defined in both frequency and direction domain instead of just parameterizing them as done in second-generation models.

Third-generations Spectral models are rapidly developing and are applied in the study Ocean waves. Examples include WAM (WAMDI Group, 1988), WAVEWATCH III (Tolman, 2009; Tolman et al., 2002), SWAN (Booij et al., 1999; Group, 1985), MIKE21, TOMAWAC etc. shown in Figure 6. With the right bathymetric data, these models can be applied in simulating any part of the

Ocean though some are better adapted to the deep Ocean while others are more efficient in shallow water (Nearshore). The differentiating parameter is mostly the source and sink terms used in these models (Tolman, 2008; Tolman et al., 2002).

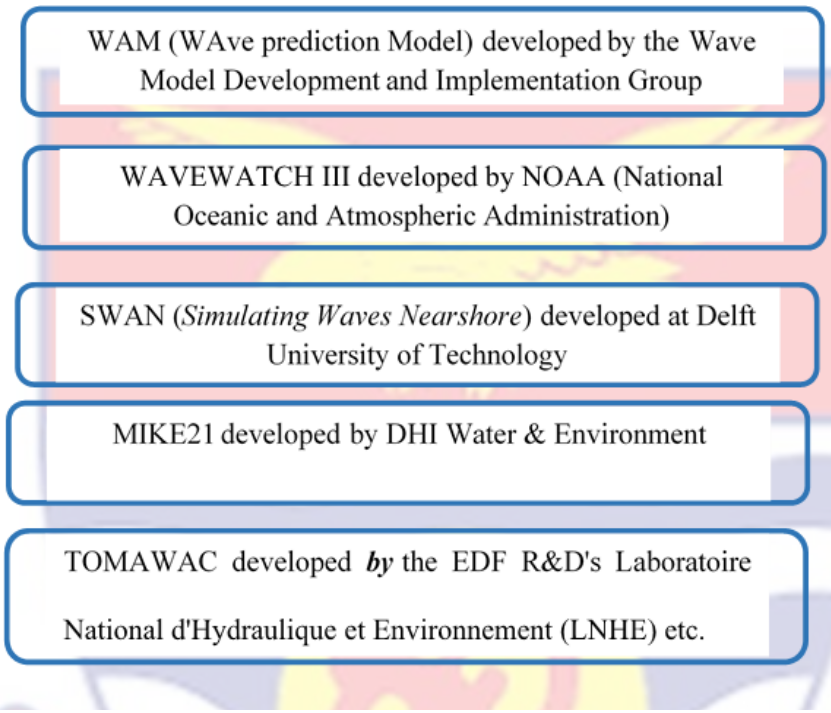

Figure 6: Some third-generation wave models used around the world and their developers.

Wave Model Processes and Scales

Most Spectral wave models generally account for processes such as wave generation by wind input, bottom friction, refraction and shoaling, nonlinear interaction, white capping and bathymetry-induced wave breaking. White capping accounts for the wave breaking in deep water, while wave breaking in shallow water is induced by water-depth relationship. The generation of a wave relies on the fetch, speed and duration of the wind. Non-linearity is resolved theoretically through either triad and quadruplet wave interaction. The white capping process

makes use of the wave action spectrum parameter. Others like bottom friction, depth-induced wave breaking, refraction and shoaling relies on the bathymetry as well as the type and size of sediment.

The phases (scales) through which wind waves pass through are generation (offshore), transformation (intermediate water) and local scale (nearshore). The wave generation phase mostly takes place in the deeper water and around the continental shelf. The predominant drivers of this phase are atmospheric/wind input, non- linear wave-wave interactions and energy is dissipated through white-capping. The wave transformation phase mostly occurs in the intermediate-shallow waters. The drivers here are wave shoaling, refraction and breaking. The local scale is seen in the shallow waters and near coastal structures, where processes like diffraction, reflection, and wave nonlinearities are the governing processes (Figure 7 and 8). Despite the fact that there are sometimes overlap between these phases, numerical models are able to resolve these efficiently.

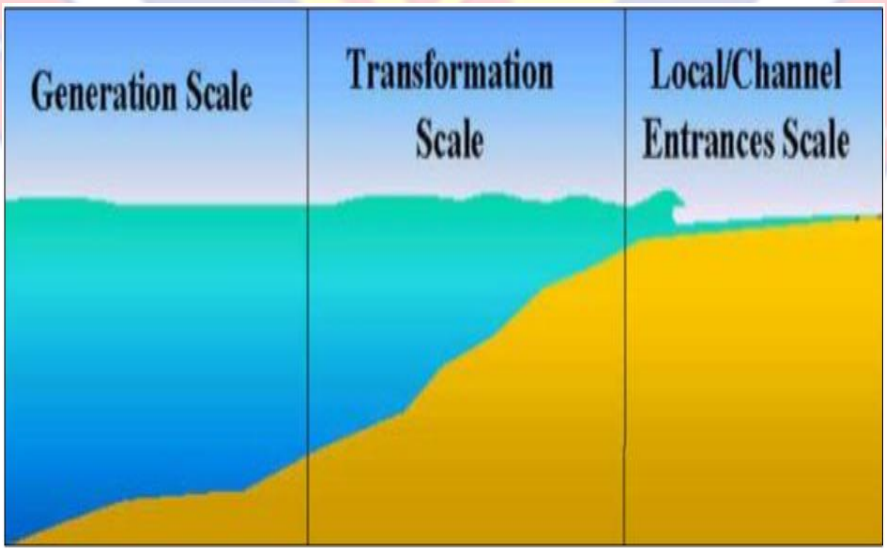

Figure 7: Phases (scales) of wave processes accounted for in Spectral models (Source: AIT et al., 2014).

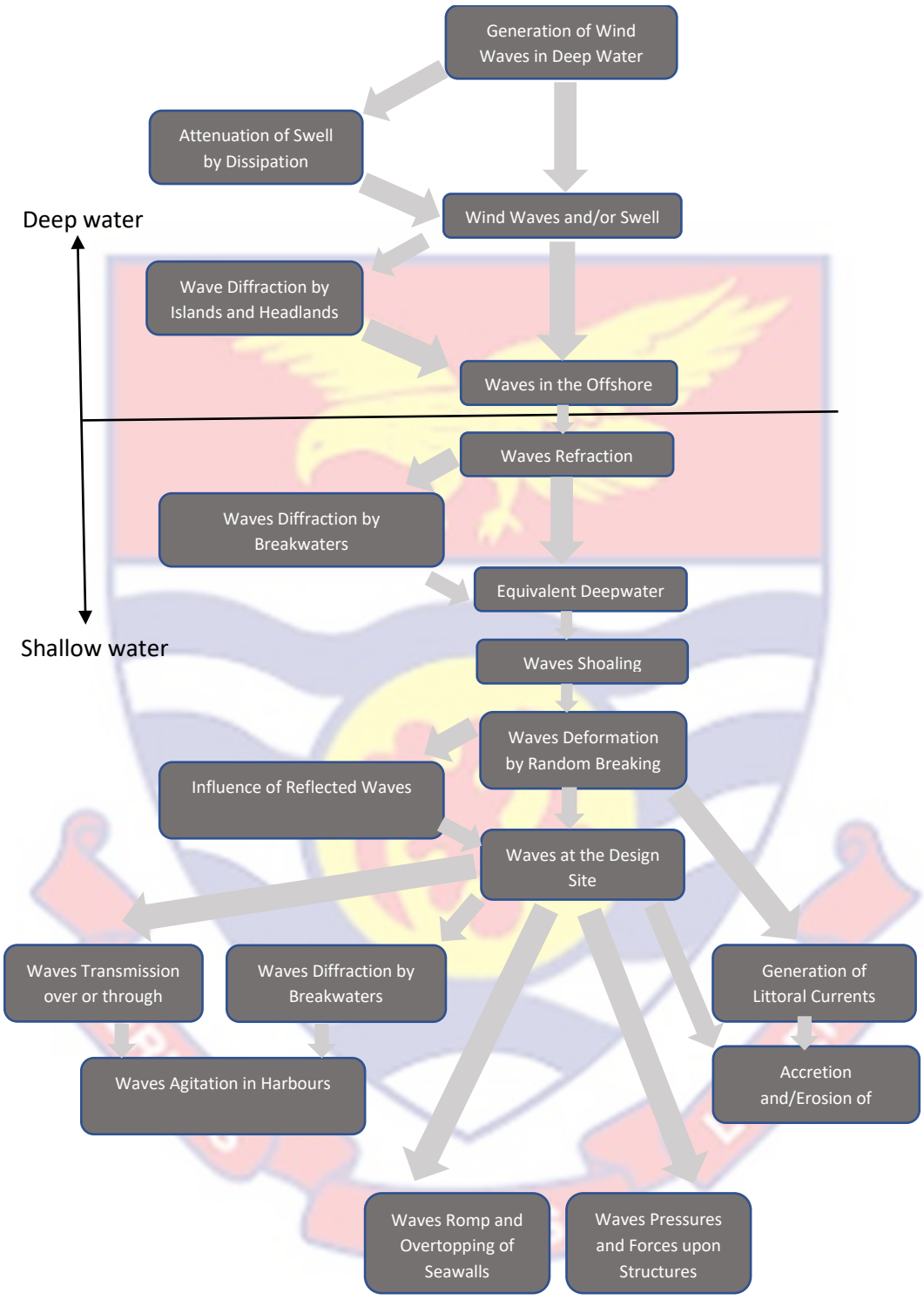

Figure 8: Flowchart showing the phases in wave movement: generation, transformation and local (actions) (Adapted from Goda, 2010).

Due to the predominance of Swells, which travel over a long distance in the tropics, wave modelling in this region is a complex task and therefore has suffered some drawbacks. These have been reported to be responsible for poor prediction of wave-heights in this region (Ardhuin et al., 2009). The overestimation of significant wave height in the tropics can be reduced by making sure numerical wave models compute parameters accounting for swell dissipation and where possible, carry out data assimilation by forcing the model with wave in-situ measurements to improve the result of the model. The application of data assimilation is not that feasible in the West African coast because of the shortage of long duration wave measurement in the region. These shortcomings have been reported to cause biases of up to 45 cm or 25 % in significant wave height and 0.8 s in wave period in the Eastern tropical Pacific (Rascle et al., 2008; Rascle and Ardhuin, 2013). Therefore, unless continuous researches on Swells in this region are carried out and improvement made on in-situ observation by installations of buoys in the Gulf of Guinea, it may be difficult to correctly predict the wave climate in this region.

WAVEWATCH III (WW3) Model

The WW3 Model was originally developed by Hendrick Tolman and it has evolved since then as a result of improvements by the developers. From WAVEWATCH I developed at Delft (Tolman, 1989, 1991) to WAVEWATCH II developed at NASA Goddard (Tolman, 1992) and to the latest WW3 developed at NCEP (Tolman et al., 2002). WW3 is now a community model through the NOAA partnership program which is dedicated for source development.

This model has been applied in simulating air–sea interactions, wave energy, wave spectral evolution, acoustic noise, nonlinear wave–wave interactions as well as Nearshore studies of Infra-Gravity waves because of its ability to adopt different gridding types (Hanson et al., 2009; Tolman et al., 2002). The grids used include:

1. Triangle mesh (unstructured), which is capable of resolving large scale and small-scale processes simultaneously.
2. Rectilinear, which is applied to remove deep water points and make use of 2-way nesting.
3. Curvilinear, which uses same Courant–Friedrichs–Lewy (CFL) timestep at low and high latitudes.

The WW3 version developed at NOAA/NCEP is similar to WAM in many ways in that it is a discrete spectral and phase averaged model capable of being applied in both regional and global scale (Bouws et al., 1998). WW3 computes the directional wave spectrum for every grid point in the model based on wavenumber-direction bands, whereas the wave field is resolved using numerical approach by computing spectral wave action balance equation.

Fundamental Equations of WAVEWATCH III (WW3)

Most wave models find solution to the spectral wave action balance equation, which assumes that the properties of the medium such as the depth of water, its currents and the wave energy change at a magnitude much larger than a single wave. The spectral wave action balance equation is given as:

$$\frac{\partial N(i)}{\partial t}+\nabla_x \cdot \left(c_g+U\right)N(i)+\nabla_i \cdot c_i N(i)=\Sigma S(i) \quad (1)$$

where $N(i)$ is the action density, i is the spectral phase space (wavenumber, frequency, direction, 2D), ∇_x and ∇_i are divergence operators, c_i, U, and c_g are characteristic and current velocities respectively and $\Sigma S(i)$ are the sources and sinks of energy/action (Tolman et al., 2002).

Equation (1) can be rewritten as:

$$\frac{\partial N}{\partial t}+\frac{\partial}{\partial t}\dot{x}N+\frac{\partial}{\partial t}\dot{y}N+\frac{\partial}{\partial t}\dot{k}N+\frac{\partial}{\partial t}\dot{\theta}N=\frac{S}{\sigma} \quad (2)$$

where t represents time, $\dot{\mathbf{k}}$ stands for wave number, $\sigma = 2\pi f$ represents the angular frequency, the dot placed on the variables represents the rate of change, and s stands for the source terms.

The total source term, S_{tot} (Equation 3), is the sum of source terms for input (S_{in}), dissipation (breaking) (S_{ds}), nonlinear interactions (S_{nl}), bottom friction (S_{bot}), depth induced breaking (S_{db}), triad interactions (S_{tr}), bottom scattering (S_{sc}), wave-ice interaction (S_{ice}), wave reflection (S_{ref}) and others that the user may see fit to include.

$$S_{tot}= S_{in}+ S_{ds}+ S_{nl}+ S_{bot}+ S_{db}+ S_{tr}+ S_{ice}+ S_{ref}+\ldots \quad (3)$$

For deep water, the total source term S_{tot} is usually a balance of the atmosphere-wave interaction source term given as S_{in}, a non-linear wave-wave

interaction source term given as S_{nl} and a wave-ocean interaction source term given as S_{ds}. S_{in} is mostly positive but may be negative for Swells and it represents the energy input. S_{ds} also account for dissipation of energy as wave breaks (Figure 9).

To properly simulate the ocean surface conditions in WW3, the spectral energy density function given as $E(\sigma,\theta)$ is used. In this function, σ accounts for the frequencies, while θ stands for the direction of propagation. The action density equation is given as:

$$N=\frac{E}{\sigma} \tag{4}$$

$$\frac{\partial N}{\partial t}+\nabla_{\vec{x}}.\left[\left(C_g+\vec{U}\right)N\right]+\frac{\partial c_\sigma A}{\partial \sigma}+\frac{\partial c_\theta A}{\partial \theta}=\frac{S_{tot}}{\sigma} \tag{5}$$

where $\frac{\partial N}{\partial t}$ accounts for the effect of time on wave action density, $\nabla_{\vec{x}}.\left[\left(C_g+\vec{U}\right)N\right]$ accounts for propagation of wave energy in 2D space, $\frac{\partial c_\sigma A}{\partial \sigma}$ accounts for the effect of shifting of the radian frequency due to variations in depth and mean currents, $\frac{\partial c_\theta A}{\partial \theta}$ accounts for bathymetry-induced and current-induced refraction, $\vec{U}$ stands for the current, $\vec{x}$ represents the spatial dimension and C_g the group velocity. The left-hand side of equation (5) is generally referred to as the kinematic part. The source

and sink terms are represented by the terms on the right-hand side of the equation (5). WW3 propagates waves based on the equations described in Equations 6 - 7

$$\frac{dN}{dt} = \frac{S}{\alpha} \tag{6}$$

where $\frac{dN}{dt}$ is the net derivative of the wave action density spectrum and S stands for the total effect of sources and sinks in the model.

The Eulerian form of Equation (6) which is applied in WW3 is given as:

$$\frac{\partial N}{\partial t} + \nabla_{\vec{x}} . \dot{x} N + \frac{\partial \dot{k} N}{\partial k} + \frac{\partial \dot{\theta} N}{\partial \theta} = \frac{S_{tot}}{\sigma} \tag{7}$$

In Equation (7), the left-hand terms i.e., the kinematic part respectively account for change in time, advection in geographical space and advection in spectral space. To properly represent the physical processes in the ocean, WW3 also employs some source and sink terms, which are referred to as switches. Wind-wave interaction, white-capping dissipation and non-linear wave-wave interaction are the physical processes that are accounted for by source terms in the deep ocean (Figure 9). Since both wind-wave interaction and white-capping dissipation are both responsible for wave growth in the model, they are treated and tuned by one switch in WW3 (WW3DG, 2019). In the nearshore where wave-bottom interaction becomes significant, the source and sink terms used are wave-bottom interaction to account for the effect of bottom friction and depth induced wave breaking. Other

sinks terms like wave-ice interactions are also available in WW3 though not used in this study since the effect of wave-ice interaction is not significant in GoG.

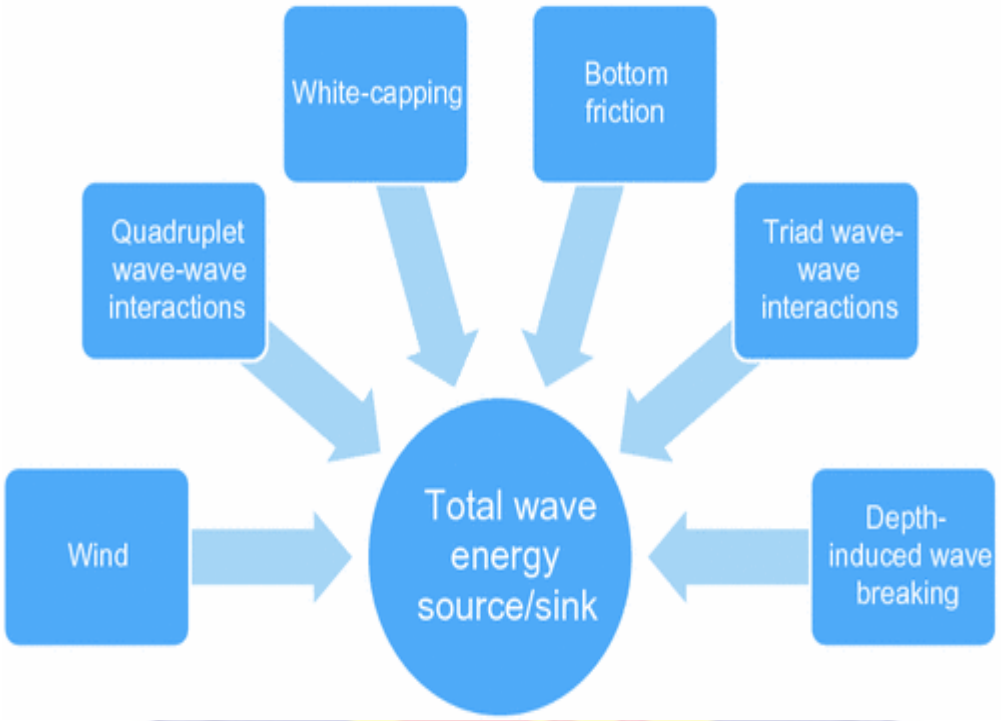

Figure 9: The various source and sink terms in ocean wave model (Source: Rascle and Ardhuin, 2013; Folley, 2017).

Climate Change and the Coast

Various studies have reported on the environmental impacts of CC globally among which statistical projections based on past weather conditions have shown the possibilities of these impacts to last up to several decades or millions of years (UNEP Programme., 2008). The major factors known to contribute to CC include Volcanic Eruption Forcing, Solar Radiation Forcing and Anthropogenic Forcing (Crowley, 2000). Nevertheless, the recent change in climate has been said to be mostly driven by human activities through an increase in the amount of Greenhouse

gases in the atmosphere (Houghton, 1996; Wigley, 2007). The major culprit in the increase of the global temperature, the greenhouse gases, include Carbon-dioxide (CO_2), Ozone (O_3), Water Vapor ($H_2O_{(g)}$), Methane (CH_4) and Nitrous Oxide (N_2O). They are referred to as greenhouse gases because they tend to provide a blanketing (enveloping) effect by trapping heat in the atmosphere to regulate the temperature on Earth. This helps to balance the incoming solar radiation and outgoing heat from the Earth but when they are in excess, they retain more heat than needed, leading to global warming. Of all the greenhouse gases, CO_2 accounts for about 35 % of the warming experienced today since the industrial age when it was used in large quantities in burning fossils fuels (IPCC., 2007).

Various impacts of increase of greenhouse gases have been reported in the literature among which are global warming and the resultant changes in global weather patterns as well as increased frequency of storminess are the most discussed. Some of the effects of global warming are increase in surface evaporation which leads to drought and various fire outbreaks and excessive precipitation, which results in flooding (Fowler and Hennessy, 1995). The rapid melting of the ice in the polar regions and the thermal expansion of the oceans have been linked to global SLR (IPCC, 2001). Of all these impacts, the increase in the frequency of storminess, which causes more storm surges and SLR are most impactful in the coastal environment (Zhang et al., 2004). SLR has been reported in every continent of the world and models have predicted a global increase in sea-level of about 0.18 – 0.59 m by 2100 (IPCC., 2007). Increased storminess is

expected to increase the impact of SLR because it tends to bring the water more inland during coastal storms (Philippart et al., 2007).

There has been growing proof of past intra- and inter-annual trends and variabilities of wave climate in the ocean surface through studies such as those making use of satellite altimeters (Hemer et al., 2013; Hemer et al., 2010; Young et al., 2011) and visual observing ships (Grigorieva and Gulev, 2008, 2006; Gulev et al., 2003) data. These observed changes are not only seen in wave height but also wave period and wave direction (Hemer et al., 2010; Morim et al., 2020). Results from various studies including observation and modelling have shown that wave height has been experiencing increase since 1975 (Caires et al., 2004; Hemer et al., 2010) and this has been associated to the global increase in 10m above sea surface wind speed (U10). This may not be directly traceable to the local wind condition due to the propagation of swell wave.

These changes are expected to lead to a modification of the equilibrium state of the coastal system and also affects engineering needs of offshore structures (Morim et al., 2020; Semedo et al., 2012). Judging from the key part played by waves in the atmosphere-ocean interactions, the observed changes are expected to also have a major impact on coupled climate system (Cavaleri et al., 2012).

Consequently, the ocean modelling groups and institution have stepped-up efforts to comprehend how the wind-wave climate reacts to climate change and variabilities to know the likely effects of these changes. This has been done in form of hindcasting historical wave climate as well as forecasting future wave climate (Cavaleri et al., 2012). Some regions of the world have done well than others in

these efforts which has led to regions at higher risks in terms of severity of hazards (level of change in wave climate) or in form of degree of vulnerability (regions with less adaptive/coping capacity) being mostly under covered. The GoG, where wave climate is a major determinant of onshore and offshore infrastructure as well as ecosystems and their services, fits into the description of highly vulnerable region to projected change in wave climate (Morim et al., 2020).

Significant wave height has been simulated using different climate models for different oceans with most reporting increase. Results have shown varying rates as well as signs for the projected significant wave height from one time to another during the century in some locations. These variations have been linked to the variations in the forcing applied in these models. Positive correlations have been found between rate of change of significant wave height and rate of increase of greenhouse gas forcing (Wang et al., 2004). In a study by (Wang and Swail, 2006), it was projected that the Antarctic region between 40^{o}S and 60^{o}S will experience rise in the significant wave height. Being the source of Swell experienced in Gulf of Guinea, similar or higher increase is expected to be observed in the Swells reaching the West African region (Ardhuin et al., 2009).

Large scale variations in ocean-atmosphere interactions has been linked to interannual variability of wave climate through correlations between average monthly significant wave height and climate indices such as ENSO (Gulev and Grigorieva, 2004), Southern Annular Mode (SAM) (Hemer et al., 2010) and NAO (Izaguirre et al., 2010, 2011; Woolf et al., 2002). Though it is known that changes in wave heights and its energy is majorly determined by changes in surface wind

energy, interannual climate phenomenon such as SAM or the Pacific Decadal Oscillation are responsible for changes on decadal basin scale (Merrifield et al., 2012; Wang et al., 2014; Yang et al., 2007). As a result, the global wave climate changes as these phenomena happen thereby leading to inter-basin teleconnections due to NAO and the ENSO.

El Niño, the positive phase of ENSO, is marked by higher seas surface temperature in the tropical Pacific Ocean and is usually accompanied by higher frequency of cyclonic activities in both the Pacific and Atlantic Oceans, through dynamic atmospheric teleconnection (Jin et al., 2014). The effect of ENSO is felt on the oceanic conditions globally (Alexander et al., 2002). In a study of the interrelationship between ocean warming and wave conditions by Reguero et al. (2019), some regions (shown in Figure 11) were selected due to their application in studying the influence of ocean swell waves to the global wind-wave climate to show that approximately 90% of the storm generated waves comes from the extratropical sub-basins. These regions also coincide with areas with different wave climates (Mentaschi et al., 2017; Rueda et al., 2017). Figure 11 also shows the region of teleconnection of SST and wave conditions. The arrows' thickness and colour show the level of correlation between the linked regions. The regions are ETNP, TPAC, ETSP, ETNA, TATL, ETSA, TIOC and ETSI (Figure 10 and 11).

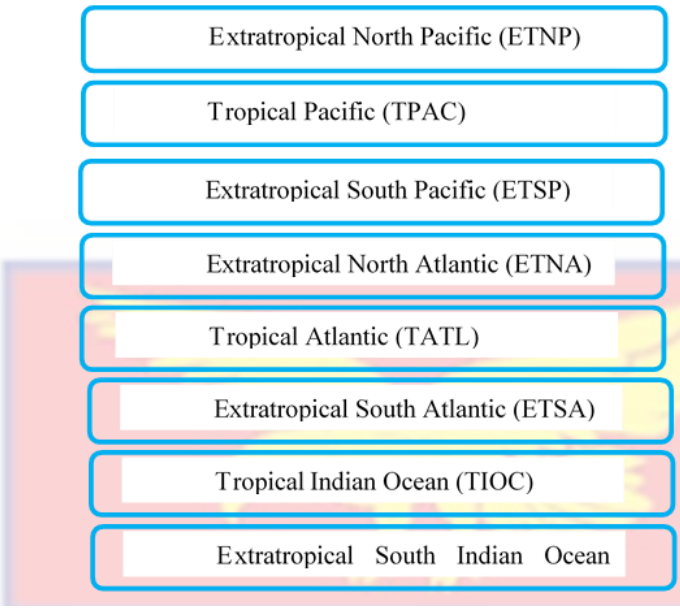

Figure 10: Regions of the global ocean based on wave conditions.

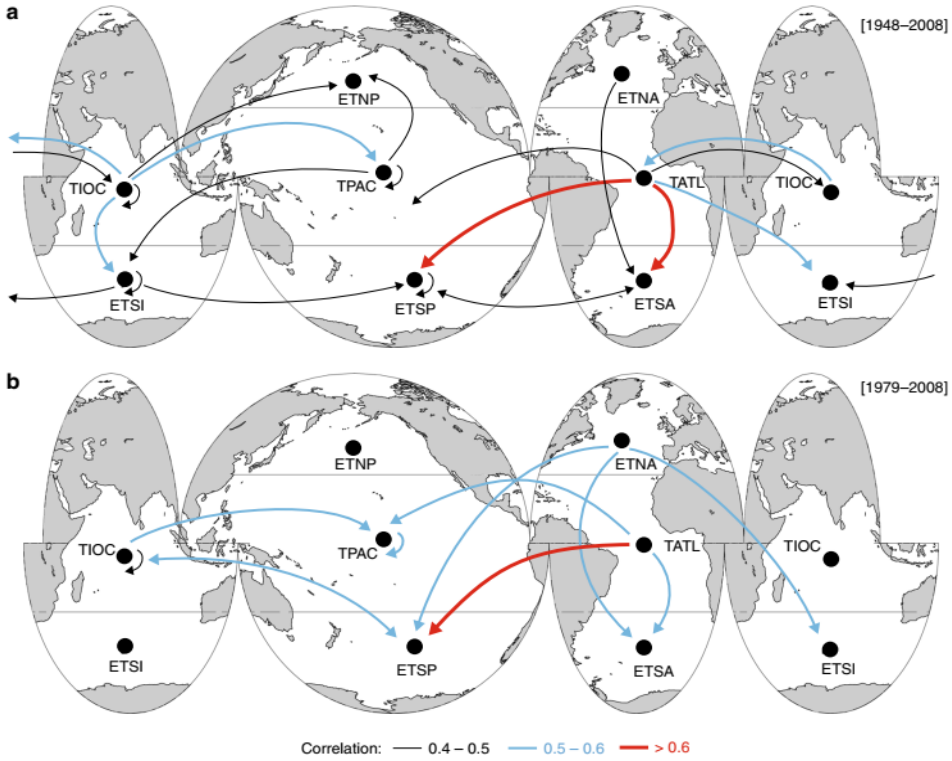

Figure 11: Inter-basin correlations of SST and Wave conditions for periods: (a) 1948–2008 (upper frame) and (b) 1979–2008 (lower frame) (Source: Reguero et al., 2019).

In a recent study by Reguero et al. (2019), calculation of correlations between the Sea Surface Temperature (SST) and Wave Power (WP) for the various swell regions of the world was done. The results show that the SST changes correlate well with changes in the WP in different ocean basins especially in mid and high latitudes. A high correlation was found between warmer eastern-central tropical Pacific and higher WP in the North Atlantic which is the same observed trend for El-Nino climate index corresponding to ENSO. This is explained by air-sea connections between sea level pressure, wind and SST in the tropical Atlantic and eastern Pacific. This remote influence happens through the Walker circulation-kind of response seen in the ENSO-Atlantic teleconnection.

It is worthy of note that the classifications shown in Figure 10 are generally used in the global assessment of model performance and their regional variability. These sub-regions of the global ocean are defined by Alves (2006) on the basis that the wave climate shows related qualitative features within such regions (Hemer and Trenham, 2016).

Wave Projections/Forecast

In the literatures, there is no standard or one globally accepted approach to scientifically analyze or predict extreme significant wave height (Bouws et al., 1998; DNV, 2017; Gumbel, 1958; Holthuijsen, 2010). Recommendations vary depending on data used, the distribution that best fits the data and the best technique that optimizes the best fit. These various extreme wave height projection methods have been reviewed and intercompared in literature (Soares and Henriques, 1996;

Soares and Scotto, 2001). These documented approaches include initial distribution approach (three-parameter Weibull distribution), the annual maximum approach (Gumbel distribution) and the peak-over threshold approach (exponential distribution).

Chapter Summary

Previous literatures on wave modelling researches have been reviewed globally and regionally to show the development phases wave modelling has passed through. The type and dynamics of wind wave was presented as a foundation for the development of the equations on which spectral models rely. The various methods that have been developed for better wave analysis and prediction have been reviewed in this chapter also. The types and generations of numerical wind-wave models were also covered in this chapter to give a historical overview of the development phases of ocean wave modelling. Also presented in this chapter are the various examples of ocean wave models currently in use, their fundamental equations as well as the processes and scales of this wave models. The historical development and features of WAVEWATCH III (WW3) model, which is the model used for this study was presented. The impacts of various air-sea interactions such as ENSO which may influence oceanic processes like waves have also been reviewed especially as they relate to climate change. This chapter was closed by reviewing the various wave projections/forecasting methods currently being used in studying ocean waves.

CHAPTER THREE

MATERIALS AND METHODS

This chapter describes the study area including the meteorology and geomorphology of Gulf of Guinea. Included here also is the spectral wave model and fundamental equations of WAVEWATCH III^{TM} presented in some sections. The various modelling steps such as input data acquisition, input data pre-processing, model set-up, model running, model output and model validation have all been detailed in this chapter.

Overview of the Study Area

This study is focused on the Gulf of Guinea region. This is because this region is affected by relatively similar wave conditions (Almar et al., 2015; Osinowo et al., 2018). As a result of this relatively uniform wave conditions, the region is affected by similar hydrodynamics problems. This regional-scale problems, such as coastal erosion, have manifested in form of knock-on effect of coastal engineering structures on neighbouring countries. For example, coastal structures in Ghana have been reported to affect the coastal areas of Togo (Guerrera et al., 2021). This issue warrants that coastal management should be done on regional scale rather than country-by-country. This was recommended by Alves et al. (2020) as a more effective and economical way of managing coastal problems in the GoG. Hence the choice to carry out wave assessment on a regional scale in this study. The GoG is located in the north-easternmost region of the tropical Atlantic Ocean and it covers an area of 2,350,000 km^2 (Osinowo et al., 2018). The

countries of the region are bounded in the southern part by the GoG and in the North they are bordered by the continent of Africa, which serves as source of numerous rivers flowing into the Atlantic Ocean (Figure 13). The stretch of the coastline cover is from Cape Palmas (4°22'8.00"N, 7°43'43.00"W) in Liberia through Niger Delta (4°48'43.02"N, 8°47'0.13"E) in Nigeria, which is approximately 2,100 km in length. According to Schwartz (2006), the drift rate in GoG is one of the strongest drift rates for sediment of about 1 m^3 per annum. This drift is reported to be mostly eastward, which accounts for the littoral transport in the coast in this region (Wellens-Mensah et al., 2002).

The atmospheric conditions in GoG are mostly driven by the position of the Inter-tropical Convergence Zone (ITCZ), which is the point where the north-east trade winds meet the South-East Trade winds. The seasonal variation of wind speed and direction is weak with average wind speed mostly between 3.7 – 4 ms^{-1} (EPA, 2009 and 2015). The dominant current in this region is the Guinea Current (GC), which is a mixture of the Canary Current and North Equatorial Counter Current (NECC) (Figure 12). The GC moves further southward to mix with the Benguela Current (BC).

The GC is weaker nearshore because of the effects of currents that are locally generated close to the coast, which are mainly wind-driven currents extending between 10 – 40 m layer of coastal water (Ukwe and Ibe, 2010). The direction of the resulting longshore currents is west-east, which indicates the direction of the effects on the shoreline of incoming waves. The magnitude of the

longshore current mostly varies between 0.5 – 1.5 ms^{-1} and on average, 1 ms^{-1}. Being wave driven, these values may be higher during stormy periods.

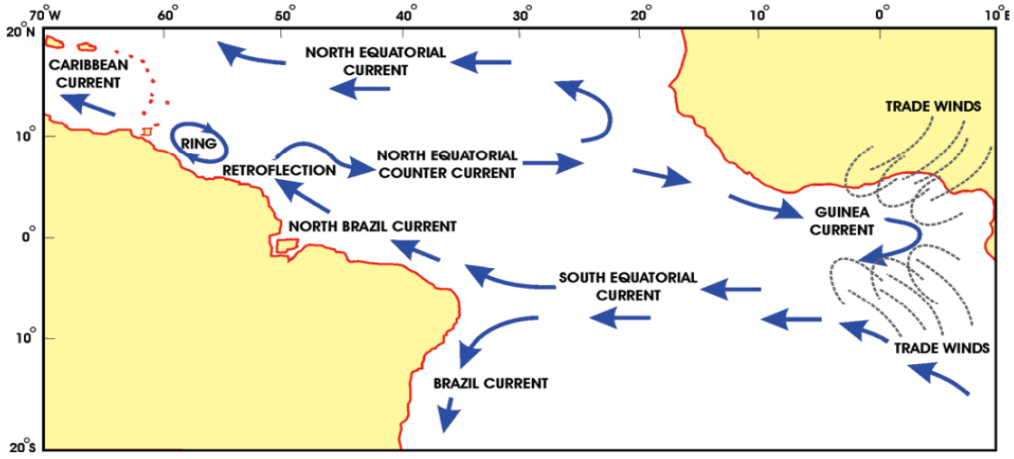

(a)

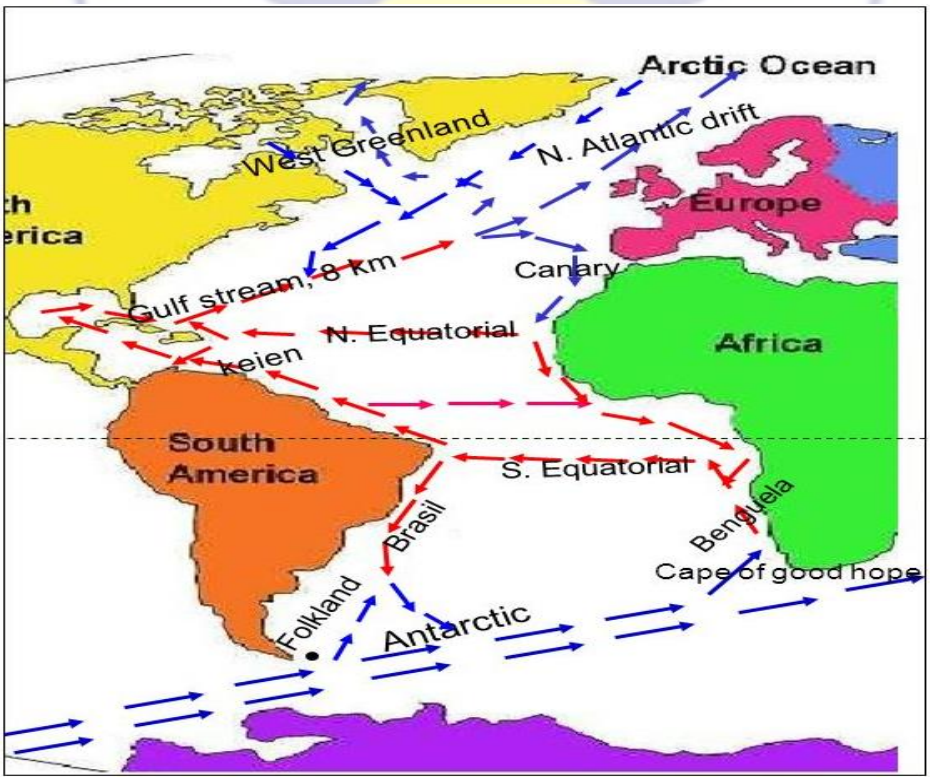

Figure 12: (a) & (b) show the mixture of NECC and Canary Current to form GC. and the Atlantic Ocean current system (Sources: Sharma et al., 2009).

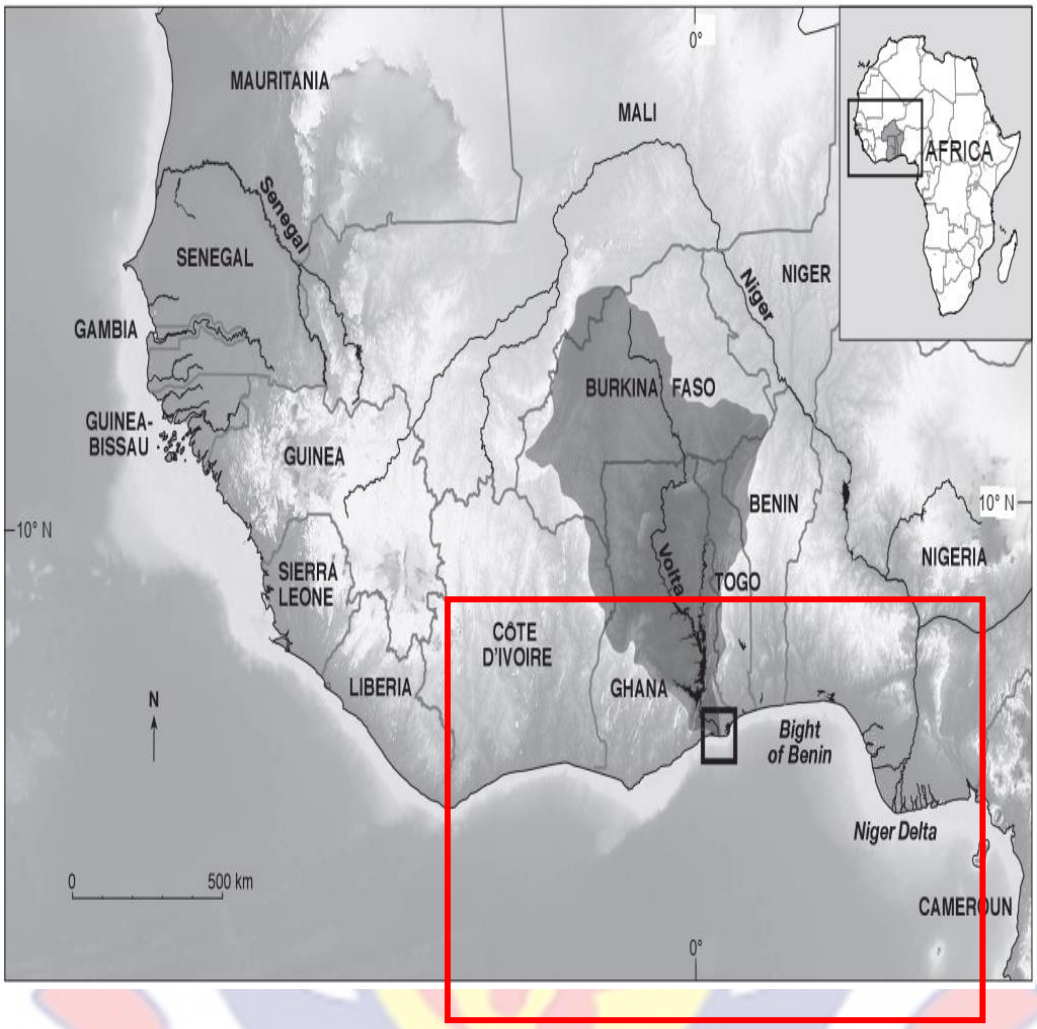

Figure 13: Map of the coast and continental shelf of West Africa with GoG enclosed in red rectangular box. Continental shelf width shown by pale area along the coast (Source: Laïbi et al., 2014).

Though the GoG predominantly experiences swells of about 1 m significant wave heights with maximum of approximately 3.3 m on annual basis, extreme wave conditions featuring 5-6 m significant wave heights have been observed to be experienced within 10-20 year return period (Short, 2012). The swell has mean wave period of approximately 7-14 s and dominantly in the south or southwest direction.

Some of the numerous rivers that flow into the GoG are the Volta and the River Niger. The coastal waters include the likes of the Bight of Bonny and the Bight of Benin. The beaches along this coast are mostly in the ‘‘reflective-to-intermediate’’ state classes (Gourlay parameter, Ω=1 using the method of Wright and Short, 1984; Relative Tide Range RTR=1, Masselink et al., 2014), and often exhibit an alongshore-uniform low-tide terrace and a steep reflective upper beach-face. The grain size is medium to coarse (Anthony and Blivi, 1999).

The nature of the climate along the coast of West Africa is equatorial, with significant differences in the volume and seasonal supply of rainfall (Allersma and Tilmans, 1993). The eastern part of the coastline is known to have less precipitation than the western part. Moving from west to east, the major rivers adding to the supply of sediments to the coast include: Sassandra, Bandama and Comoé all in Côte d'Ivoire, Pra and Volta in Ghana, Mono in Togo, Oueme in Benin. The Volta River contributes the largest sediment supply of the rivers in the region.

The Meteorology and Geomorphology of Gulf of Guinea

The wind system in GoG consists mostly of south-east trade winds, which is season dependent having a monthly average wind speed of about 5 m/s in the boreal summer. This weak but steady wind becomes even weaker during boreal winter, having values of approximately half their summer equivalence (Brink and Robinson, 2005; Houghton, 1996). Studies have shown that in the central and equatorial Atlantic region in which Gulf of Guinea belongs, the effect of wind variation is more noticeable, especially when the ITCZ extends to the equator

during the boreal winter. This seasonal changes in the location of the ITCZ in turn determines the seasonal variations in rainfall (Hastenrath, 2012).

The coastline of GoG has been observed to have two unique parts with one in the zonal direction and the other in the meridional found in the northern and eastern borders, respectively. The continental shelf which extends from the coast up to the shelf break is relatively narrow covering about 30 km expanse with 100 – 150 m water depth. Nevertheless, wider continental shelves are found in some places like south-eastern part of Takoradi in Ghana and along the Niger River Delta in Nigeria (Figure 13). Various submarine canyons have been discovered in the GoG including Avon Canyon, Mahin Canyon and Calabar Canyon in Nigeria as well as Trou sans Fonds in Ivory Coast. These are in addition to others like the Congo-Zaire Canyon south of Pointe Noire in this region of Atlantic Ocean. This narrow and shallow nature of the continental shelf in GoG is the reason offshore swells are able to travel far into this region and dominate the impact of wave at the coast (Brink and Robinson, 2005).

Spectral Wave Model: WAVEWATCH III™

Wave generated by winds are usually of varying heights, periods and directions because of the incessant changes in the nature of the generating winds. As a result of this haphazard nature, the surface of the ocean is constantly changing which is why the deterministic method of solving wave equations is not a viable approach in this case (Tolman, 2010).

To efficiently study the trends of wave climate in GoG, three of the bulk wave parameters vis-à-vis significant wave height (*Hs*), mean wave period (*Ts*) and mean wave direction (*Dm*) of locally generated wind waves (sea) as well as offshore storm generated swells are needed. In this study, these data were obtained by running a hindcast simulation of the wave conditions between 1980-2019 for the mid-Atlantic between longitudes 80° W-15° E and latitudes 40° N-30° S. The simulation was run for the entire mid-Atlantic to avoid the error due to model boundary conditions in the area of interest which is GoG. The study duration, 1980-2019, has been chosen to enable validation of models and comparison of results since in-situ data are available for this period, and have been used for similar studies.

The WW3 Model version 3.14, a third-generation spectral wave model, was employed in this study. The version of wave model used in this study was developed in 2009 by the Marine Modelling and Analysis Branch (MMAB) of the Environmental Modelling Center (EMC) of the US National Centres for Environmental Prediction (NCEP). This model was built primarily for ocean wave simulations, to predict wave conditions through forecast. The current version of the model is an improvement on the former WAVEWATCH II of NASA Goddard Space Flight Center from the initially built WAVEWATCH I by Delft University of Technology, and (Tolman, 2009; Tracy et al., 2007). WW3 differs from the previous versions in terms of features. These differences include improvements in the governing equations, the structure of the model, the numerical methods used in

solving the various equations. It also differs in terms of the parameterization approaches adopted in this latest version of the model.

The application of WW3 in the modelling of sea-state and wave climate on a large scale, using coarser regular (rectilinear) grids and fine-resolution unstructured grids in the offshore and coastal areas, respectively is well known (WW3DG, 2019).

As a spectral model (phase-averaged), WW3 is able to forecast and transform deep-wave conditions to the shore by solving the spectral wave action/energy balance equation. Like other spectral models, WW3 accounts for the constant changes in the ocean surface conditions and other physical processes through the energy density spectra, as well as some source and sink terms (Tolman, 2014).

Like other third generation spectral model, WW3 is based on finding solution to the random phase spectral action density balance equation for wavenumber-direction spectra. This approach is based on the assumption that the characteristics of the ocean such as the bathymetry, current and wave field change on spatial and temporal scales, which are higher than the scale at which a single wave may change. WW3 is applicable for both nearshore/shallow-water studies as well as offshore modelling because of features like drying and wetting of grid points, regular and irregular grids, single-grid or multi-grid option etc. WW3 has also been improved in terms of the source terms, which are used to properly parameterize oceanic physical processes such as white-capping, surf-breaking, bottom friction and sub-grid blocking, due to unresolved islands (WW3DG, 2019).

WW3 is written in American National Standards Institute (ANSI) standard Formula Translation -FORTRAN 90 in a modular format. The wave energy spectra in WW3 are evenly distributed in all directions, making use of wavenumber grids that are increasing from one grid point to another in all directions. WW3 has the option of compiling in parallel using OpenMP or Message Passing Interface (MPI) compiler (Tolman, 2014).

Input data Acquisition

The bathymetric data used for this study is from the National Geophysical Data Center (NGDC) now NOAA's National Centres for Environmental Information (NCEI) ETOPO1 data. This water depth field was extracted at a resolution of 0.017° × 0.017° over the mid-Atlantic Ocean (https://maps.ngdc.noaa.gov/viewers/grid-extract/index.html) (Figure 14 and 15). The subset bathymetric download or extraction can be done by using either the grid extract option in which a highlight of region of interest is done by click and drag on the interactive map (Figure 15) or manually inputting the coordinates of the region of interest as shown in the Figure 14.

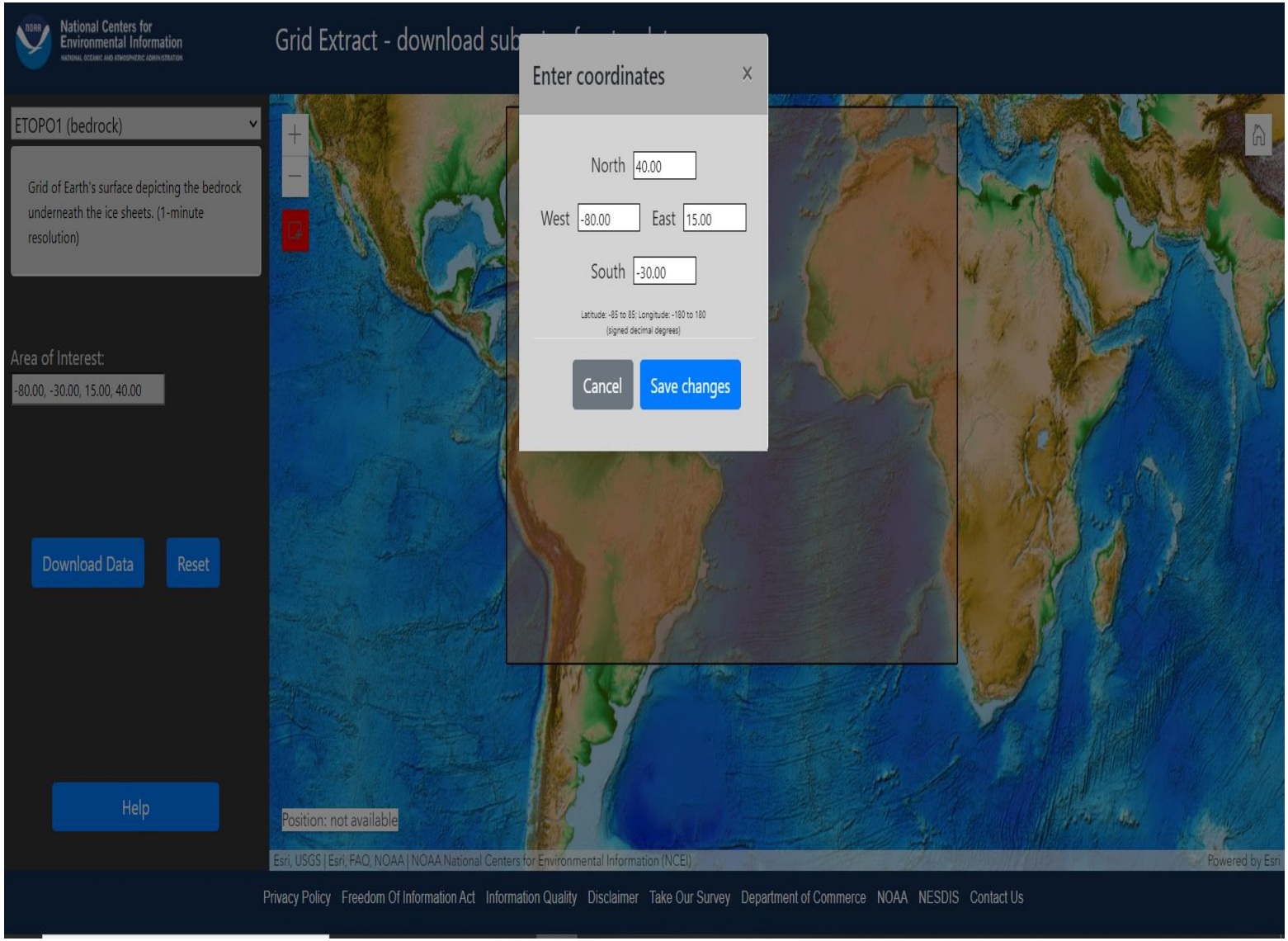

Figure 14: Manual Coordinate Input option for ETOPO1 bathymetric data extraction.

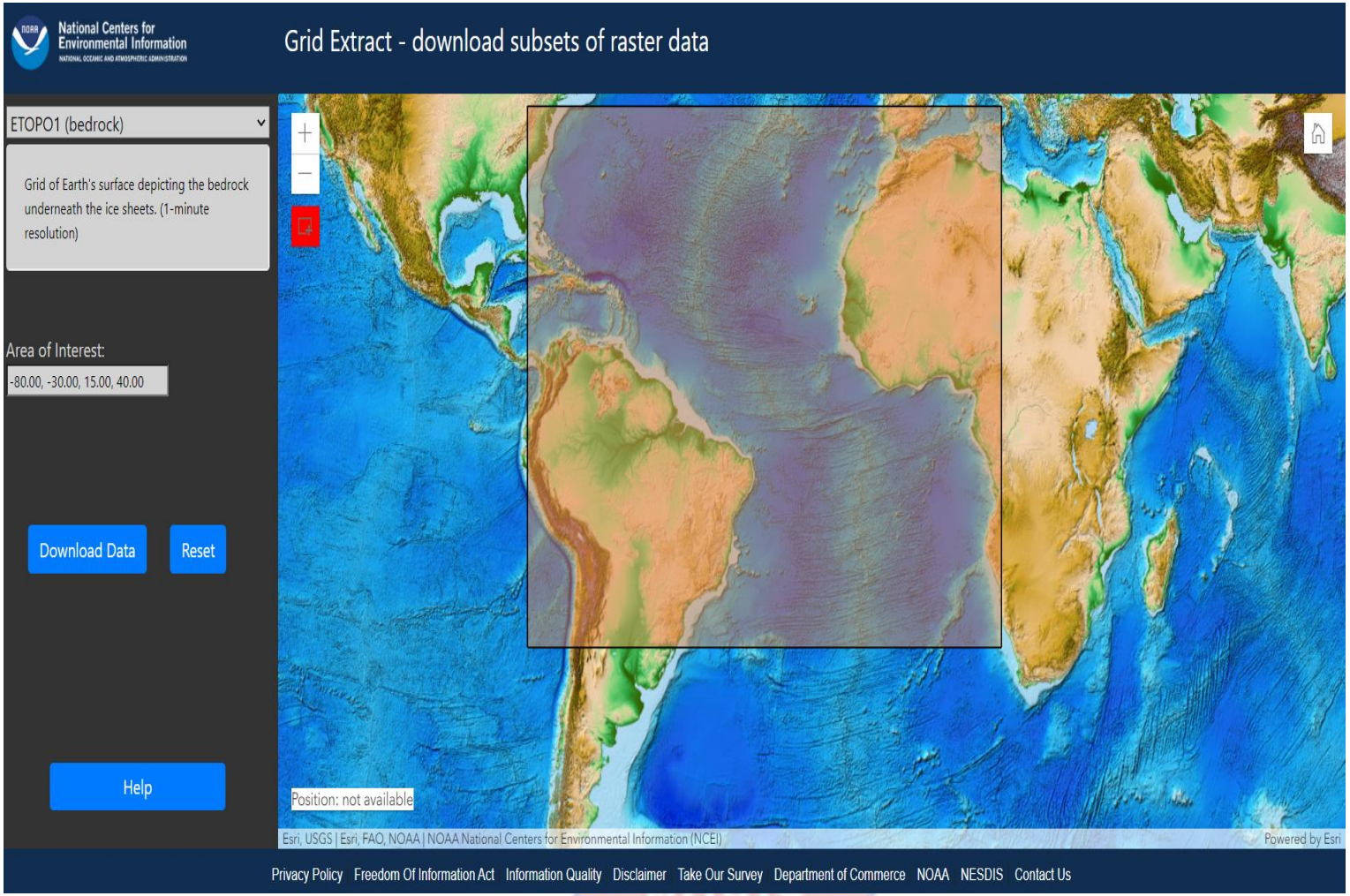

Figure 15: Grid Extract option for ETOPO1 bathymetric data extraction.

The 6-hourly reanalysis wind-fields that was used was extracted from the European Centre for Medium-Range Weather Forecasts (ECMWF) ERA5 hourly data on single level from 1979 to present dataset from 1980 to 2019 on a 0.125° x 0.125° over the mid-Atlantic (https://www.ecmwf.int/en/forecasts/datasets/reanalysis-datasets/era-5) (Hersbach, 2016).

The steps involved in this extraction are highlighted in Figures 16 - 19. The first step is to select the data type from the various data provided by ECMWF, in this case, ERA5 hourly data on single level from 1979 to present. Then the product type i.e., reanalysis followed by the variables of interest i.e., 10m u-component of wind and 10 m v-component of wind which are the zonal and meridional wind components respectively (Figure 16). After variables selection, is the selection of year, months, days and hours (Figure 17 and 18). This has to be done in batches as there is a cap on the maximum data that can be requested at a single download. The separate files were later extracted and concatenated.

After the selection of the various date and time parameters, the region of interest (whole mid-Atlantic) was selected between longitudes 60^{o}W - 15^{o}E and latitudes 20^{o}N - 10^{o}S (Figure 18). Then the file format was selected as NetCDF (Network Common Data Form) as it is a lot easier for pre-processing (Figure 19). The form is submitted for approval and provision of download link by the data provider (Figure 19).

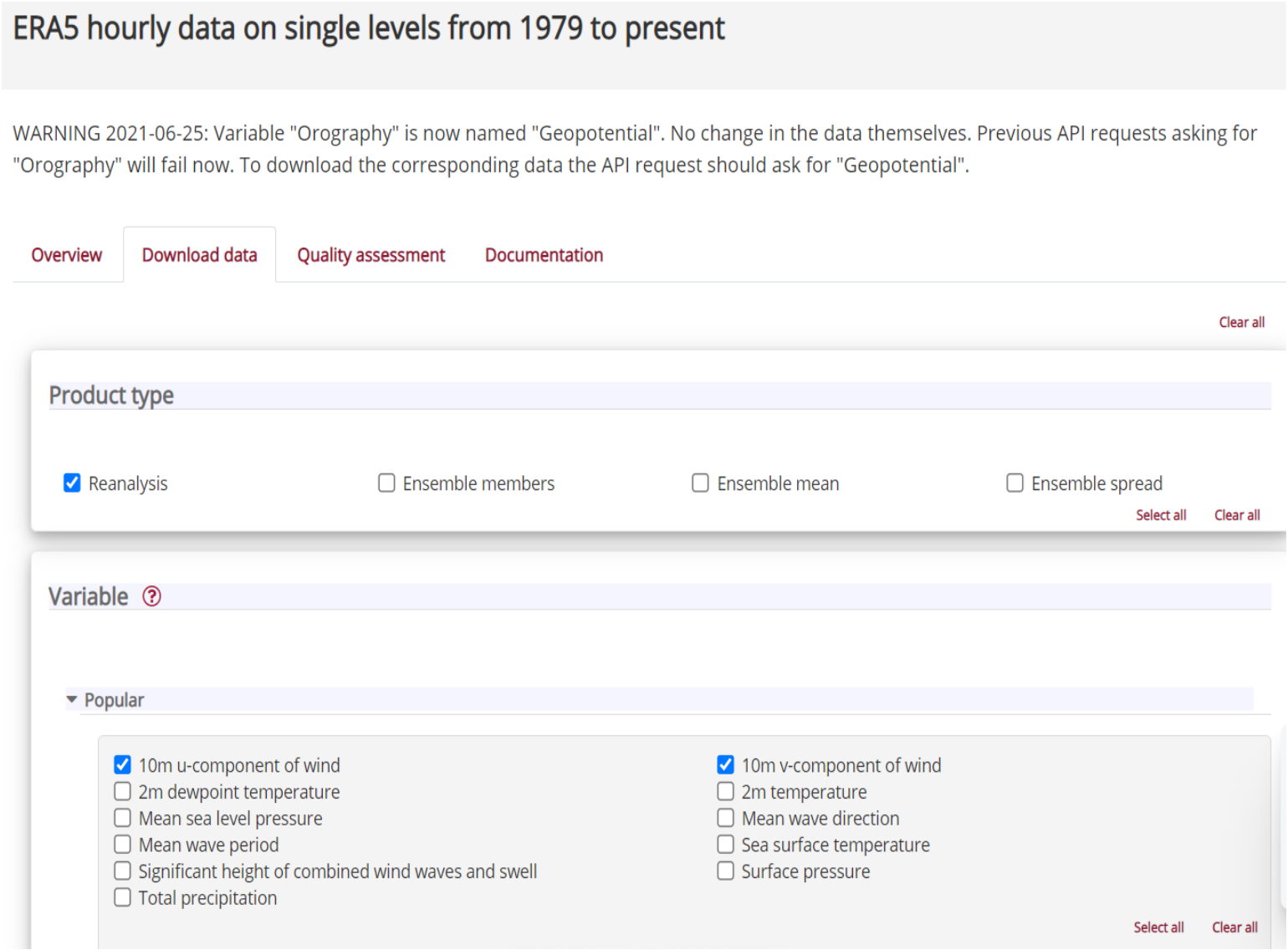

Figure 16: Product type and variables selection phase of extracting the ERA5 data.

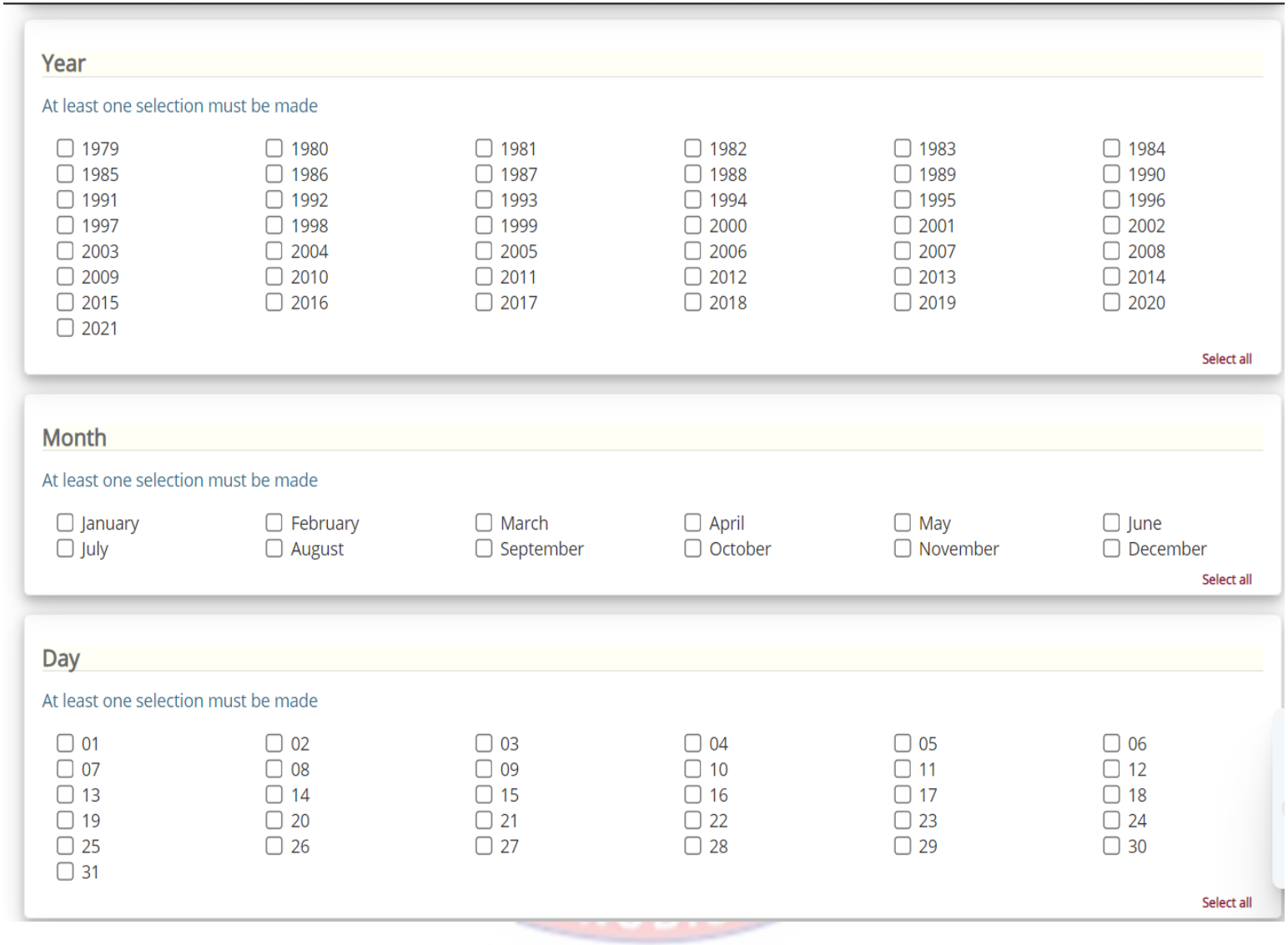

Figure 17: Date (Years, Months and Days) selection phase of extracting the ERA5 data.

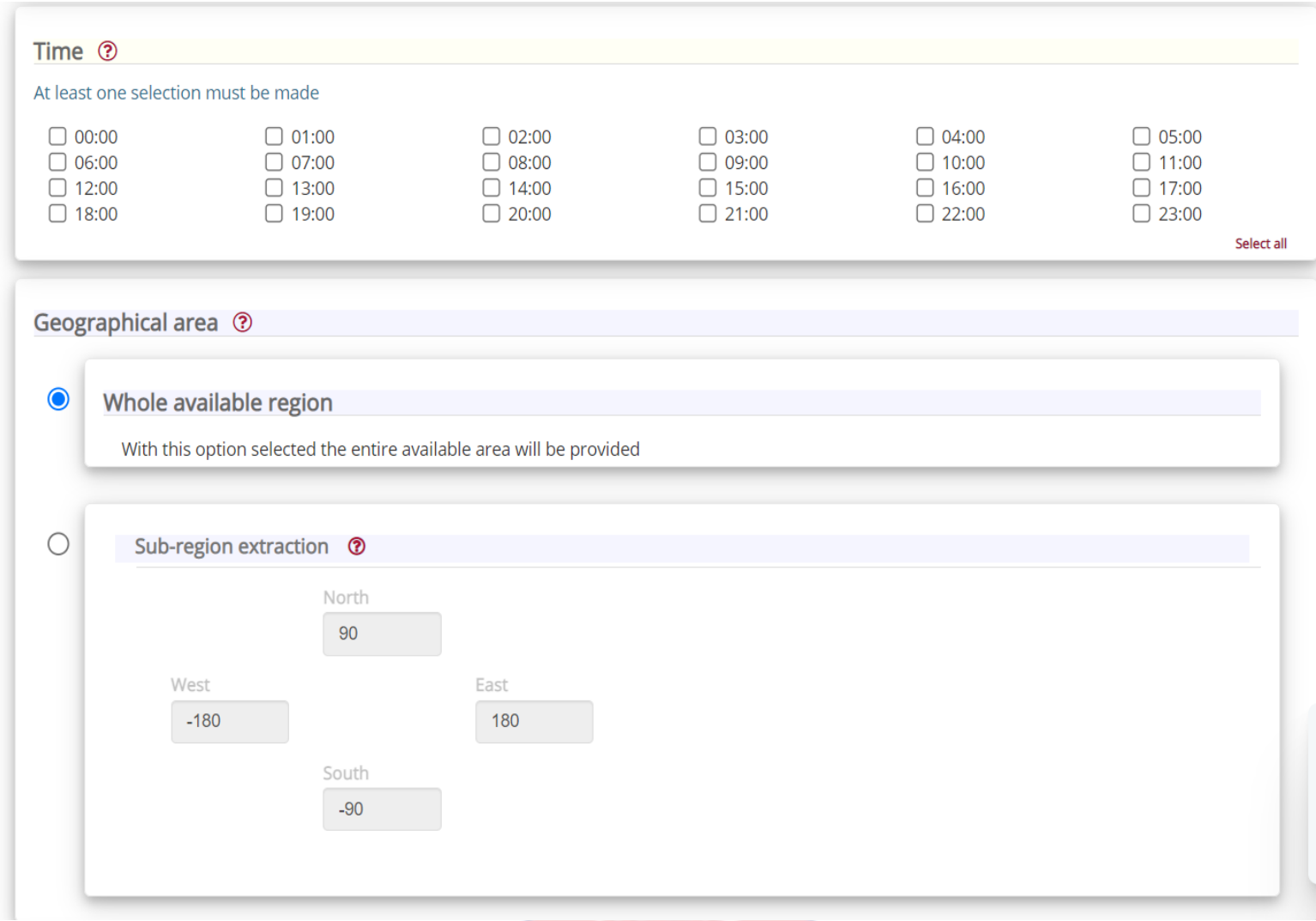

Figure 18: Time and spatial coverage (longitudinal and latitudinal coordinate) selection phase of extracting the ERA5 data.

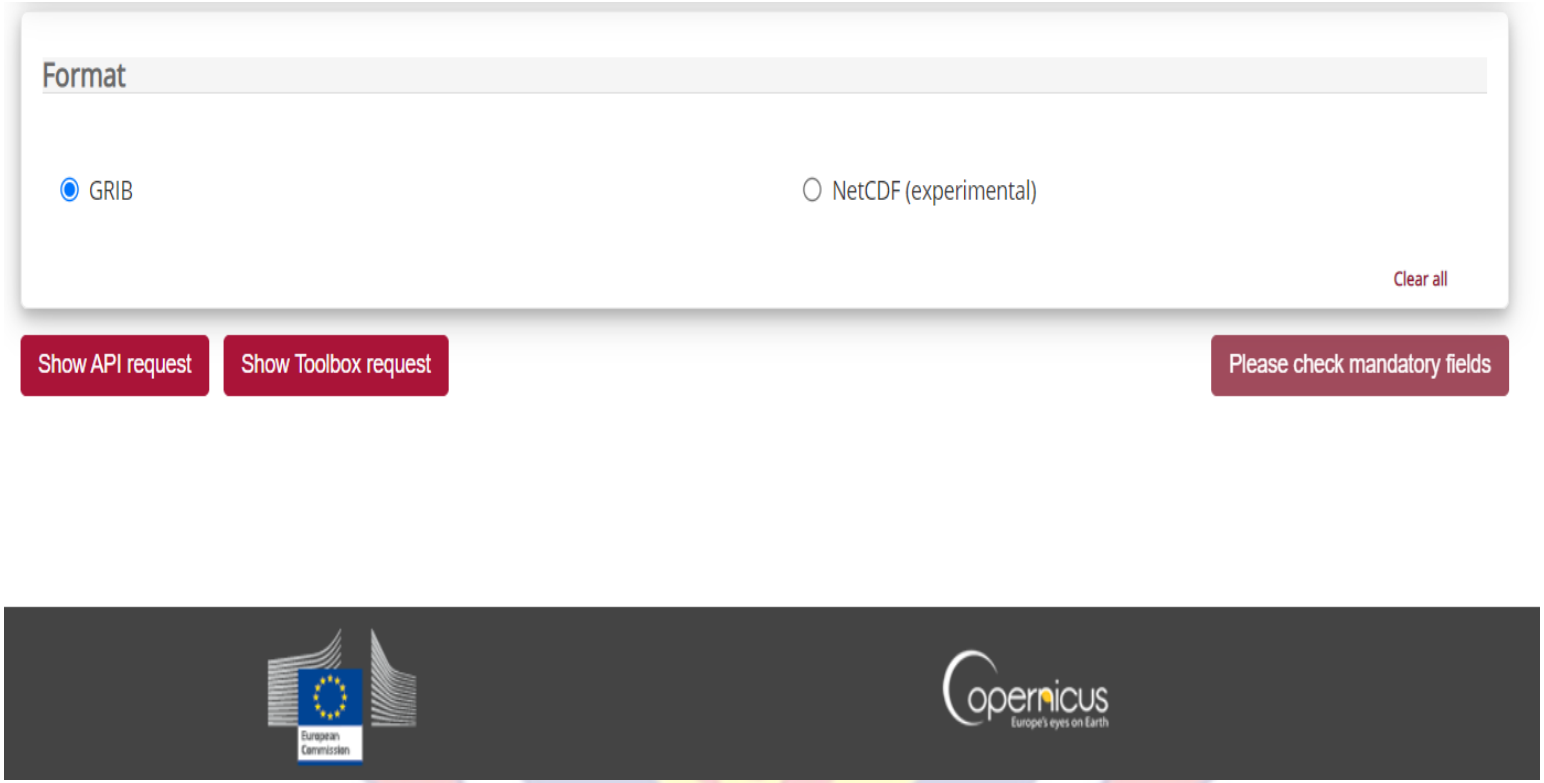

Figure 19: Data format selection phase of extracting the ERA5 data.

Input Data Pre-processing

The pre-processing was carried out using the Gridgen 3.0 packet, which is a software package that was developed for generating grids for WW3 in MATLAB for effective gridding (Chawla and Tolman, 2007). This algorithm was developed to aid accurate gridding and development of obstruction for sub-grid modelling. It also helps to reduce the number of hours that will be spent on manually generating these grids used in WW3 modelling.

Gridgen makes use of two global datasets as input files which are: (1) a high-resolution global bathymetry which is either ETOPO1 or ETOPO2 i.e., a 1 or 2 arc-min bathymetry set respectively. ETOPO1 has been chosen for this current work. (2) a high-resolution shoreline database, which has been chosen to be the MATLAB format (.mat) of **GSHHS** - **G**lobal **S**elf - consistent **H**ierarchical **H**igh - resolution **S**horeline (Wessel and Smith, 1996).

GSHHS was chosen because its polygons are able to properly define the coastal boundaries, which makes it better at resolving small islands, jetties as well as other coastal and oceanic structures. Gridgen consists of various modules, which include a grid generation module, a boundary module, a land mask module, a wet cell module, a sub-grid module and a mask modification module (Chawla and Tolman, 2007). Figure 20 shows the steps in the pre-processing done in Gridgen.

The pre-processed input files are in ASCII (American Standard Code for Information Interchange). The parameters for ETOPO1 bathymetric data are longitude, latitude and depth, while that of ERA5 wind field data are longitude, latitude, date, U10 and V10.

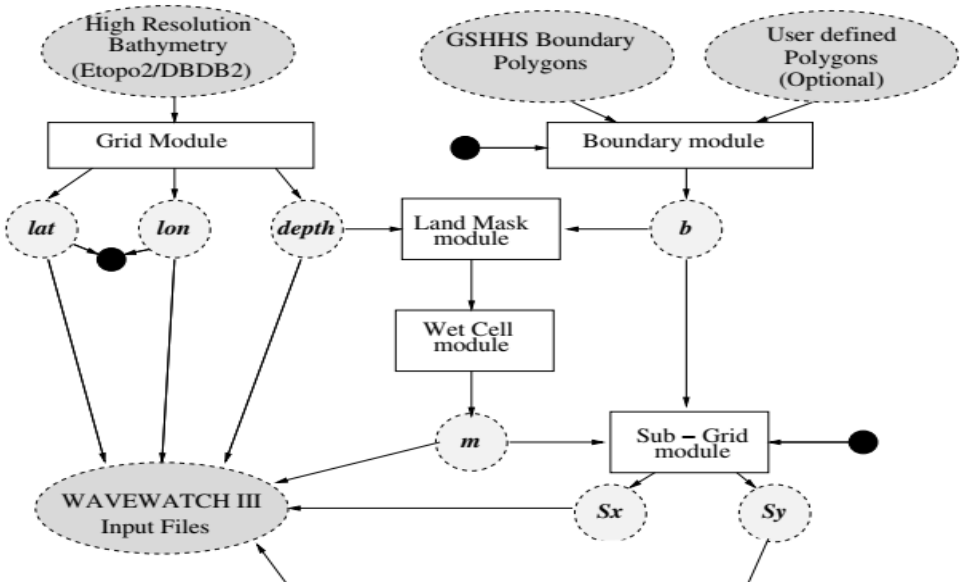

Figure 20: Flow Chart of the various modules in Gridgen (Source: Gridgen user manual, Eskeland, 1982; Steinbrenner et al., 1991).

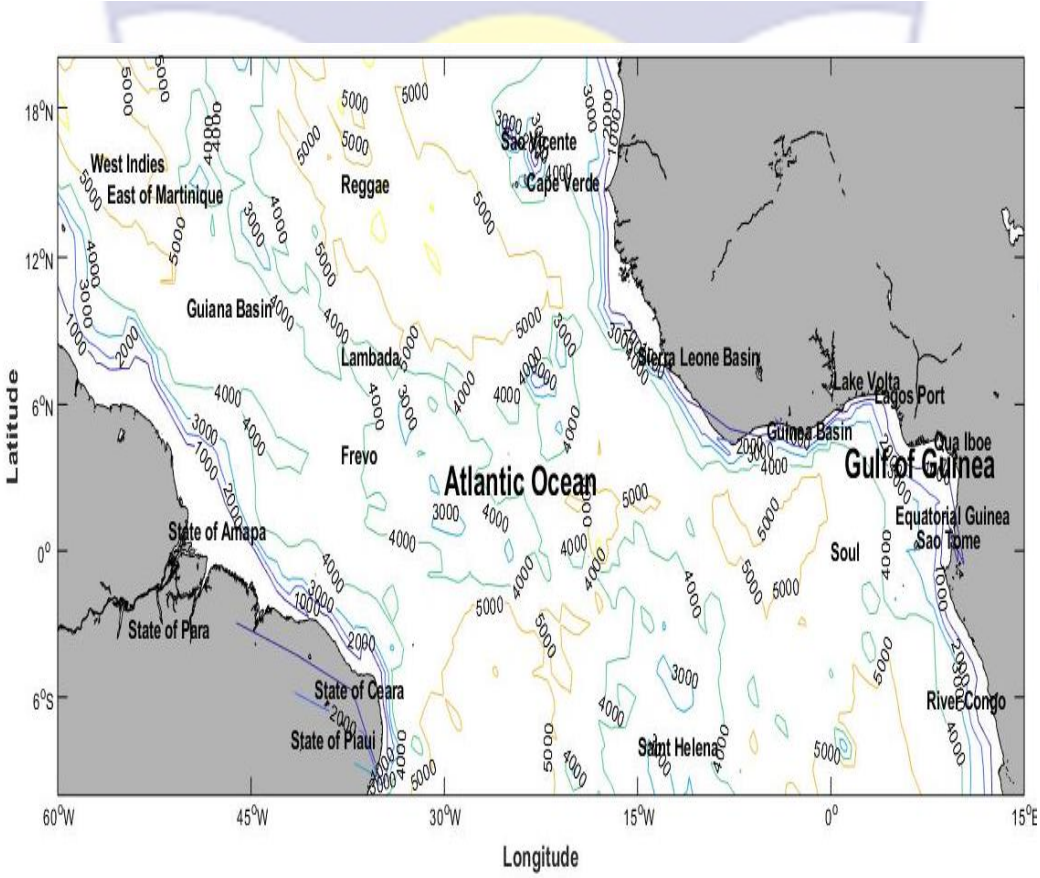

Figure 21: Map of the bathymetric data covering the mid-Atlantic used for this study.

Model Set-up

WW3 makes use of various switches to set-up the model for running. These include:

(i) ww3_grid.inp (The terrain data-related parameters are set in this file).

(ii) ww3_strt.inp (Initial conditions input file).

(iii) ww3_prep.inp (Wind field data related parameters are set in this file).

(iv) ww3_shel.inp (In this file, the start and end times, the wave parameters to be given as output, and the type of data required as output are set).

(v) Others are: ww3_outf.inp, mod_def.ww3, water-depth.dat and wind.ww3

For this study, the major set-up done in the model include setting the source terms for energy spectra to default. The model was set to integrate the spectrum to a cut-off frequency (3 Hz) and above this frequency, a parametric tail is applied (WAMDIG, 1988). The boundary condition is defined to be cyclical. The other optional settings are set to 36 directions and 24 discrete wavenumbers (0.0412–0.4060 Hz, 2.4 – 24.7 s).

The whole of the mid-Atlantic (Figure 21) was covered within the model spatial grid, including the study area in GoG with a 0.1° x 0.1° resolution. This is to enable simulation of wave condition over the selected buoy for model validation. The model, in an operational/forecasting mode, is forced with both the wind field and bathymetric data on a Gaussian grid.

Model Running

WW3 is compiled by running the following commands one after another as shown in the schematic diagram in Figure 22.

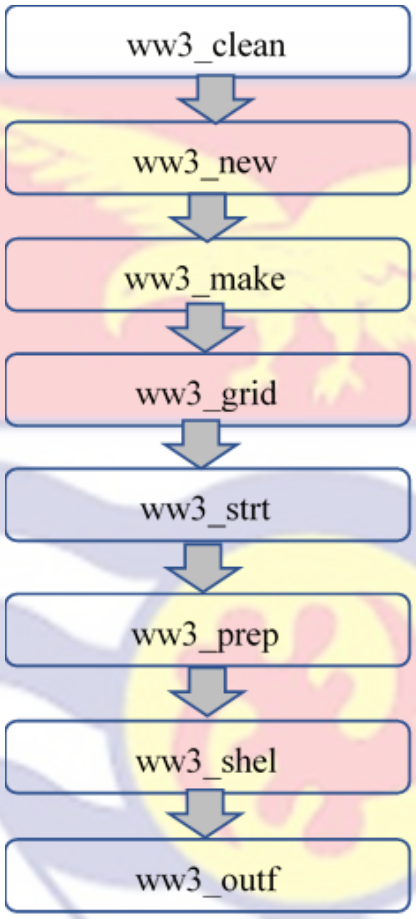

Figure 22: Schematic diagram showing the steps involved in compiling WW3 model.

Model Output

The model output is mainly 2D wave energy spectrum generated for every grid point between 1 January 1980 and 31 December 2019 every 6-hours. These outputs include wave parameters such as wave spectra, Significant Wave Height (*Hs*), mean wavelength (Ls), mean wave period (*Tm*), mean wave direction (*Dm*),

peak frequency (fp) and peak direction of which Significant Wave Height (*Hs*), mean wave period (*Tm*), mean wave direction (*Dm*) and 10 m wind speed (U10) are kept for further analysis.

Model Validation

There is a need to validate the wave climate results produced by the model (WW3) to see how well the model is able to reproduce the reality of the wave conditions (Observation/In-situ). To do this, a point validation was done using the National Data Buoy Center (NDBC) buoy data as against model data.

Comparisons between observations and simulations for significant wave height, mean wave period and wind speed for the year where observation data can be acquired (2012) were conducted. The performance of model was examined with the buoy from the US National Data Buoy Center (NDBC) for buoy 41040 located in the mid-Atlantic about 470 nautical miles East of Martinique.

The corresponding Significant Wave Height (*Hs*), mean wave period (*Tm*), mean wave direction (*Dm*) and wind speed (U10) computed by the model over the coordinates of the in-situ data was compared with observational data to see if there is a reasonable correlation between observations and simulations. The accuracy of the wind and wave parameters computed by the model was evaluated through conventional statistical analysis (Wilks, 2011) that includes calculating Correlation Coefficient (cc), Root Mean Square Error (RMSE) and Bias as used in previous studies of (Osinowo et al., 2016; Osinowo et al., 2018). These validation statistics are given by equations 8-10:

$$cc = \frac{\sum_{i-1}^{n}(x_i - \bar{x})(y_i - \bar{y})}{\sqrt{\sum_{i-1}^{n}(x_i - \bar{x})^2 \sum_{i-1}^{n}(y_i - \bar{y})^2}} \quad (8)$$

$$Bias = \bar{y} - \bar{x} \quad (9)$$

$$RMSE = \sqrt{\frac{1}{N}\sum_{i-1}^{n}(y_i - x_i)^2} \quad (10)$$

where, x_i represents the buoy data, y_i represents the model data, $\bar{x}$ and $\bar{y}$ are mean values of buoy and model data, N is the total number of observations.

Intercomparison of WW3 and other Wave Databases

A spatial validation was done against other wave model databases like ERA5 from ECMWF and MFWAM from Copernicus Marine Environment Monitoring Service (CMEMS) wave databases in form of intercomparison of their performance using WW3 as reference.

The **GLOBAL_REANALYSIS_WAV_001_032** also referred to as WAVERYS under some other wave modelling projects was used in this intercomparison. It is a globally available reanalysis describing the sea conditions from January, 1993 to December, 2019. The product is produced using Meteo France WAve Model (MFWAM) which is a third-generation model run on a spatial resolution of 0.2^o x 0.2^o and temporal resolution of 3-hourly. The details of the model algorithm, forcings (Atmospheric, Current, Bathymetry), initial conditions, assimilation approach and assimilated data are given by Chune et al. (2019).

Another globally available database used was the ECMWF ERA5 wave database named **ERA5 hourly data on single levels from 1979 to present** which is the 5th generation wave reanalysis data replacing ERA-Interim. As a reanalysis, this product makes use of both model and observation data through data assimilation. This approach is done by regularly adding observation data to model data called analysis to produce a reanalysis every few hours. This leads to improvement in the output as the reanalysis is forced to conform to observation as best as possible. The past, present and future projects for ERA5 is given at https://confluence.ecmwf.int/display/CKB/ERA5%3A+data+documentation (Hersbach, 2016; Hersbach et al., 2020).

The Taylor and Target diagrams are ways to diagrammatically give summary of how similar models are to one another in reference to a particular model or observation (Taylor, 2001). This closeness between different models is measured based on their coefficient of correlation (cc), centred root-mean-square difference (CRMSD) and standard deviations (SD). The usefulness of these diagrams has been confirmed in effectively assessing different aspects of complex models and estimating the comparative reliability and performance skill of different models (IPCC, 2001).

The three various statistics i.e., cc, CRMSD and SD can be shown at the same time on the 2D-space of the Taylor diagram because these different statistics are inter-dependent as shown by the following equations 11 - 16:

$$E'^2=\sigma_f^2+\sigma_r^2-2\sigma_f\sigma_r R \quad (11)$$

$$R=\frac{\frac{1}{N}\sum_{n=1}^{N}(f_n-\bar{f})(r_n-\bar{r})}{\sigma_f\sigma_r} \quad (12)$$

$$E'^2=\frac{1}{N}\sum_{n=1}^{N}\left[\left(f_n-\bar{f}\right)-(r_n-\bar{r})\right]^2 \quad (13)$$

$$\sigma^2{}_f=\frac{1}{N}\sum_{n=1}^{N}(f_n-\bar{f})^2 \quad (14)$$

$$\sigma^2{}_r=\frac{1}{N}\sum_{n=1}^{N}(r_n-\bar{r})^2 \quad (15)$$

$$\text{Bias}=\frac{1}{N}\sum_{n=1}^{N}(f_n-r_n) \quad (16)$$

where **R** stands for the **cc**, **E'** represents the **CRMSD** and $\boldsymbol{\sigma_f}$ and $\boldsymbol{\sigma_r}$ are the variances between the WW3 (reference data) and other models (ERA5 and MFWAM) with values $\mathbf{f_n}$ and $\mathbf{r_n}$, respectively.

Data Analysis

MATLAB version R2019a was used to write the algorithms (codes) developed for the analysis in this study in producing regional maps showing trends of the *Hs*, *Tm*, *Dm* and wind speed (U10) on monthly, annual, decadal and seasonal basis. Statistical tests for checking equality of means were done for ENSO/NAO influenced periods preceding or following years with these oceanic phenomena. Coastal structures influence were checked in periods preceding and following their constructions based on equality of mean test that was done.

One-way ANOVA was used to check for the trends of wave climate by testing for equality of means on yearly, seasonal and decadal basis and Tukey honesty significant difference was used to ascertain the particular mean that is different where applicable. The results are all presented in chapter four.

The spatial resolution used for the model produced 1569 longitudinal and latitudinal data points for *Hs, Tm* and 10 m wind speed (U10) for the entire mid-Atlantic Ocean. Since the model outputs data every six hours meaning it produces four data per point in a day. It is expected that this will amount to 365 (366) times four giving 1460 (1464) for normal years (leap years), respectively. Between 1980-2019, there are a total of ten leap years: 1980, 1984, 1988, 1992, 1996, 2000, 2004, 2008, 2012 and 2016. This gives a total of thirty normal years which makes the number of data points for the study duration to be (365 x 4 x 30) + (366 x 4 x 10) = 58440. The MATLAB algorithms written for this work treat these data points as matrices of dimensions 58440 x 1569 except for the wave direction which has dimension of 58440 x 3904. Upon restriction to Gulf of Guinea, 457 grid points were captured for analysis.

Chapter Summary

The modelling techniques employed in this research, as well as the study area have been thoroughly described in this chapter. The various validation statistics and database intercomparison applied as well as the software employed for the data analysis have all been discussed in this chapter.

CHAPTER FOUR

RESULTS AND DISCUSSION

In this chapter, the results from the assessment of the wave parameters in GoG will be presented and discussed. The nature of the wave climate under various return periods using the Gumbel analysis approach will also be presented.

Model Validation Statistics

Comparisons of wave and wind parameters obtained from observations and simulations carried out for period spanning 01-January-2012 to 08-November-2012 are shown in the Figures 23 - 28. As seen in Figures 24, 26 and 28, which are presented after each time-series plots for *Hs*, *Tm* and U10 respectively, it is obvious that the wave and wind parameters simulated by the model and observations from buoy are highly correlated with the correlation coefficient (cc) higher than 0.8 for *Hs*, *Tm* and U10. Also, the mean bias error (MBE) computed for these parameters is low with values of 0.094 m for *Hs*, 1.2722 ms^{-1} for U10 and 1.2804 s for *Tm*, which showed that the model outputs are a little lower than observational data from buoy. Likewise, the root mean square error (RMSE) of the comparison is generally low ranging from 0.221 m for *Hs*, 0.5509 ms^{-1} for U10 to 1.3608 s for *Tm*.

The fitted linear regression lines in Figures 24, 26 and 28 are the identity lines (1:1 lines), which represents the line on which the difference between the simulated and observed data is zero. It shows the level of underestimation or overestimation of the model compared to observation data. In general, the model

was able to reproduce a real-time data, making WW3 a useful tool for producing surface waves in general in the GoG.

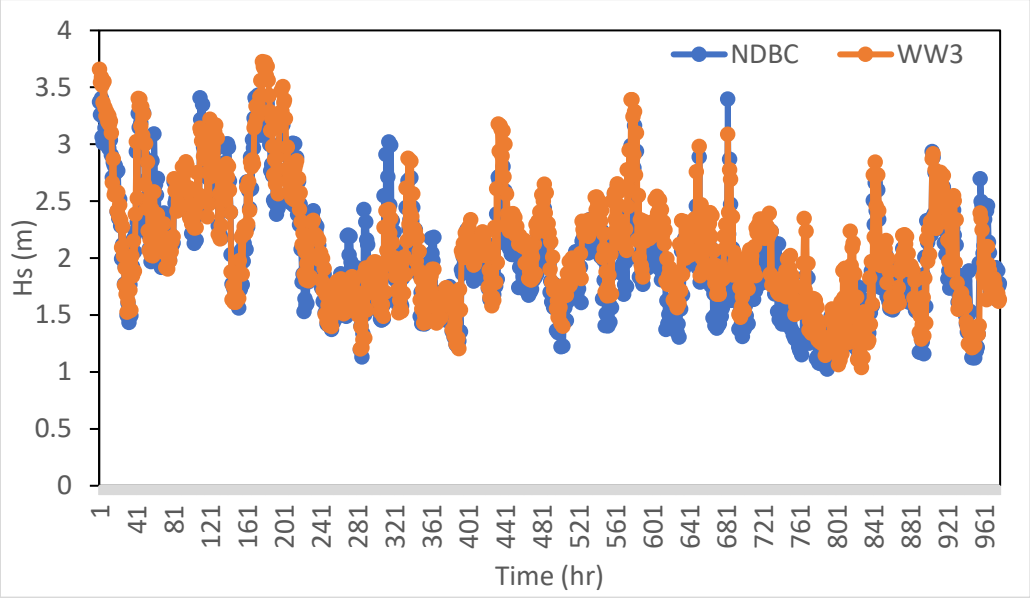

Figure 23: Time-series of *Hs* for NDBC and WW3.

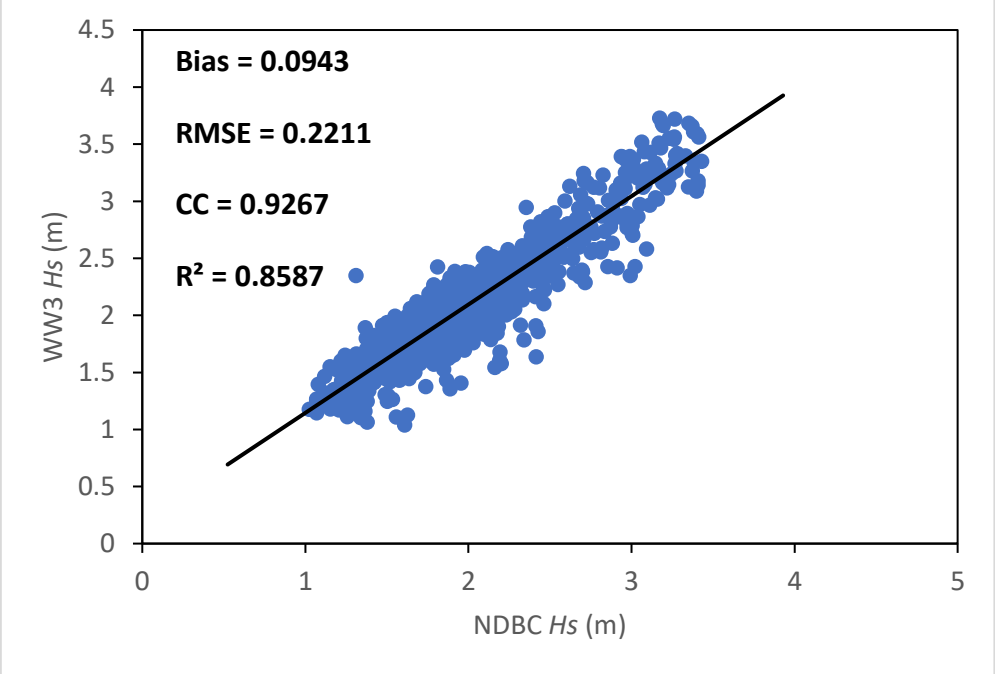

Figure 24: Comparison (Scatter Plots) of *Hs* for NDBC and WW3.

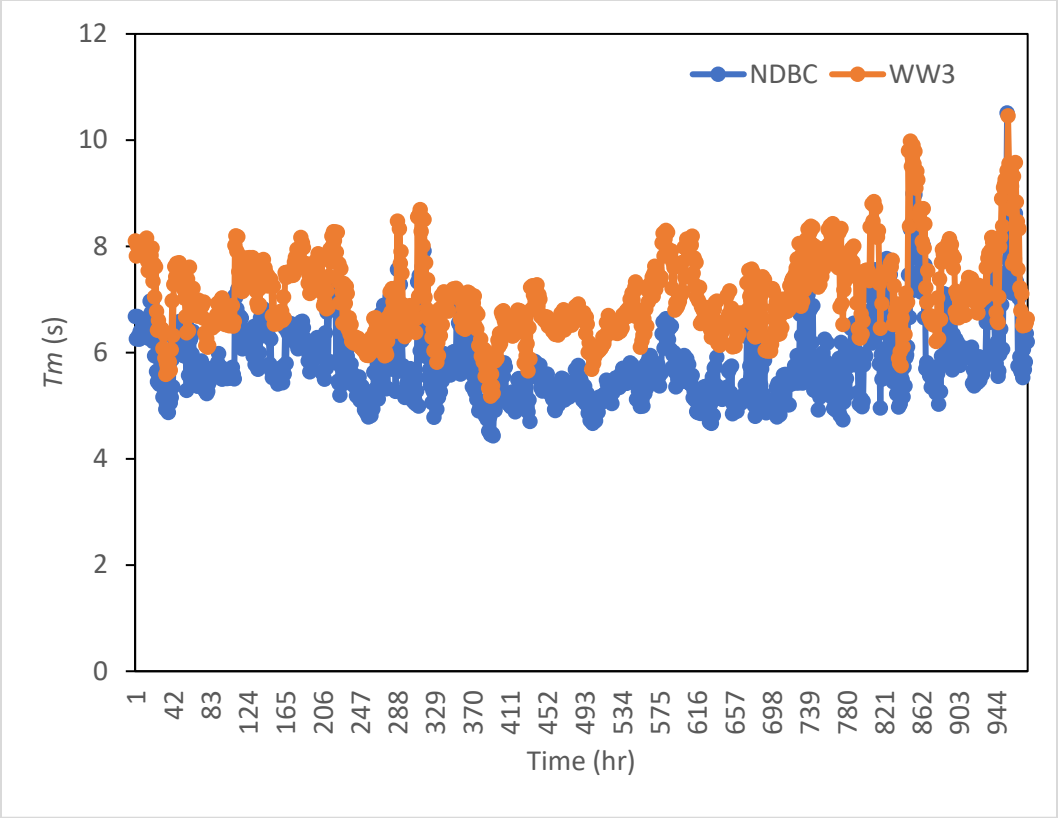

Figure 25: Time-series of *Tm* for NDBC and WW3.

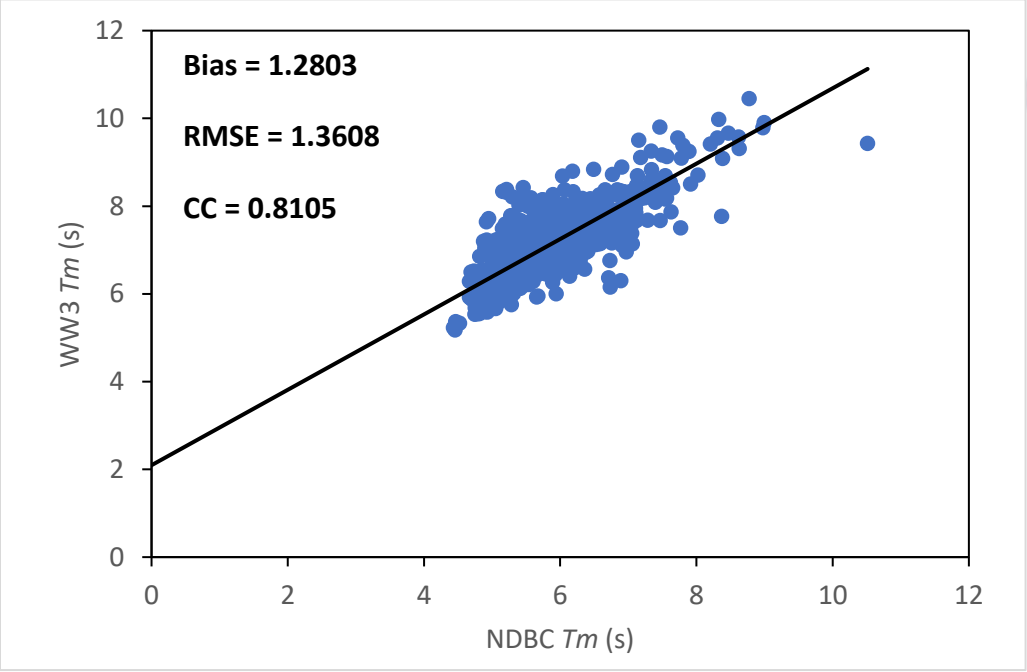

Figure 26: Comparison (Scatter Plots) of *Tm* for NDBC and WW3.

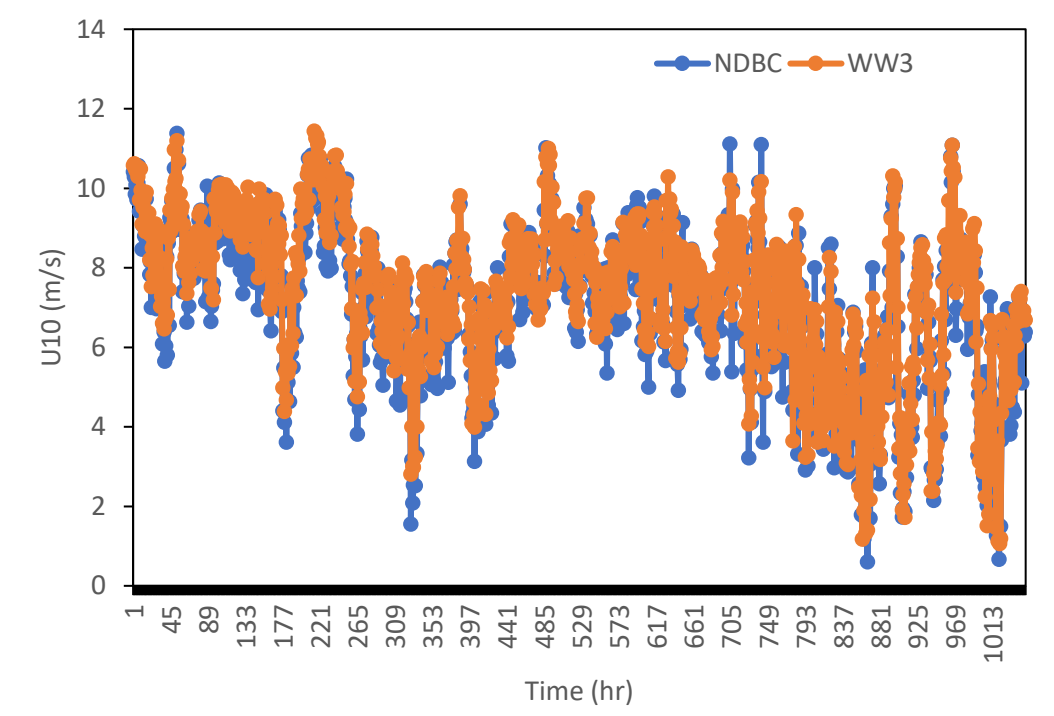

Figure 27: Time-series of U10 for NDBC and WW3.

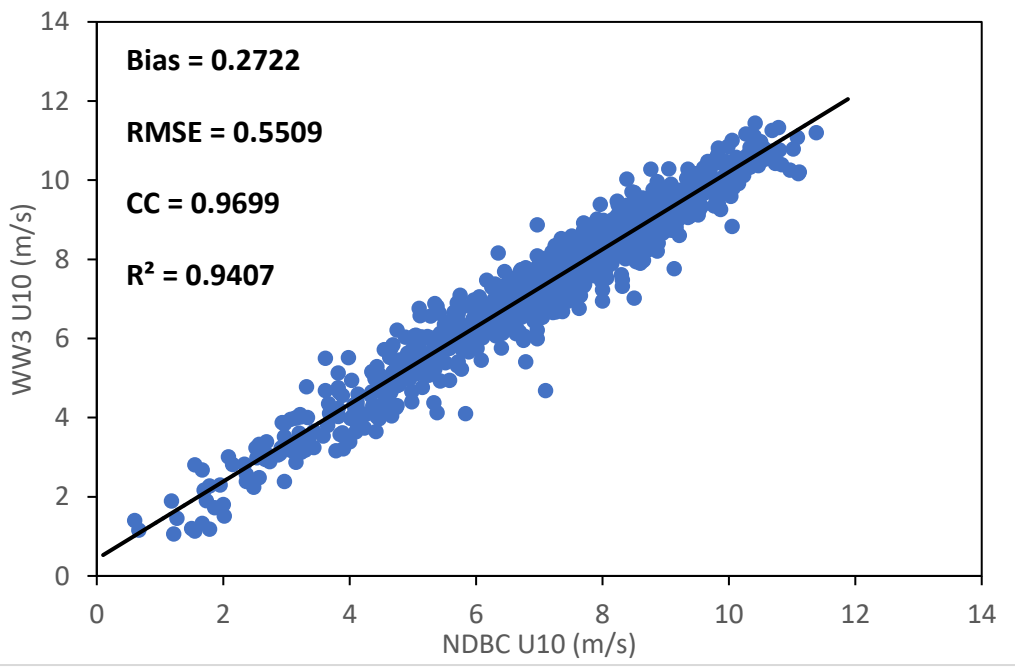

Figure 28: Comparison (Scatter Plots) of U10 for NDBC and WW3.

Intercomparison of Database

To access the agreement between WW3 and other globally available database popularly used for studies in GoG i.e., ERA5 and MFWAM, an intercomparison was done. The results of the validations done against MFWAM and ERA5 are shown in Figures 29 - 34. The time-series and statistics shown by Figures 29 - 32 show that both ERA5 and MFWAM have similar trend with WW3. It can be observed that both MFWAM and ERA5 generally overestimate the *Hs* values in comparison with WW3. The statistics summarized in Table 1 is also confirmed through the bias of -0.42048 m and -0.41668 m for ERA5 and MFWAM, respectively. These bias values have magnitudes that are relatively high when compared with the bias of 0.094311 m between WW3 and NDBC.

A relatively high correlation higher than 0.7 was shown by both ERA5 and MFWAM though this is also less than a value higher than 0.9 shown by WW3 and NDBC. All these results including a lower root-mean-square error between observation and WW3 compared to other models confirms the better performance of WW3 in GoG. This is most likely due to the finer resolution of WW3 compared to other models. This is further proven by the better performance of MFWAM, which has a spatial resolution of 0.2^o x 0.2^o and temporal resolution of 3-hourly compared to ERA5 with 0.5^o x 0.5^o and 6-hourly respectively. These results confirm that the higher the spatio-temporal resolution of a model, the better the chance of performing well.

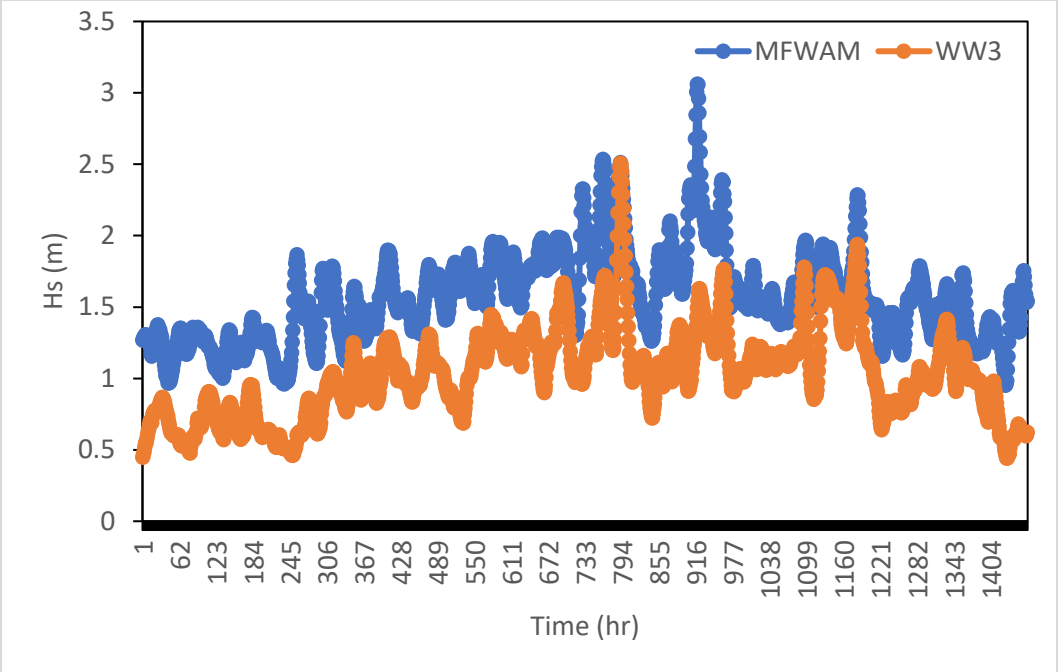

Figure 29: Time-series of *Hs* for MFWAM and WW3.

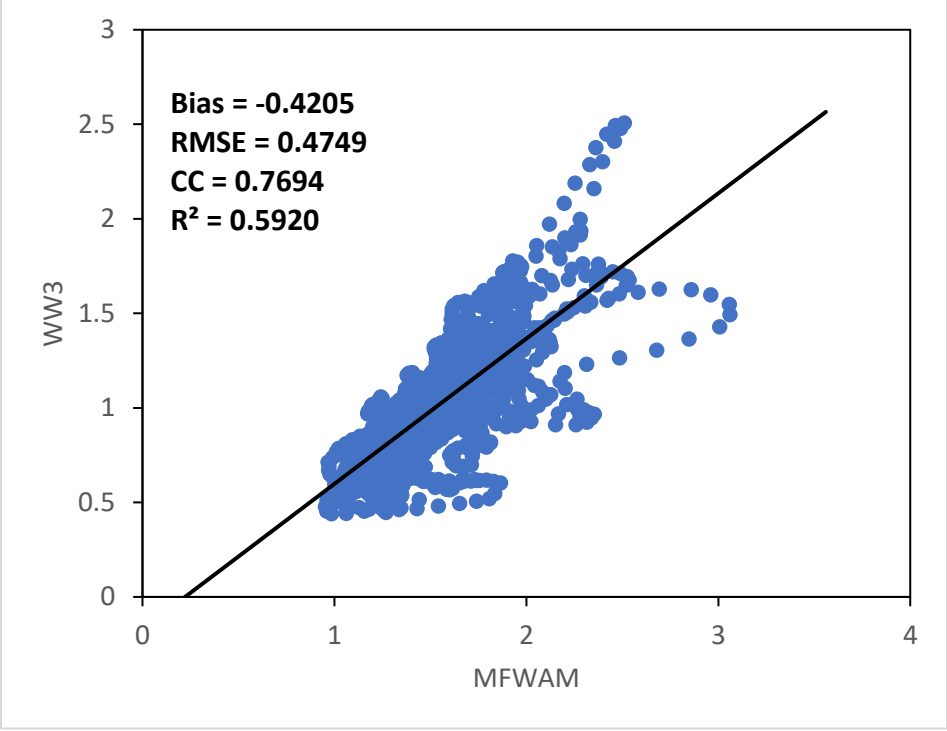

Figure 30: Comparison (Scatter Plots) of *Hs* for MFWAM and WW3.

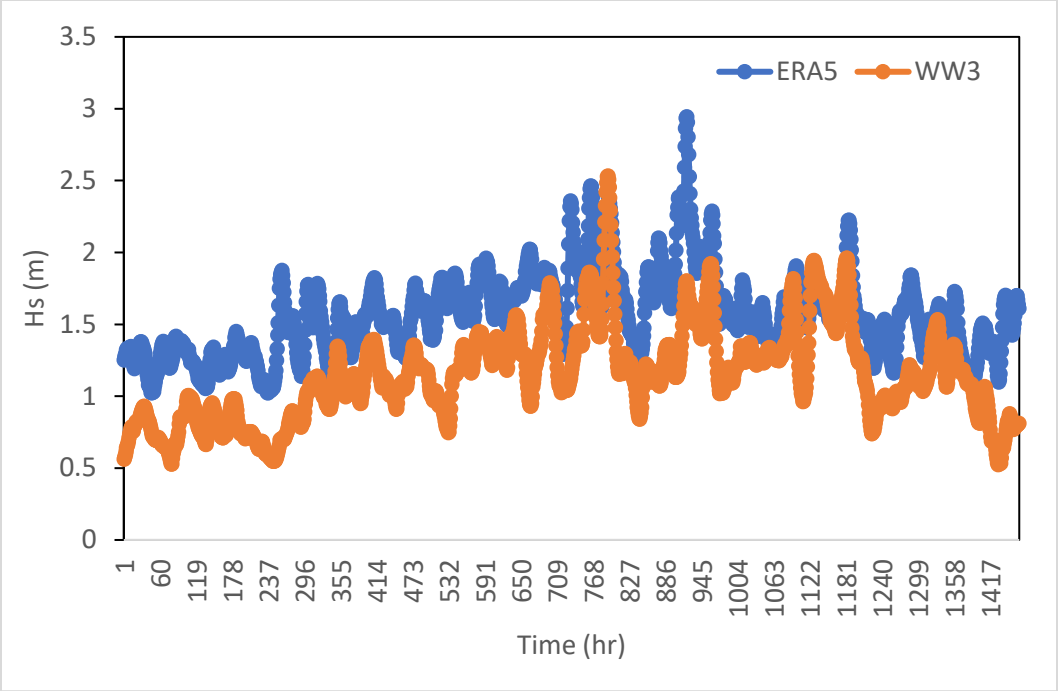

Figure 31: Time-series of *Hs* for ERA5 and WW3.

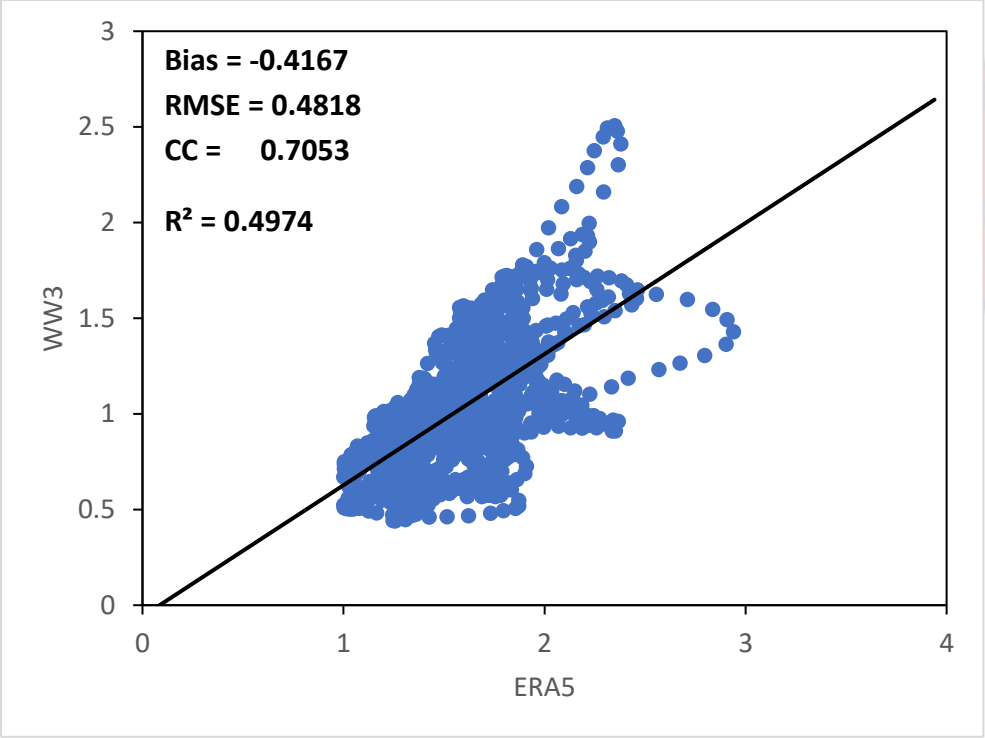

Figure 32: Comparison (Scatter Plots) of *Hs* for ERA5 and WW3.

Table 1: Summary of Validation Statistics for *Hs*

Source	Bias (m)	RMSE (m)	CC	R^2
WW3/NDBC	0.094311	0.220917	0.926671	0.858719
WW3/WFWAM	-0.42048	0.474921	0.769445	0.592046
WW3/ERA-5	-0.41668	0.481816	0.70527	0.497406

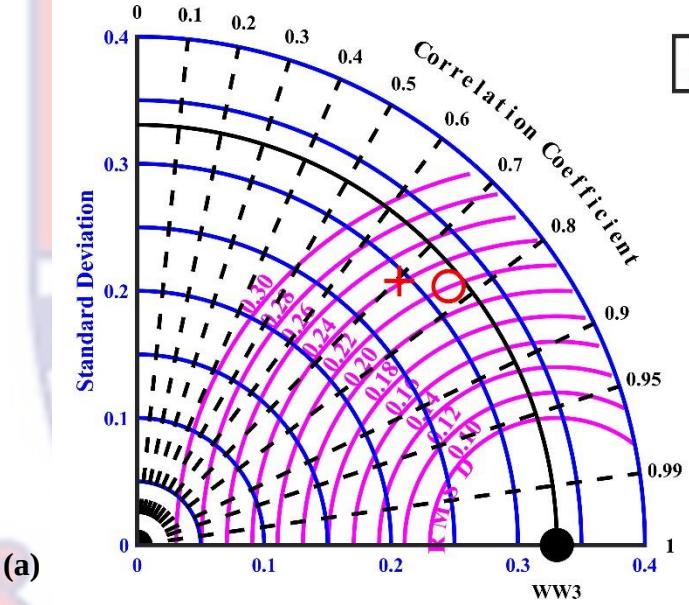

(a)

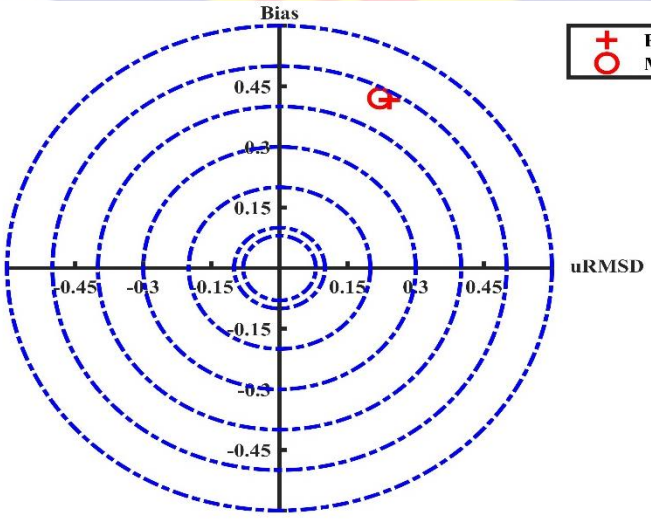

(b)

Figure 33: Comparison of WW3 with ERA5 and MFWAM databases using (a) Taylor diagram and (b) Target diagram.

The CRMSD is represented by the magenta-coloured contours in Figure 33(a) and it is estimated as the difference between the WW3 and other models. It is the same as the distance of the marker denoting the models to point on the x-axis marked **WW3**. The RMSD is close to 0.22 m for MFWAM and 0.24 m for ERA5. The SD of the models is shown by the radial distance from the origin by the blue arcs and black arc for WW3. The SD for both ERA5 and MFWAM is less than that of WW3 as seen in Figure 33(a). Both ERA5 and MFWAM also have relatively high correlation between 0.7-0.8 as shown by the radial dotted black lines in Figure 33(a). The bias as shown by Figure 33(b) depicts similar values for the two databases considered.

The error metrics shown by the comparisons as summarized in the Table 1 confirm that they all follow similar trends, though the NDBC observation (Figures 23, 25 and 27) shows a better overlap than the two other models i.e., MFWAM (Figure 29) and ERA5 (Figure 31). It can be seen that the other models give Significant Wave Height values that are higher than that of WW3. The other validation parameters i.e., Bias, Root Mean Square Error (RMSE), Correlation Coefficient (cc) and R-Squared, which is the square of cc, all show values comparable to other previous studies like (Osinowo et al., 2016; Osinowo et al., 2018).

To see the overestimation observed in the MFWAM and ERA5, a spatial distribution of bias shown in the colour maps was produced. In Figure 34, higher values of bias can be seen closer to the coast meaning that the differences WW3 dataset and both ERA5 and MFWAM datasets are more pronounced in the coastal

area than offshore. This can be explained by the inefficiency of these globally available databases to properly resolve bathymetry close to the coast due to the spatial resolution on which they are run, which is coarser than the WW3 used for this study. This can be confirmed especially close to small islands, which are captured around latitudes 0°-4°N and longitudes 6°E-12°E (Figures 34(a) and (b)).

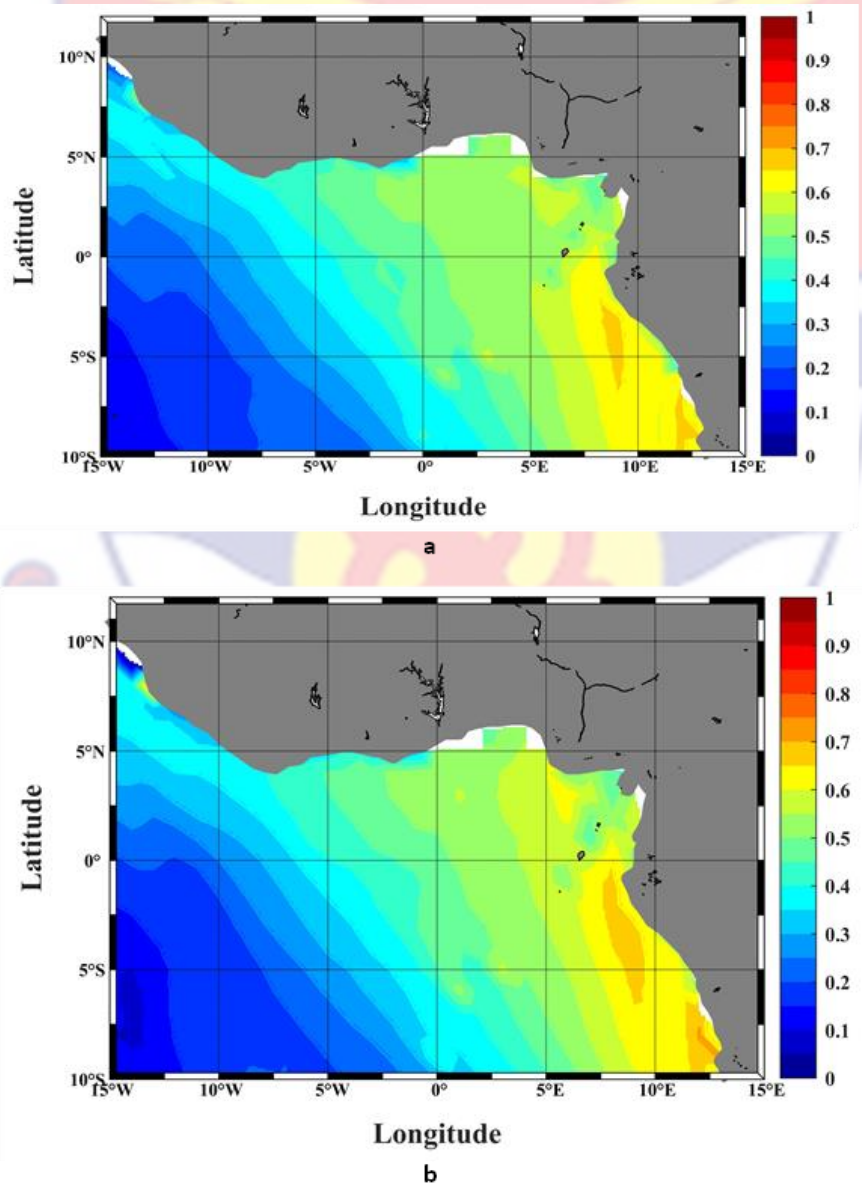

Figure 34: Regional distribution of bias for (a) MFWAM-WW3 (b) ERA-Interim-WW3.

Significant Wave Height (*Hs*)

Annual and Seasonal Analysis

The overall mean of the *Hs* at each grid point between 1980 and 2019 is shown in the map in Figure 35, which shows that during the period covered the average Significant wave heights close to the coast of GoG generally range between 0.2 m and 1.0 m. The average *Hs* for the region shown in the spatial distribution is 1.0836 m. From the spatial distribution shown in Figure 35, it can be confirmed that waves of higher *Hs* are observed farther from the coast i.e., *Hs* decreases coastwards. It can also be deduced that the GoG region has very uniform wave condition except around Niger Delta in Nigeria, where relatively lower wave are seen compared to those observed from Cape Palmas through Ivory Coast, Ghana, Togo, Benin to the south-western part of Nigeria.

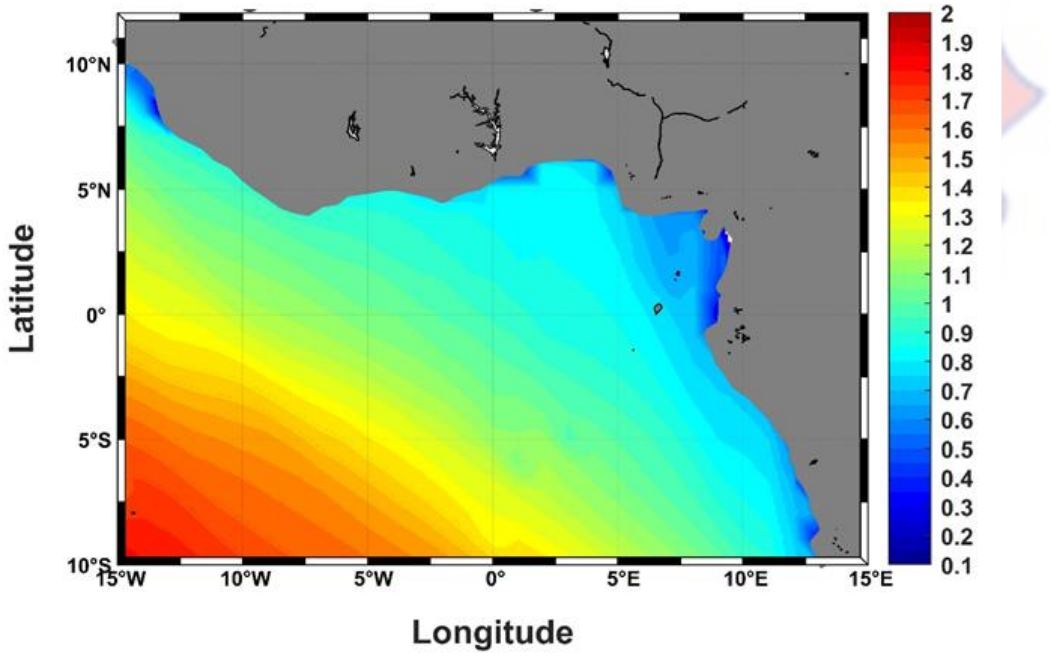

Figure 35: Regional distribution of the mean *Hs* in GoG between 1980-2019.

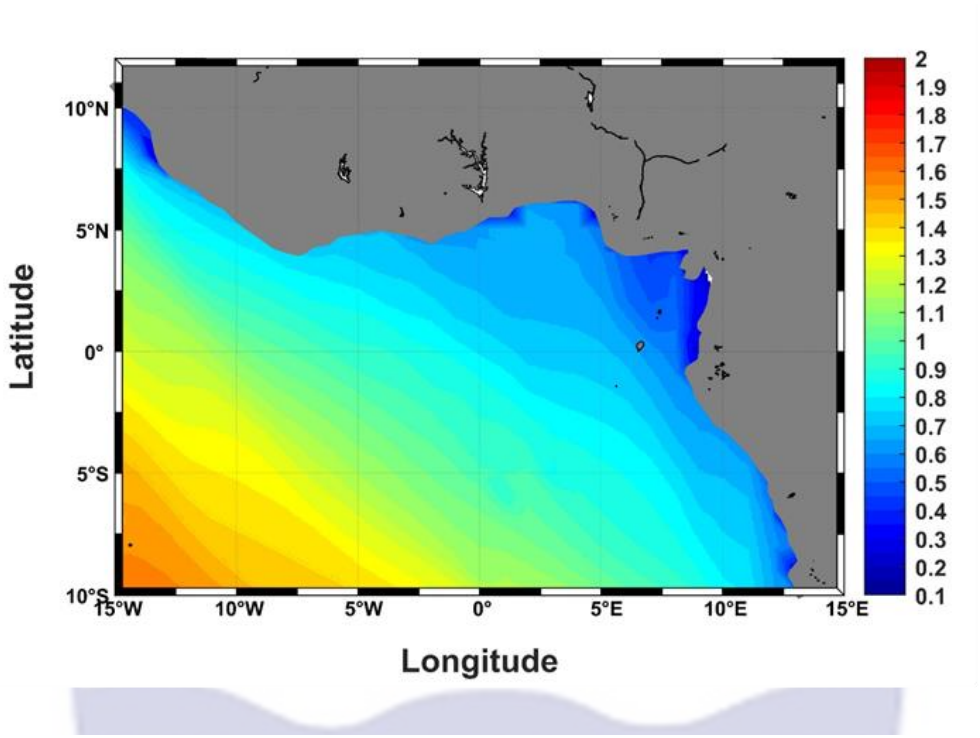

Figure 36: Regional distribution of the mean *Hs* in GoG during winter between 1980-2019

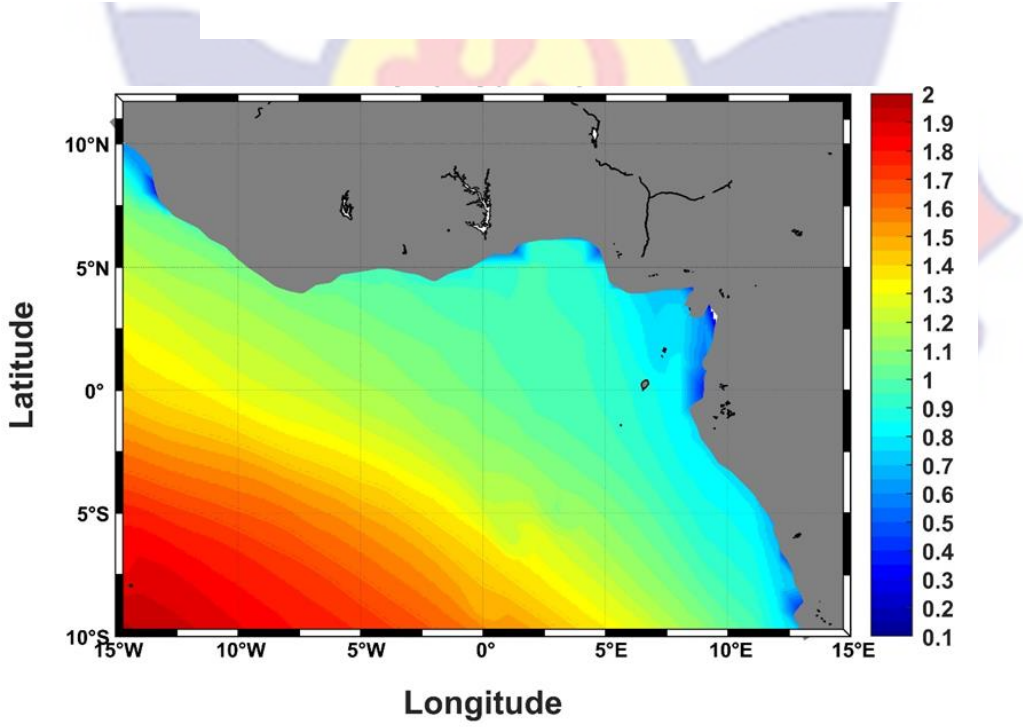

Figure 37: Regional distribution of the mean *Hs* in GoG during summer between 1980-2019.

The seasons for this study are according to the boreal season, which has boreal winter (dry season) and boreal summer (rainy season). The boreal winter defined for this study covered a total of five months, which includes the months of November, December, January, February, and March, while months in boreal summer covered a total of seven months which are April, May, June, July, August, September and October.

The mean of the seasonal distribution of *Hs* in GoG for Winter and summer between 1980-2019 are shown by the maps in Figures 36 and 37 respectively. It can be observed from these Figures that higher waves are found in the coast of GoG during summer than in winter. The average *Hs* for winter was found to be 0.9312 m, while that of summer was calculated as 1.1913 m.

For a clearer understanding of the emergence of variations within the seasons, *Hs* distributions between April and May mark the beginning of summer, June-August represent the maximum of summer variation and September-October signify the fading period of summer influence. Likewise for winter, October-November stand for the beginning of winter, December-February mark the maximum of winter variation and March-April denotes the fading period of winter influence.

Monthly Analysis

Data for every month were grouped together and averaged between 1980-2019 and the resulting spatial distribution of *Hs* in GoG are shown in the subplot regional maps in Figure 38 and the average values are summarized in Table 2. Maps showing bigger versions for each month are presented in Appendix A.

Table 2: Monthly averages of significant wave height (*Hs*)

Month	Average *Hs* (m)
January	0.8392
February	0.8368
March	0.9437
April	1.0912
May	1.1671
June	1.2174
July	1.2645
August	1.2474
September	1.1894
October	1.1603
November	1.0855
December	0.9477

The average of *Hs* on monthly basis is as shown in Table 2. These results which confirm the result shown by the seasonal analysis show that *Hs* on average starts increasing in April-May marking the onset of summer, the reduction starting from August which marks the transition from summer to winter and the winter months are observed to have generally low average *Hs* with even most less than 1.0 m starting from December-March.

The general uniform wave conditions shown by the annual average *Hs* distribution can be observed not to be throughout the year as shown by some months in Figure 38. This non-uniformity is seen mostly at the peak of summer between June and August when relatively higher waves are seen closer to the coast in the westernmost part of the GoG compared to the eastern parts toward Nigeria.

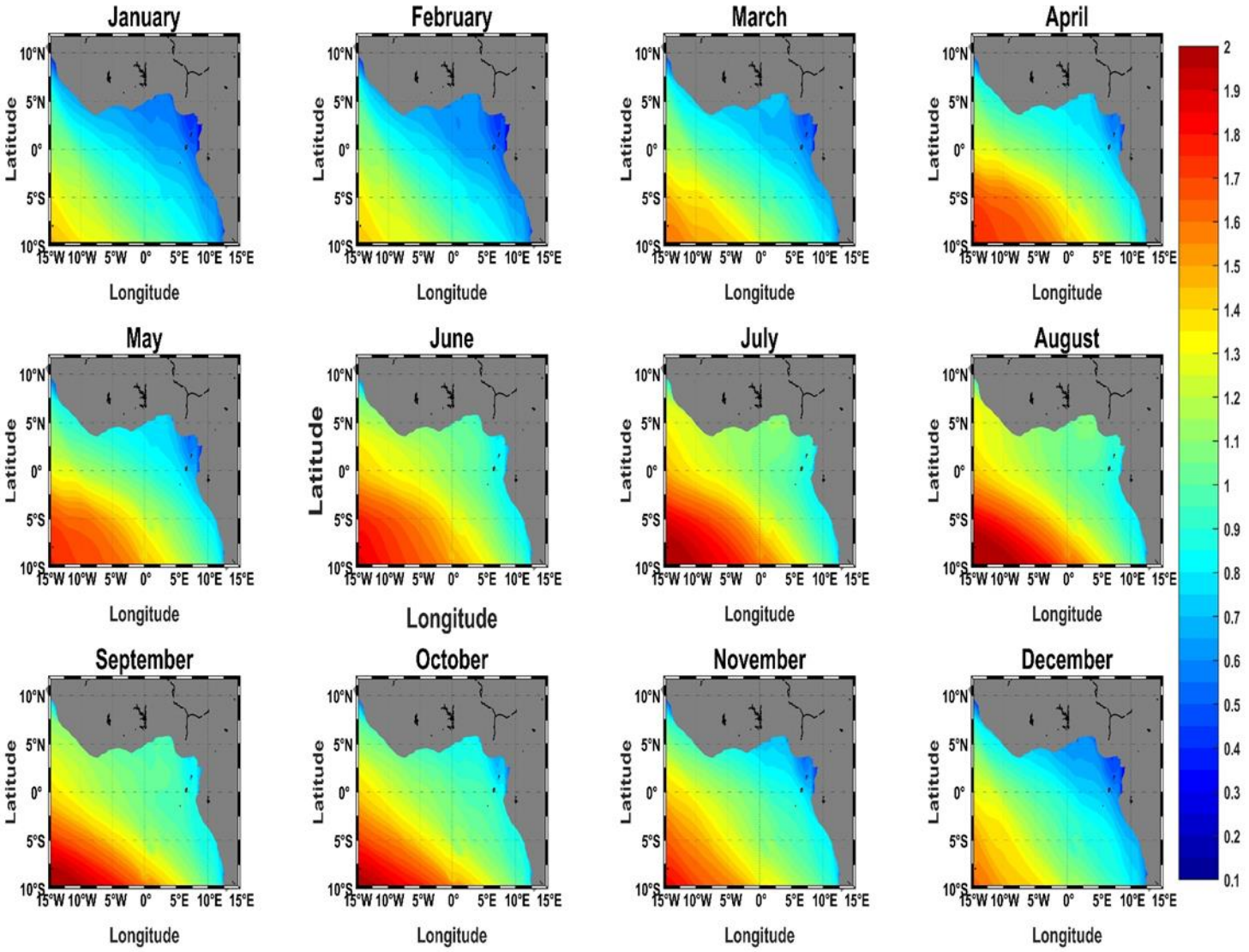

Figure 38: Regional distribution of the mean *Hs* in GoG on monthly basis between 1980-2019.

These monthly variations agree with patterns seen in other oceanographic properties including upwelling in the GoG. The summer is known to mark the peak of these phenomena in the GoG region. Since these other oceanic events are wind driven too, they follow similar spatio-temporal patterns to the wave conditions. Another reason that has been linked to this variation is movement of the longshore drift which goes from west to east reported in Laïbi et al. (2014). This follows the in the direction of the predominant Guinea current in the GoG.

Mean Wave Period (*Tm*)

Annual and Seasonal Analysis

The distribution of the mean *Tm* at each grid point between 1980 and 2019 is shown in the map in Figure 39, which shows that during the period covered, the average wave period close to the coast of GoG generally ranges between 5 s and 6 s with almost no variation from offshore. This is expected since wave period is relatively unaffected by bathymetry changes. The average wave period for the area covered by this study was found to be 5.3897 s between 1980-2019.

Waves of higher periods can be seen in the equatorial region of the mid-Atlantic Ocean. This can be linked to another source of wave generation from the north-western part of Atlantic, which differs from that observed within the GoG region. This was confirmed during a study under the West African Swell Project (Forristall et al., 2013; Prevosto et al., 2013). It was confirmed that during the boreal summer, the predominant swells in West African coast come from the south to south-westerly direction i.e., from those generated by storms in the South Atlantic (40°S-60°S). While during boreal winter, north-westerly swells are seen emerging

from North Atlantic. These can be confirmed by observing the wave period around 5N-5S, 10W-15W in Figures 39 - 41. It is seen that the *Tm* is higher in that region due to the influence from North Atlantic and even higher during the winter because this influence is stronger during this period of the year.

It can be observed from the spatial distribution of mean wave period in Figures 40 - 41 that wave period is slightly higher in GoG during summer than in winter. The average *Tm* for winter was found to be 5.3876 s, while that of summer was calculated as 5.3911 s. These values are withing range of the peak period reported by Almar et al. (2015) and Laïbi et al. (2014) though lower than the 9.4 s reported since the peak period only describe the period corresponding to the most energetic wave in the region.

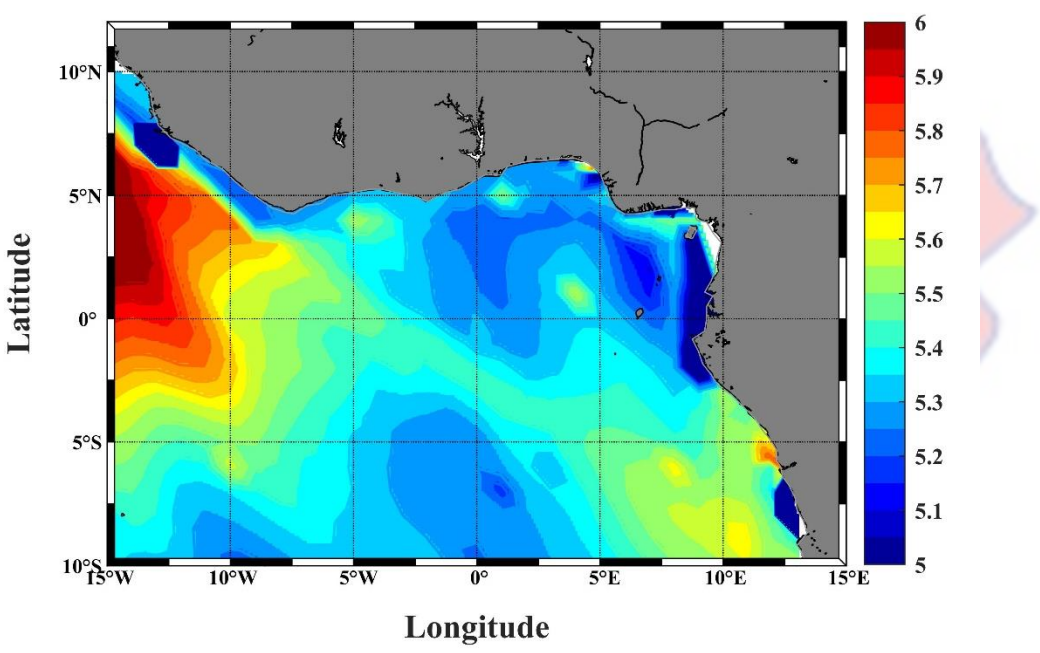

Figure 39: Regional distribution of the mean *Tm* in GoG between 1980-2019.

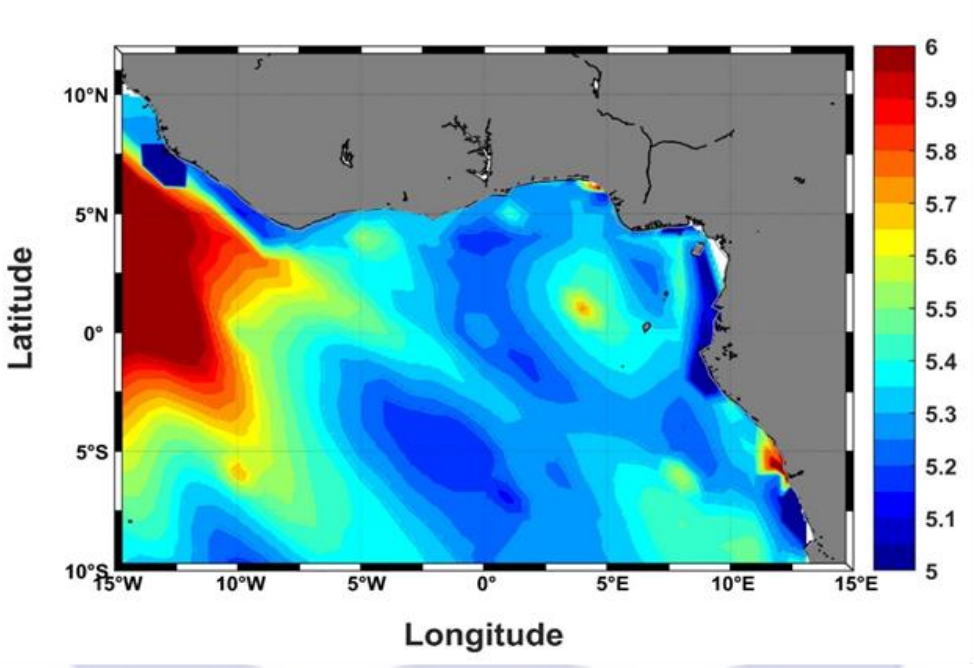

Figure 40: Regional distribution of the mean *Tm* in GoG during winter between 1980-2019.

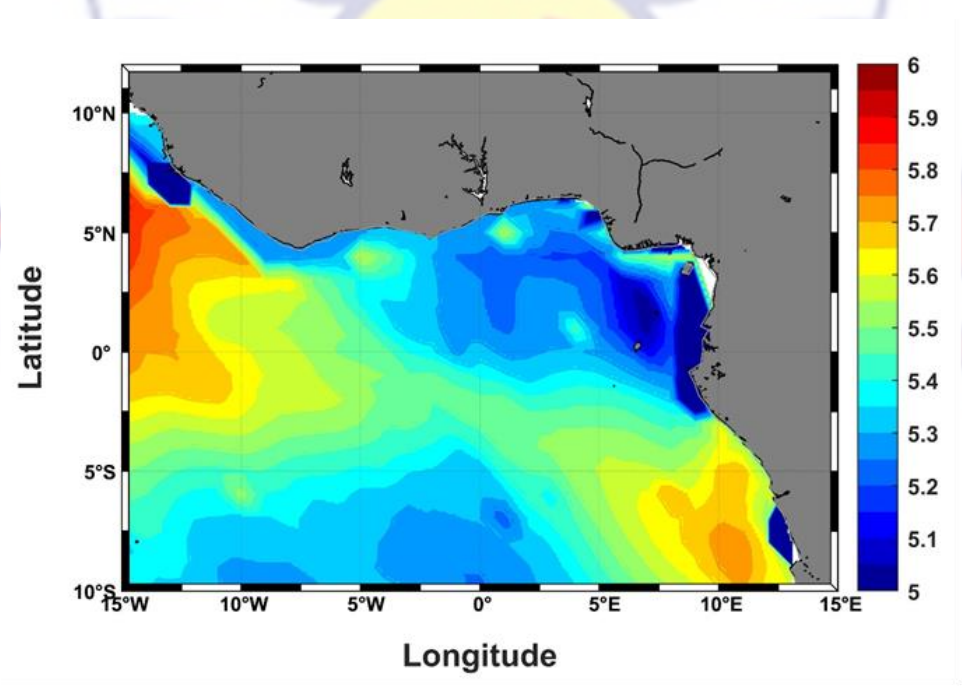

Figure 41: Regional distribution of the mean *Tm* in GoG during summer between 1980-2019.

Monthly Analysis

Tm distributions show similar monthly variation as seen in *Hs* with March-April marking the beginning of summer effect which peaked between September-October unlike *Hs*, which has maximum values between June and August. The effect of winter becomes more obvious between December and March with reduced mean wave period (Table 3). Generally, from the spatial distribution of *Tm* in Figures 39 - 42, it can be observed that despite the relatively uniform nature of the *Tm*, waves of lesser periods are observed closer to the coast.

Table 3: Monthly averages of wave period (*Tm*)

Month	Average *Tm* (s)
January	5.2876
February	5.4704
March	5.5243
April	5.4253
May	5.1974
June	5.2274
July	5.3951
August	5.4419
September	5.5038
October	5.5466
November	5.3562
December	5.3064

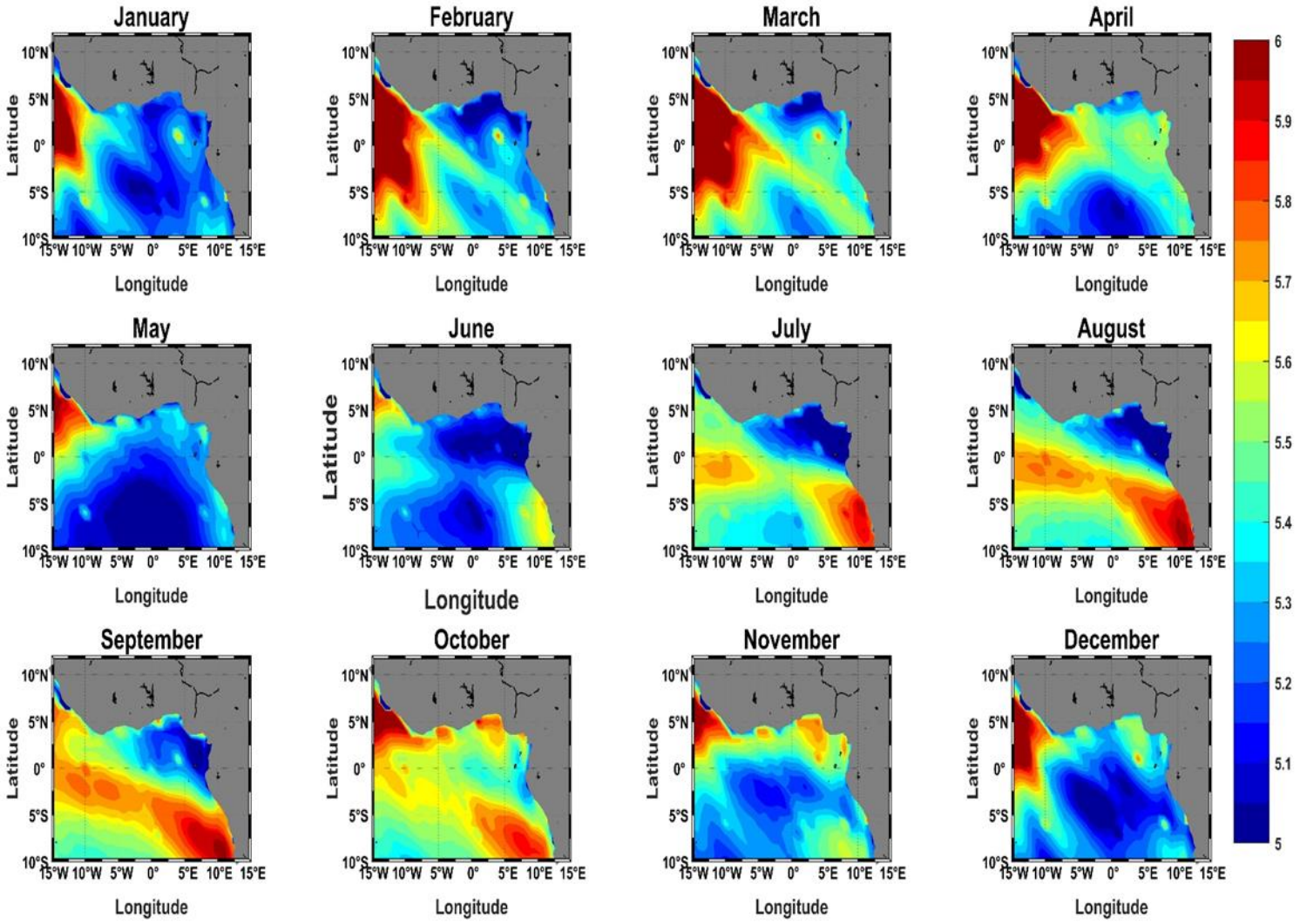

Figure 42: Regional distribution of the mean *Tm* in GoG on monthly basis between 1980-2019.

Wind Speed (U10)

Annual and Seasonal Analysis

The distribution of the annual mean wind speed 10 m above the sea surface (U10) at each grid point between 1980-2019 is shown in Figure 43. This Figure shows that during the period covered, the average wind speed close to the coast of GoG generally varies between 2 m/s and 7 m/s. The annual average wind speed is 4.7001 m/s between 1980-2019. The usual uniform distribution seen for *Hs* and *Tm* is also observed for U10 close to the coast. The wind speed can be seen to decrease as it approaches the coastal areas of GoG. This trend is seen all year round, both in summer and winter. The east to west increase observed in *Hs* can also be seen in the distribution of U10 with regions towards Niger Delta having winds of lesser speeds.

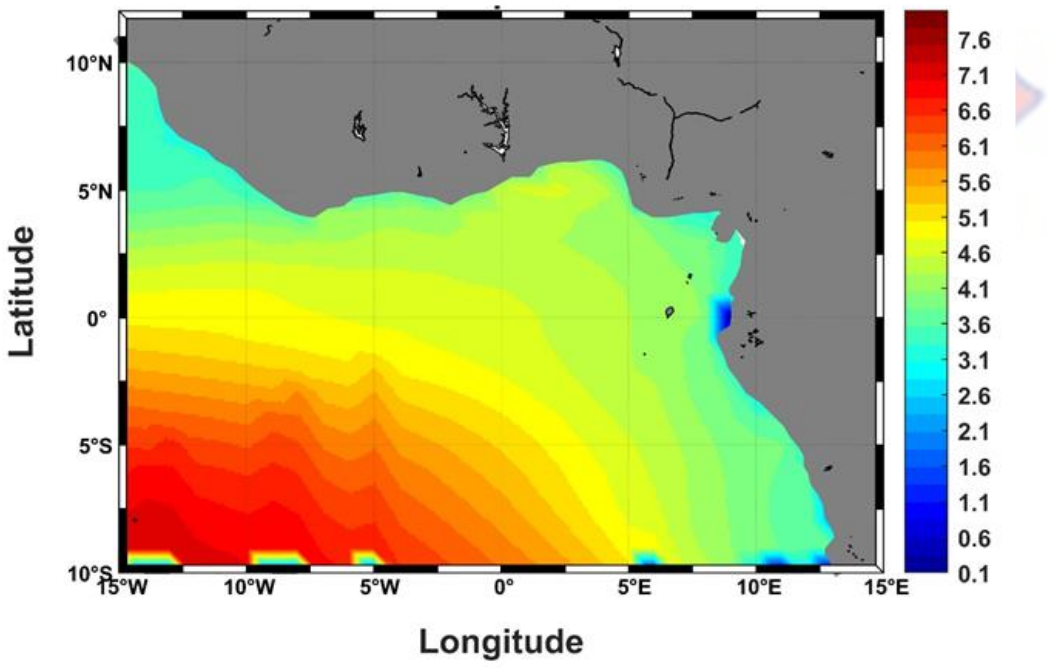

Figure 43: Regional distribution of the mean U10 in GoG between 1980-2019.

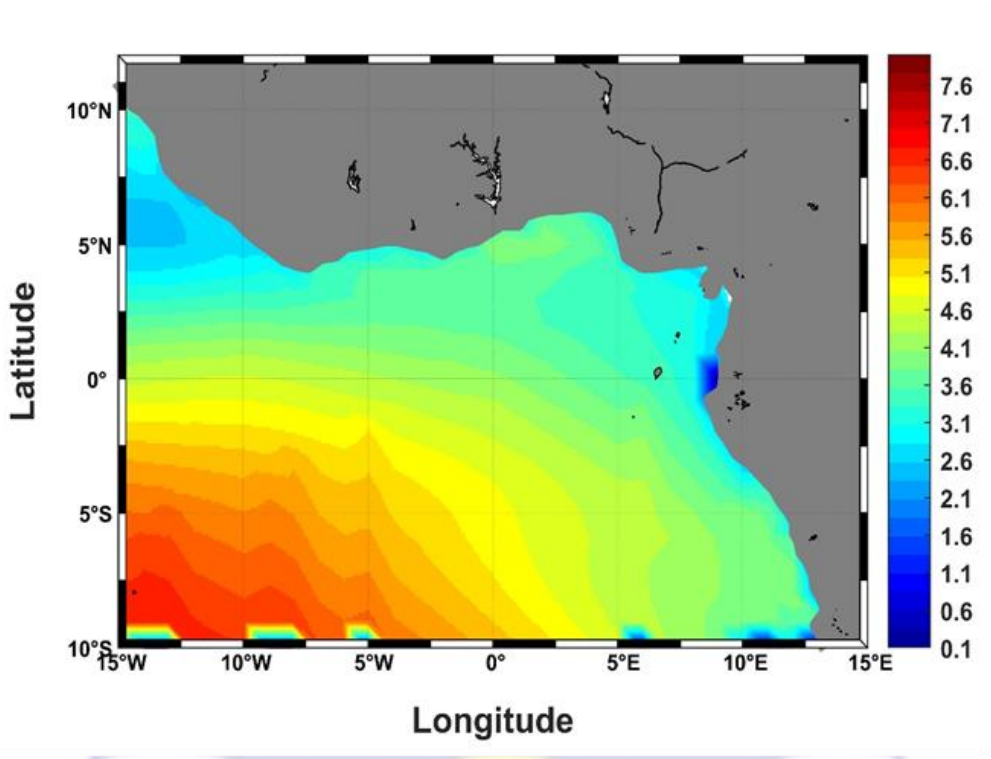

Figure 44: Regional distribution of the mean U10 in GoG during winter between 1980-2019.

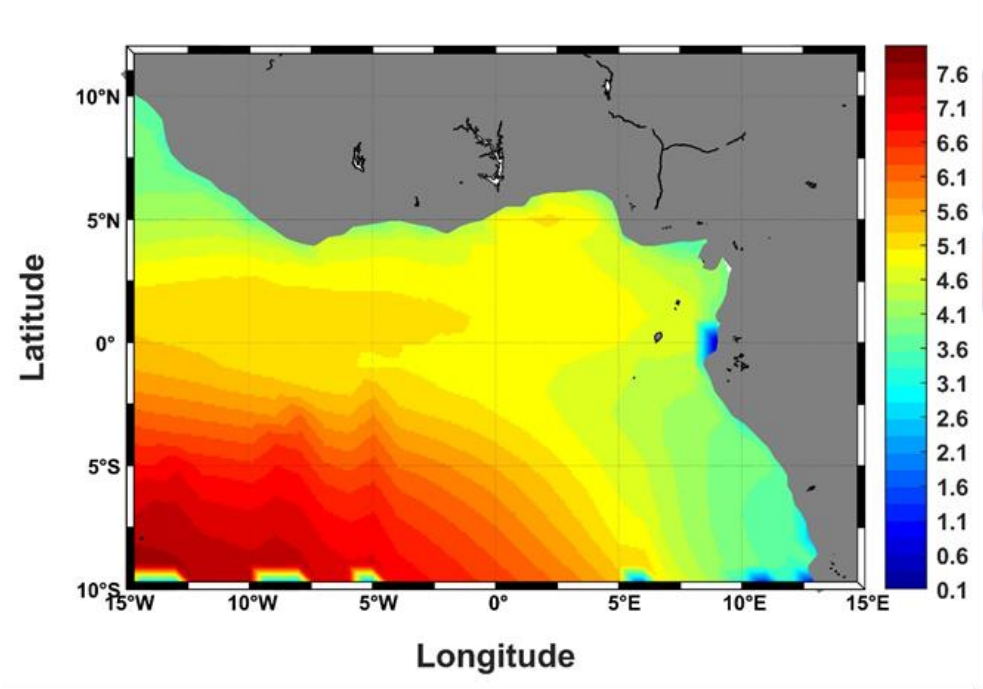

Figure 45: Regional distribution of the mean U10 in GoG during summer between 1980-2019.

From Figures 44 and 47, which show the spatial distribution of mean wind speed for winter and summer respectively, it can be observed that it is slightly higher in GoG during summer than winter. The average U10 for winter was found to be 4.2344 m/s, while that of summer was calculated as 5.0292 m/s. In the summer, winds with high speed can be seen offshore of the cape between Ghana and Togo. This seemingly faster wind spread offshore Togo and Benin which corresponds to the eastern part of the GoG where higher *Hs* are observed. The zonal sorting of winds from offshore is similar to the trend seen in the wave fronts observed from the distribution of *Hs*.

Monthly Analysis

Figure 46 and Table 4 summarizing the monthly evolution of the wind speeds hereby confirm that the summer months show higher wind speed peaking between June-July, when the zonal distribution seen in the average annual, winter and summer distribution are overturned to a more or less meridional distribution of wind speed.

Table 4: Monthly averages of wind speed (*U10*)

Month	Average U10 (m/s)
January	3.9909
February	3.9944
March	4.1417
April	4.5088
May	4.9992
June	5.3116
July	5.3185
August	5.262
September	4.9974
October	4.7989
November	4.7011
December	4.3382

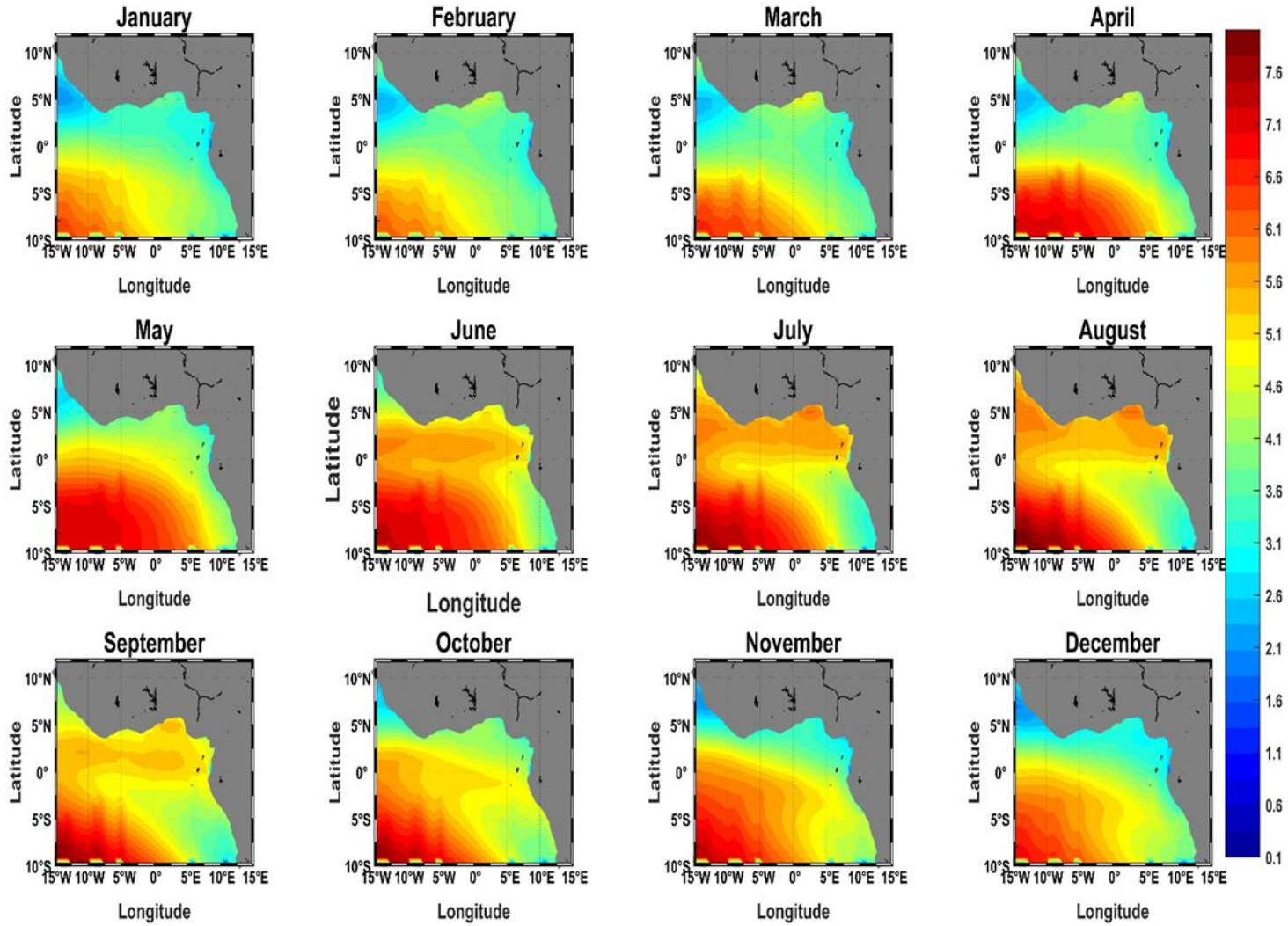

Figure 46: Regional distribution of the mean U10 in GoG on monthly basis between 1980-2019.

Wave Direction

Annual and Seasonal Analysis

The analysis for wave direction is done by calculating the magnitude of both zonal and meridional components of the wave velocity i.e., u and v components in x- (East) and y- (North) axes, respectively. Both the annual (Figure 47) and seasonal analysis (Figures 48 and 49) have similar pattern showing the wave directions have similar direction throughout the year. The wave directions as shown by these Figures confirm that the waves emanate from the southern Atlantic. Since the lengths of the arrows were scaled by *Hs*, it can be seen that longer arrows seen offshore of GoG are heading outside the GoG, while those waves heading for GoG become smaller on their approach to the coast. This direction agrees with the predominantly S-SW drection reported by Laïbi et al. (2014).

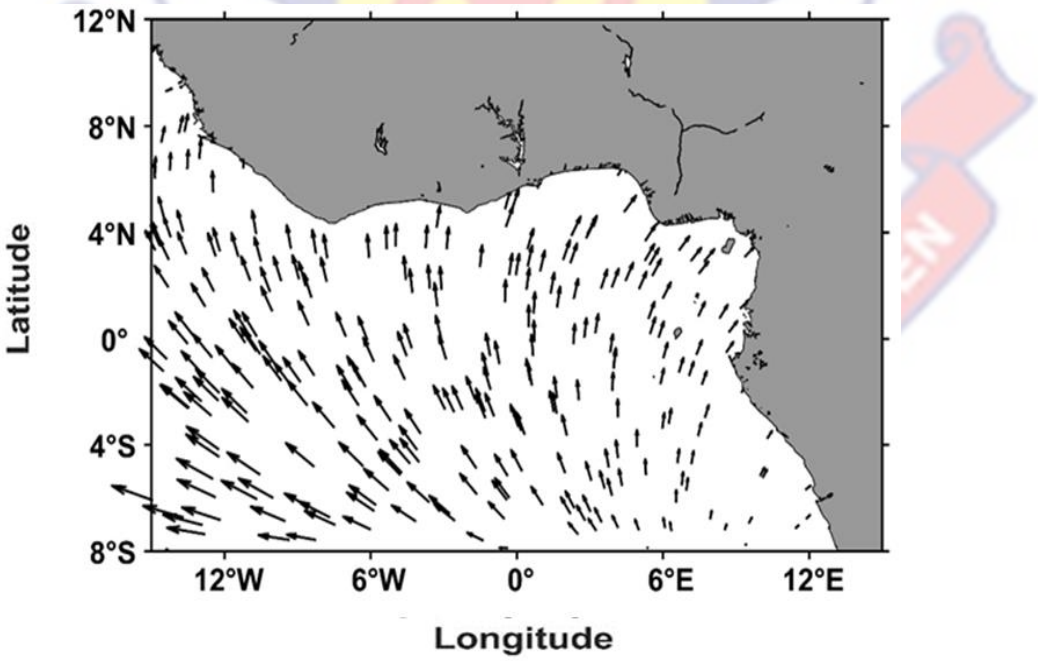

Figure 47: Regional distribution of the wave direction in GoG between 1980-2019.

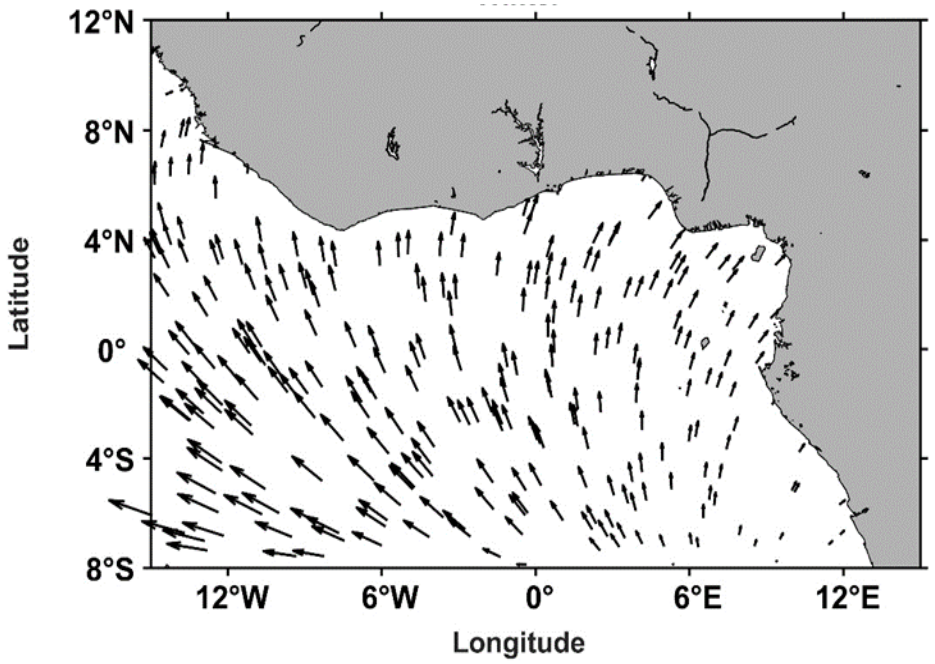

Figure 48: Regional distribution of the wave direction in GoG during winter between 1980-2019.

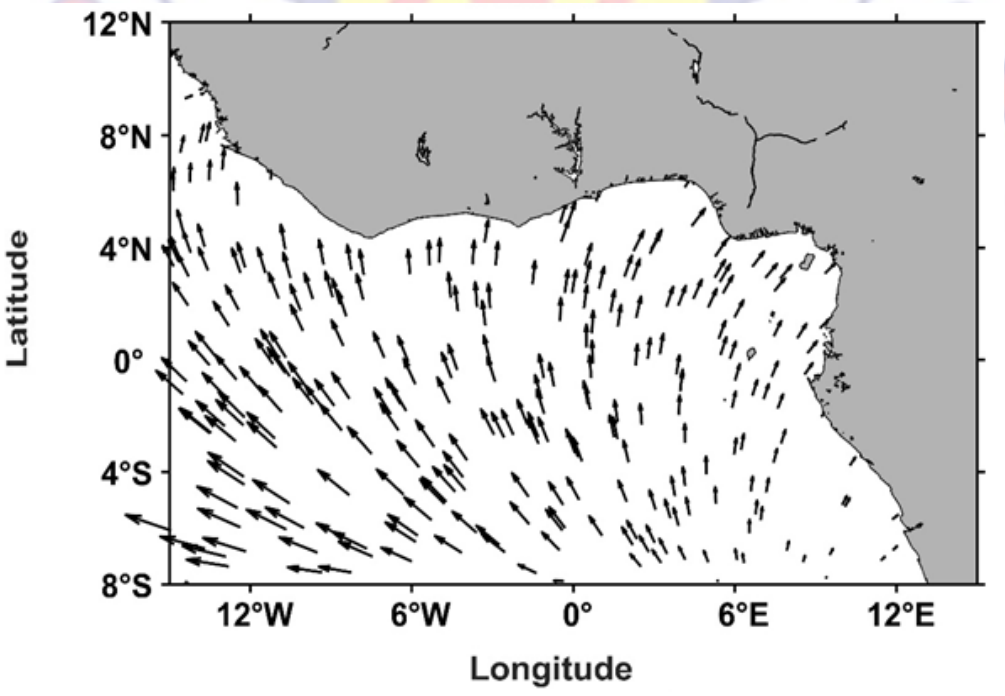

Figure 49: Regional distribution of the wave direction in GoG during summer between 1980-2019.

From the results presented so far, it was seen that though the approaches for studying or modelling are different, all the results presented for *Hs*, *Tm*, U10 and wave direction are similar to those derived from previous studies on waves in the GoG region. These are confirmed in studies by Almar et al. (2015), where the responses of some parts of the GoG coastline to anthropogenic and natural forcing were examined through modelling. The study of the variability of the swell in the coastline of northern part of the GoG using modelled and remotely sensed data by Toualy et al. (2015) also showed similar results. The differences between these results have been linked to the Tolman-Chalikov parameterization used in WW3 set-up for this study similar to that employed by Osinowo et al. (2016). These previous studies also confirmed the trend of east-west and south-north decrease of *Hs* previously mentioned. For the U10, the spatio-temporal distributions also tally with the spatio-temporal variation of the upwelling system in the easternmost part of the GoG (Wiafe and Nyadjro, 2015).

Spatio-Temporal Trends of Significant Wave Height (*Hs*)

Annual and Seasonal Analysis

To get a clearer picture of the changes of wave height between 1980-2019, a trend analysis was done. This was done by applying the linear regression approach to the annual and seasonal averages of *Hs*. This analysis was done using the MATLAB function **polyfit** which works by finding the coefficient of the polynomial P(X), which in this case is the number of years (40 years), that fits the data Y (the mean value of *Hs*) best in a least-squares sense. This provided the

gridded trend data with the same dimension as the input which is *Hs* in this case for both annual and seasonal analysis.

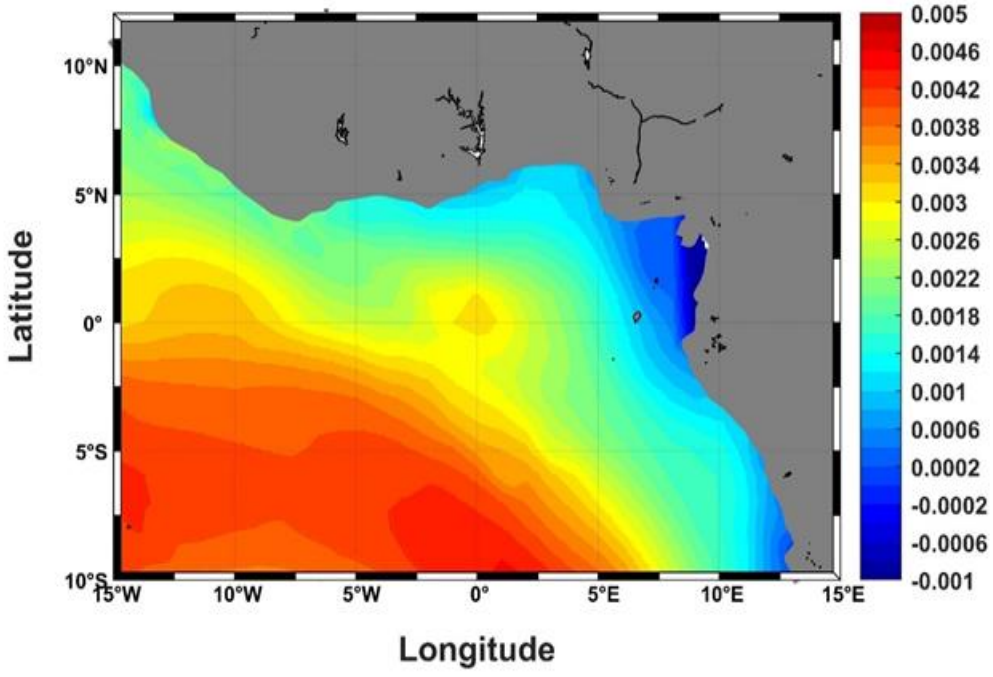

Figure 50: Spatial distribution of annual trends in *Hs* between 1980-2019.

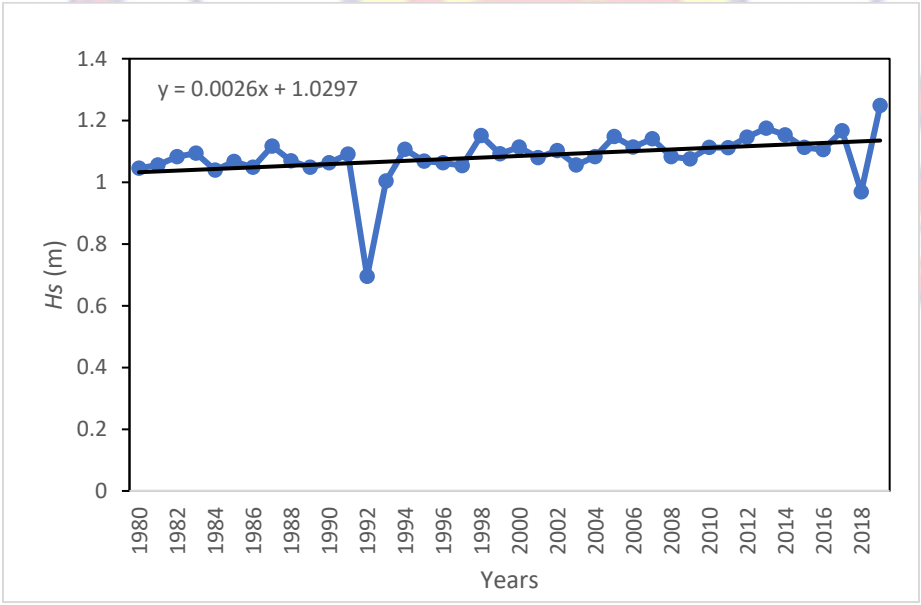

Figure 51: Annual temporal trends in *Hs* between 1980-2019.

Figure 50 shows the annual spatial trend of *Hs* between 1980-2019 with the average result showing an increase of about of 2.6 x 10^{-3} m in the *Hs* per year. This is shown by the slope of the equation of linear fitting shown in Figure 51. The rate of increase of *Hs* follows the same east-west and south-north increasing pattern shown by the distribution of *Hs* earlier presented. Generally, the average yearly *Hs* for GoG is above 1 m except for the years 1992 and 2018 (Figure 51)

The seasonal analysis of *Hs* shows a trend of increasing *Hs* both in winter and summer. The increase rate in summer, which is higher than winter, is about 3.4 x 10^{-3} m per year, while winter *Hs* has been increasing at an average rate of 1.6 x 10^{-3} m per year between years 1980 and 2019 (Figures 53 and 55). The yearly trend evolution for winter and summer shown by Figures 53 and 55 respectively shows that in winter the average *Hs* is usually above 0.8 m and 1 m for summer except for years 1992 and 2018.

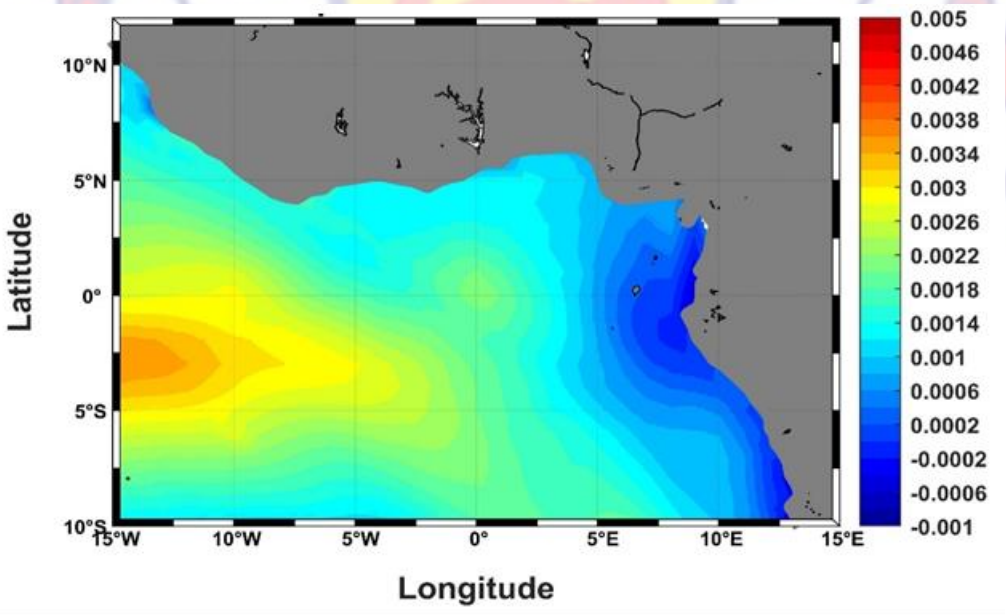

Figure 52: Spatial distribution of winter trends in *Hs* between 1980-2019.

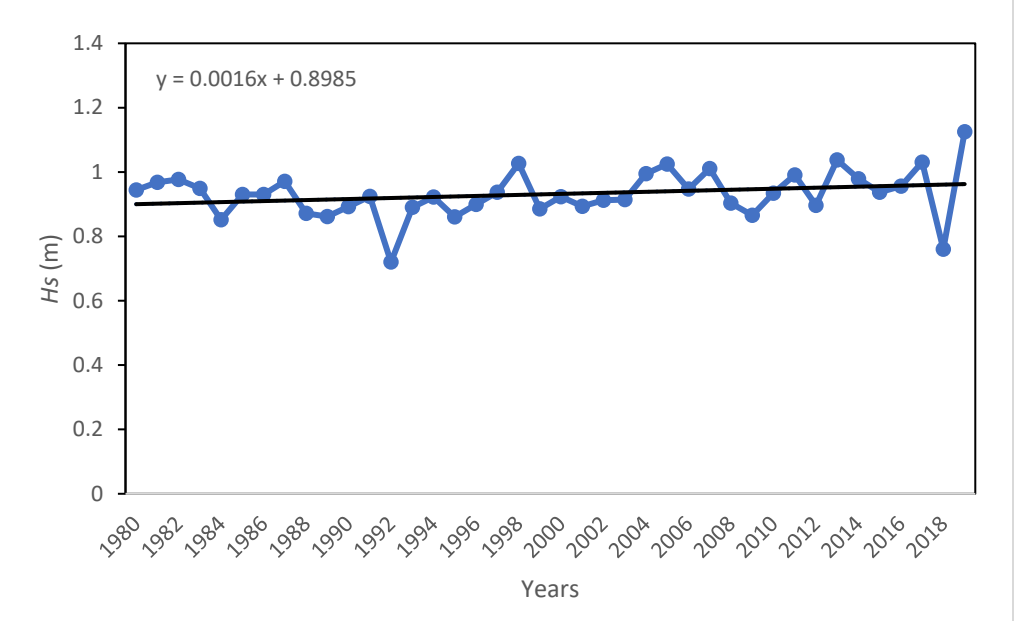

Figure 53: Winter temporal trends in *Hs* between 1980-2019.

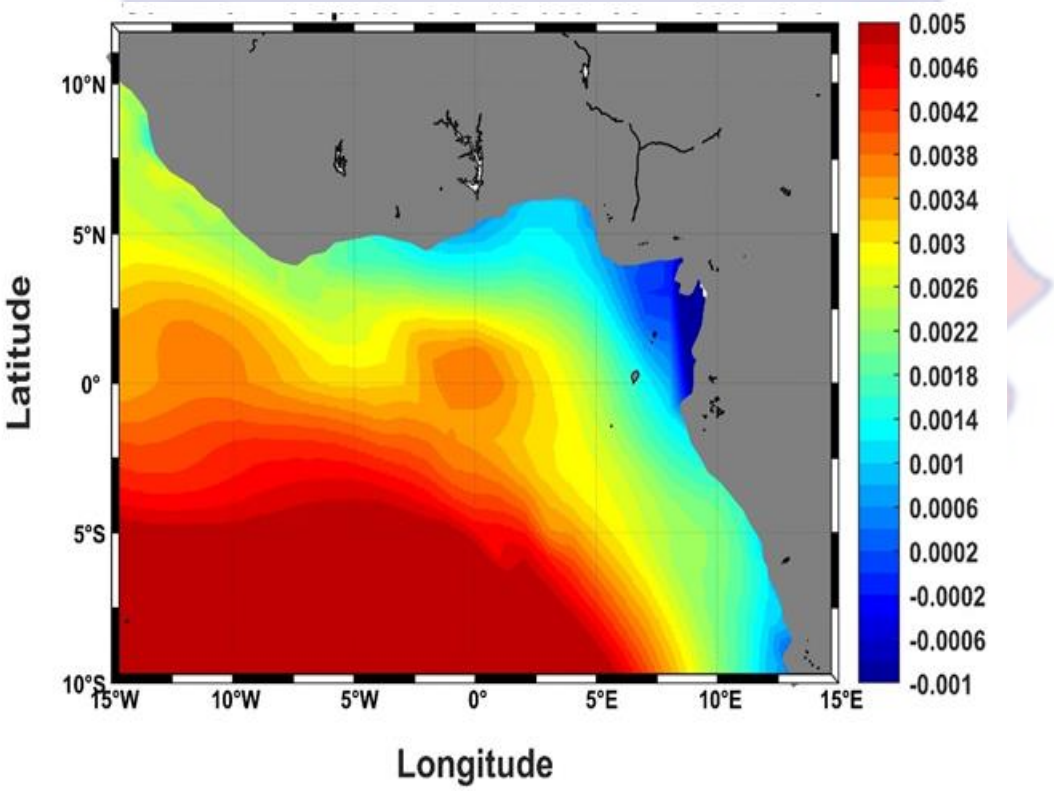

Figure 54: Spatial distribution of summer trends in *Hs* between 1980-2019.

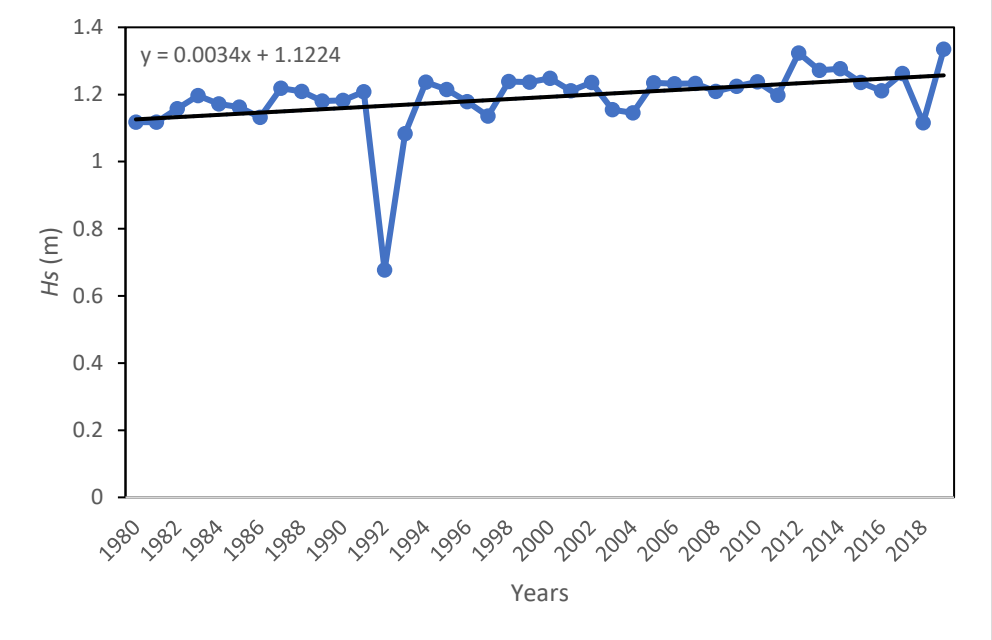

Figure 55: Summer temporal trends in *Hs* between 1980-2019.

The trendlines in Figures 51, 53 and 55 represent the average changes *Hs* has undergone between 1980-2019. The rate of change is given by the coefficient of x in the equation of the regression line. This value is similar to that obtained when the average of the trends shown in the spatial distribution in Figures 50, 52 and 54 are calculated for confirmation. From Figures 52 and 54, it can be observed that the trend during summer (rainy season) shows high rate of increase from offshore even very close to the coast. This can be linked to the rapidly increasing frequency of severe perennial flooding experienced in the low-lying coastal communities in the north-eastern countries of GoG like Ivory coast and Ghana as reported in Toualy et al. (2015) and Alves et al. (2020).

Monthly Analysis

It can be observed from the spatial distribution of trend of *Hs* in Figure 56 and the summary of monthly trends in Table **5** that all the months have been experiencing relatively small increase in *Hs*. This generally observed increase also shows a south to north increment for most months except for a few months in the winter, where decrease in wave height closer to the coast and offshore is observed. This reverse pattern is seen in December, January and March. This shows that the winter months have a different pattern of trend over the past four decades except for the return to summer condition seen in February. The values in Table **5** also show a trend where most months with higher increasing trend are followed by months of lower increasing trend forming a uniform oscillation throughout the year.

Table 5: Monthly averages of spatial trends in *Hs*

Month	Average *Hs* trend (m per year)
January	5.48×10^{-4}
February	2.26×10^{-3}
March	9.18×10^{-4}
April	18.17×10^{-4}
May	35.23×10^{-4}
June	32.95×10^{-4}
July	44.08×10^{-4}
August	36.9×10^{-4}
September	42.27×10^{-4}
October	25.49×10^{-4}
November	29.85×10^{-4}
December	13.85×10^{-4}

These results of the trends of *Hs* agree with the findings of other studies both globally and regionally. Increase in heights has been observed over the past decades in most parts of the world (Wang et al., 2009; Wang and Swail, 2001, 2002; Young et al., 2011). This increase has been observed to be higher for the extreme wave conditions than the average wave climate. For example, in the study by Young et al. (2011), an increase of 0.25% per annum was observed for the 90^{th} percentile of wave height while the 99^{th} percentile showed an increase of 0.5% per annum globally. These same trend of increase has been reported for wave period and wave direction with wave direction changing from the predominant south-west direction to more south orientation in the GoG (Reguero et al., 2019).

In a study of the wave conditions in the GoG using 37 years wave hindcast data, Osinowo et al. (2018) found out that the *Hs* has been increasing at an average rate of 0.0014 m and 0.0017 m per year for the annual and summer analysis with a weak decreasing trend in the winter. This is comparable to the results of the trends in this study though increasing trend is seen throughout the year. It is worthy of note that the rate of increase has almost double from 2016 to 2019 when compared with the results from Osinowo et al. (2018). Since similar modelling approach was employed, the yearly variations in this study agree with Osinowo et al. (2018) especially the sharp decrease in 1992 which has been linked to the influence of the El-Nino event in the Pacific Ocean which weakened the West African Monsoon in the GoG during that period. The effects of the La-Nina events are also seen in the years after 1992 as sharp increase in the wave height for the region.

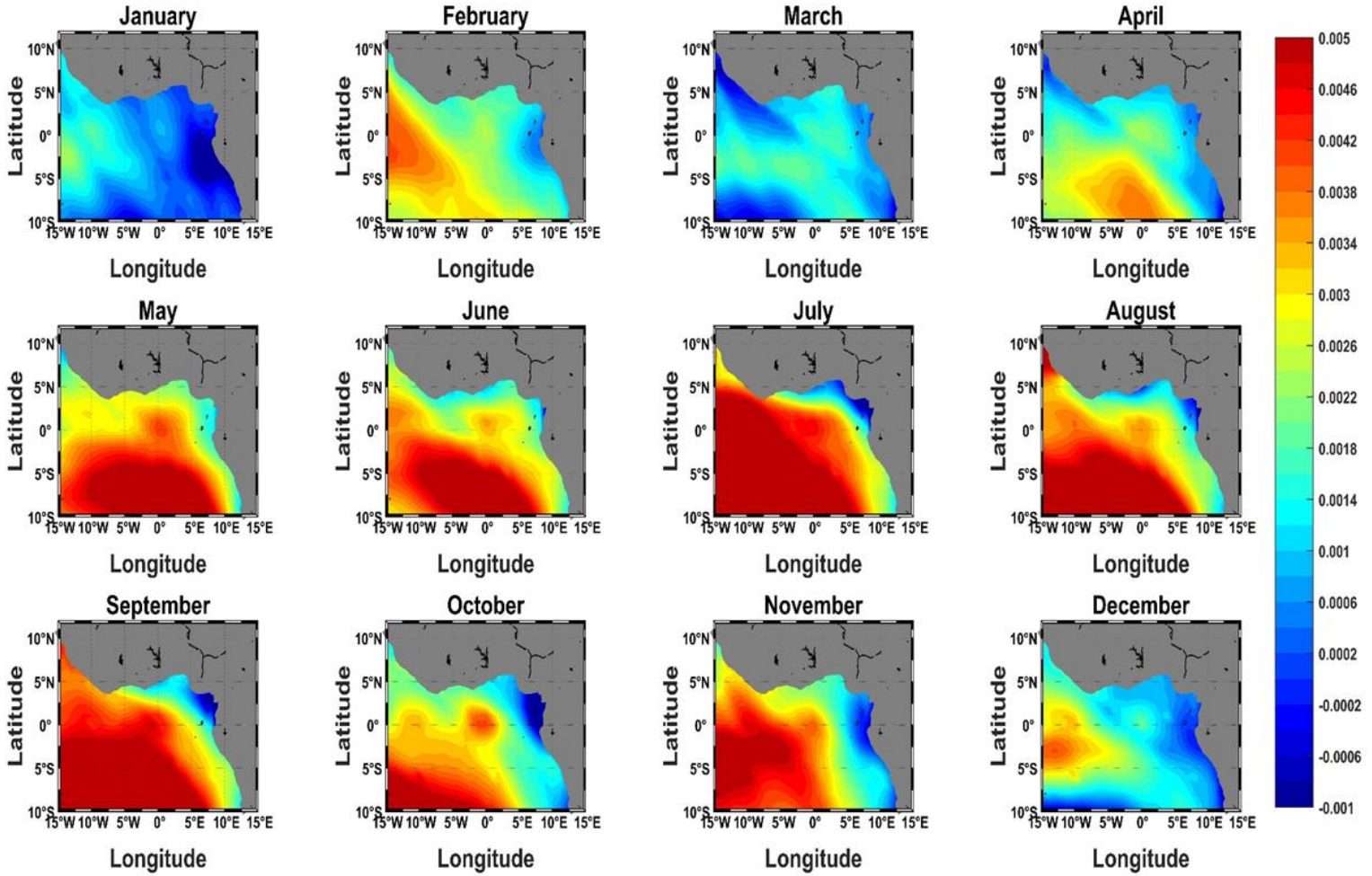

Figure 56: Spatial distribution of monthly trends in *Hs* between 1980-2019.

Spatio-Temporal Trends of Mean Wave Period (*Tm*)

Annual and Seasonal Analysis

Figure 57 shows the annual spatial trend of *Tm* between 1980-2019 with the average result showing an increase of about of 6.1353 x 10^{-4} s in the *Tm* per year. This is an order of magnitude lower than the trends shown by *Hs* between the same period. An increase of trend can be seen towards the coast with values as high as 10.5 x 10^{-3} s. This is shown by the slope of the equation of linear fitting shown in Figure *58*. Most of the regions offshore are showing lower increasing trend of *Tm* compared to what is seen in the coastal areas. These lower increasing trend values are seen to change from positive trend sign to negative meaning decreasing trend in *Tm* in some offshore region as seen in Figure 57.

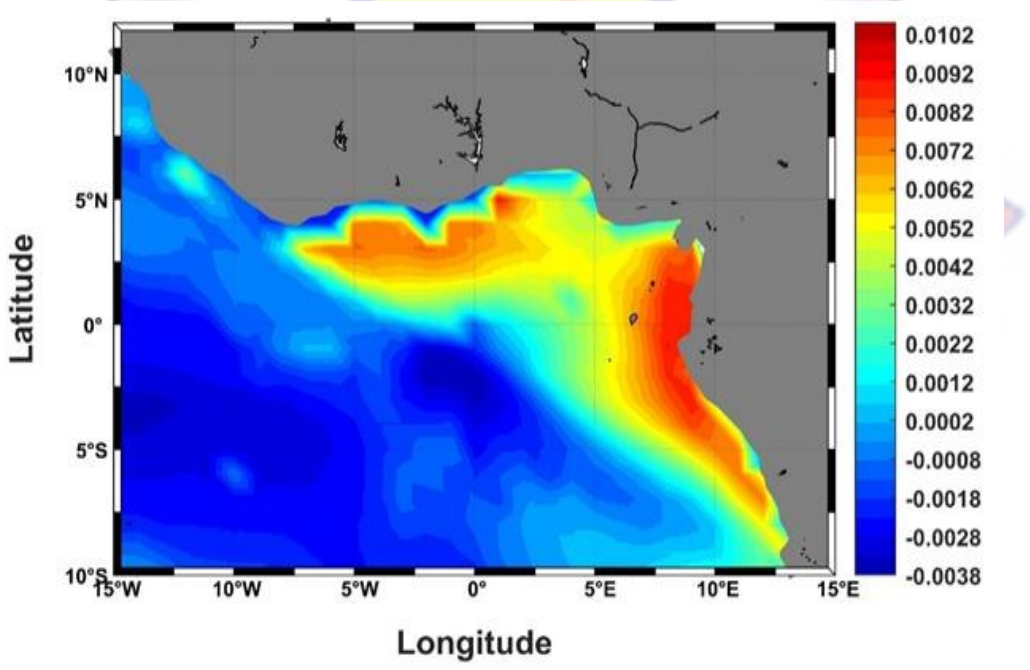

Figure 57: Spatial distribution of annual trends in *Tm* between 1980-2019.

The seasonal analysis of *Tm* shows a trend of decrease in winter and increase in summer. The decrease rate seen in winter is -1.7 x 10^{-3} s per year on average (Figure 60), while summer *Tm* has been increasing at an average rate of 2.3 x 10^{-3} s per year (Figure 62) between years 1980 and 2019. Though the offshore mean wave period seems to be experiencing a reduction per year, both in summer and winter with a decrease as high as -3.8 x 10^{-3} s per year experienced during winter (Figure 59). An increase as high as 10.2 x 10^{-3} s per year is also experienced during summer (Figure 61).

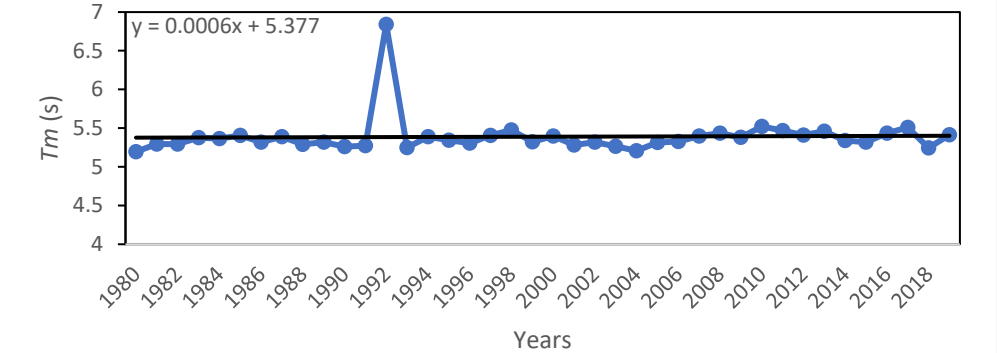

Figure 58: Annual temporal trends in *Tm* between 1980-2019.

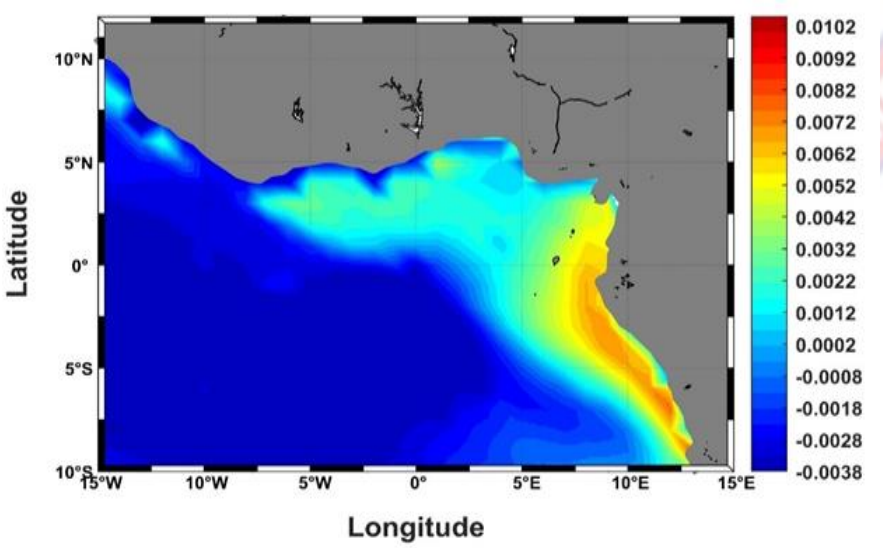

Figure 59: Spatial distribution of winter trends in *Tm* between 1980-2019.

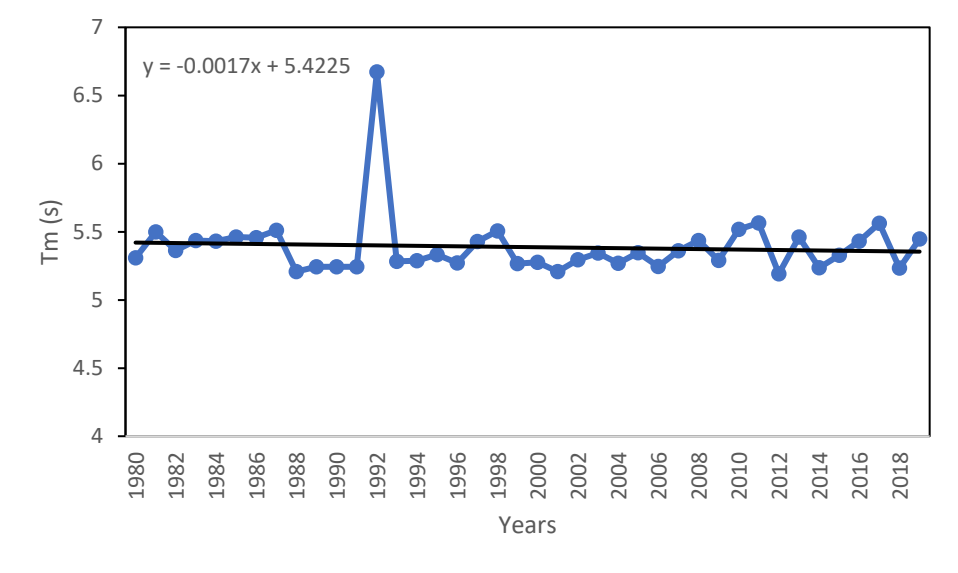

Figure 60: Winter temporal trends in *Tm* between 1980-2019.

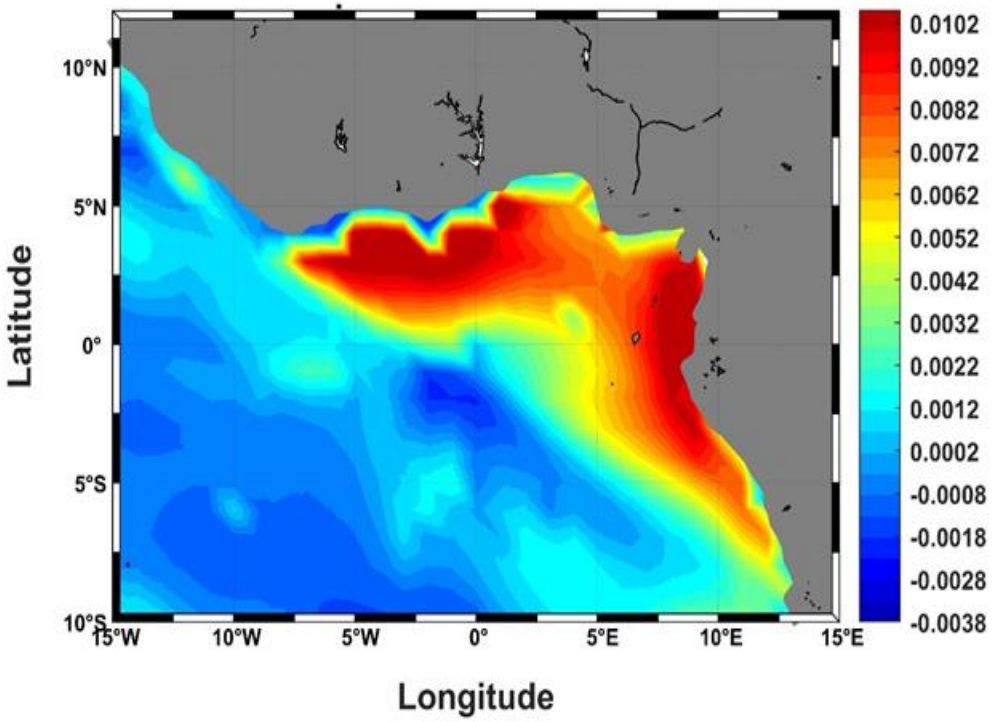

Figure 61: Spatial distribution of summer trends in *Tm* between 1980-2019.

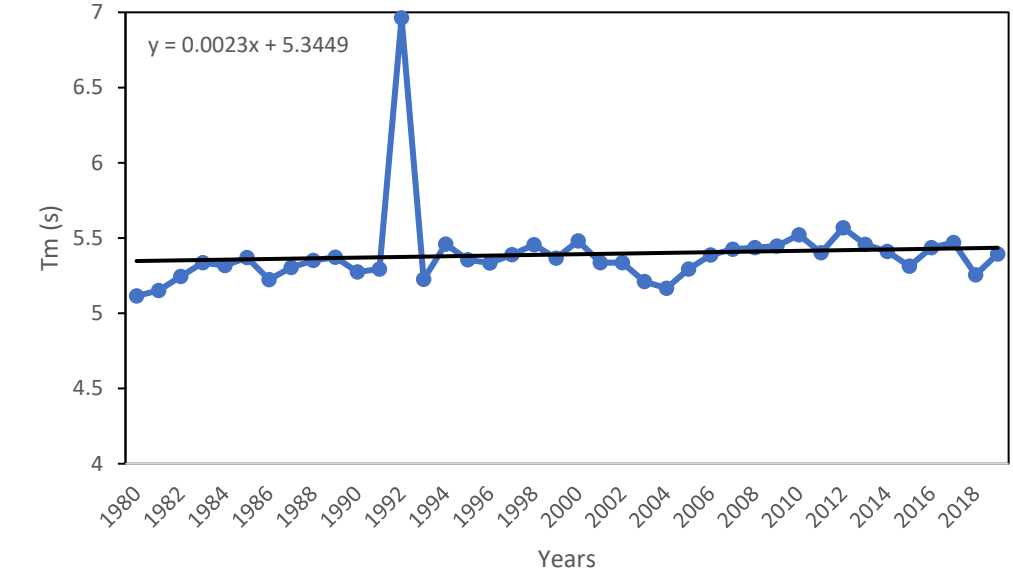

Figure 62: Summer temporal trends in *Tm* between 1980-2019.

Monthly Analysis

The spatial distribution and monthly average of trends shown in Figure 63 and Table 6 respectively confirmed the result shown by the season analysis with all the winter months except February, showing a trend of decrease in mean wave period, while the summer months from May-October depicts that the *Tm* has been on the increase in these months. The observation of the February map of spatial distribution (Figure 63) shows a trend similar to the unique deviation seen in February for *Hs* suggesting that there is almost no time lag between this temporary change in trend. It can be seen that unlike other winter months, February has a decreased *Tm* close to the coast and increase of *Tm* offshore, which is similar to the reverse observed for the February *Hs* trend.

Table 6: Monthly averages of spatial trends in *Tm*

Month	Average *Tm* trend (s per year)
January	-9.5×10^{-4}
February	14.84×10^{-4}
March	-36.7×10^{-4}
April	-28.0×10^{-4}
May	30.32×10^{-4}
June	17.18×10^{-4}
July	26.36×10^{-4}
August	28.97×10^{-4}
September	36.93×10^{-4}
October	44.6×10^{-4}
November	-8.6×10^{-4}
December	-41.9×10^{-4}

The mean wave period trend carried out by Osinowo et al. (2018) gave values of 0.0054 s, 0.0088 s and 0.0006 s per year for annual, summer and winter trends, respectively. These values confirms that the *Tm* values have been increasing at faster rates in the summer than in the winter. Though contrary to the findings in this study which shows that winter has been experiencing a decrease in *Tm*, Osinowo et al. (2018) found a very low increasing rate which was described as insignificant. These differences can be as a result of different spatio-temporal coverage of the estimation which caused the averaging of values to give slightly different results.

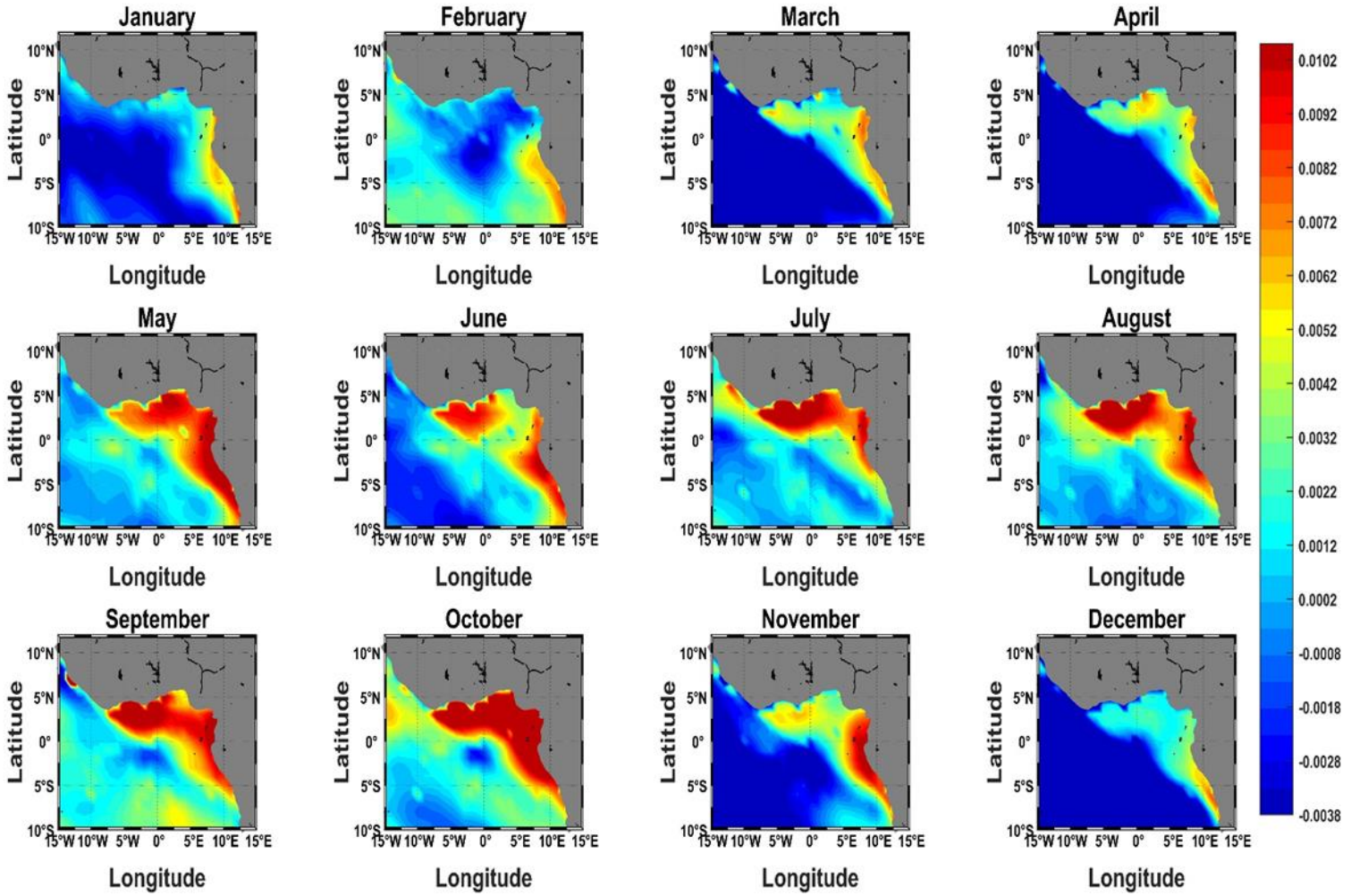

Figure 63: Spatial distribution of monthly trends in *Tm* between 1980-201

Spatio-Temporal Trends of Mean Wind Speed (U10)

Annual and Seasonal Analysis

Figure 64 shows the annual spatial trend of U10 between 1980-2019 with the average result showing an increase of about of 3.5 x 10^{-3} m/s (Figure 65) in wind speed per year. This is the same order of trends shown by *Hs* between the same period. It can be observed that the wind speed is generally experiencing a decrease close to the coast which is expected to lead to a weaker wind sea (locally generated waves). In contrast, the strong increase in the offshore wind speed bears witness to increase in height of the swell (offshore generated waves), which is the major type of wave experienced in the GoG region. A decrease as high as 14.9 x 10^{-3} m/s per year is seen in the coast of the GoG except areas close to the coast of Togo, Benin down to the Niger Delta where these reductions have lesser magnitudes (Figure 64).

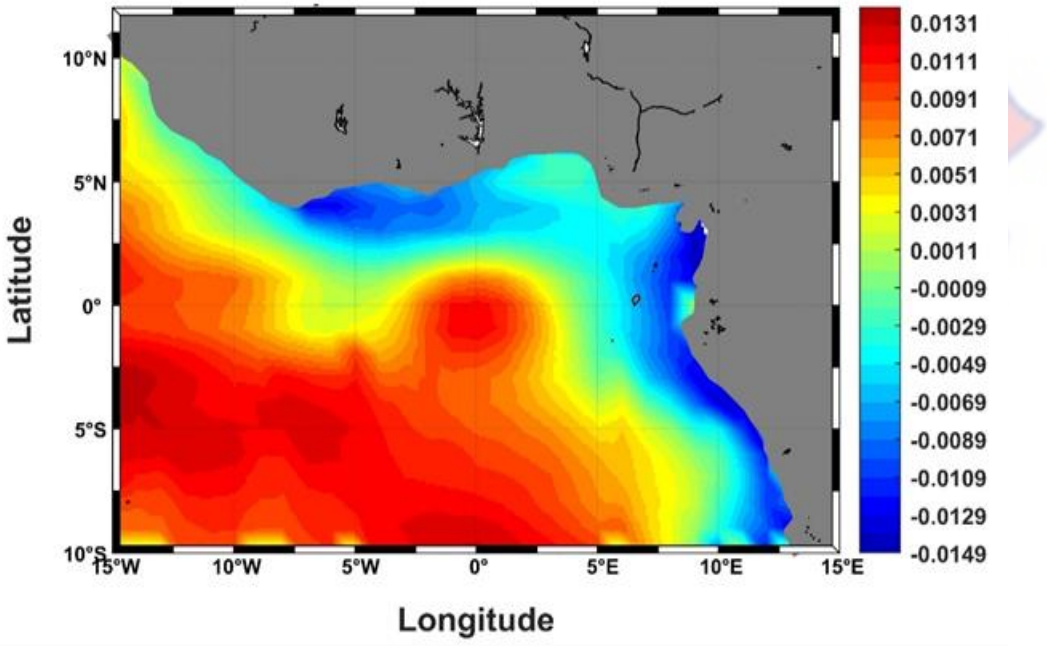

Figure 64: Spatial distribution of annual trends in U10 between 1980-2019

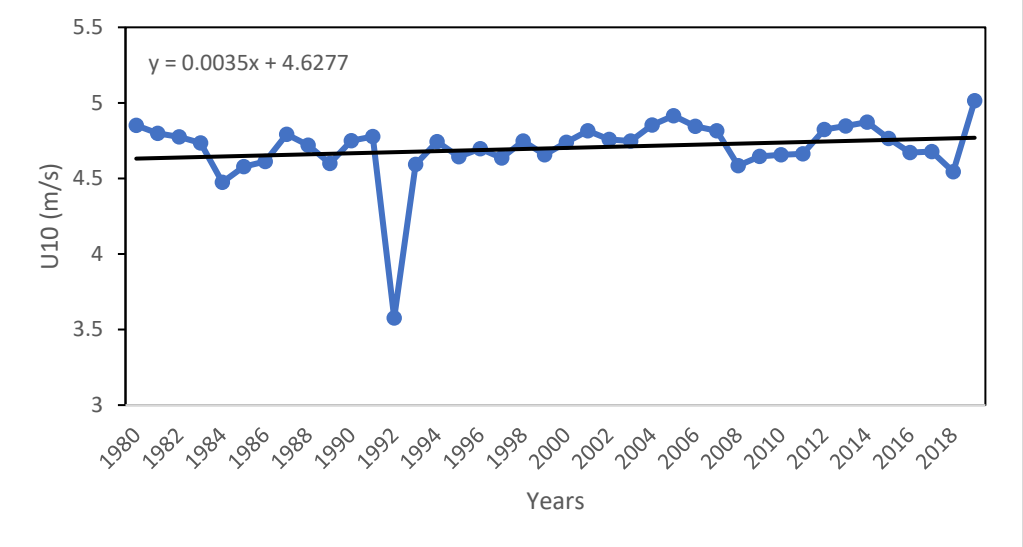

Figure 65: Annual temporal trends in U10 between 1980-2019

The seasonal analysis of U10 presented in Figures 66 - 69 show, on the average, an increasing trend for both winter and summer in GoG region. In contrast to what was seen for *Hs* and *Tm*, the rate of increase of averagely 4.2 x 10^{-3} m/s per year (Figure 67) seen during winter is higher than that observed for summer which is averagely 3.1 x 10^{-3} m/s per year (Figure 69). Though, on average, both seasons show decreasing trend in coastal wind speed and increase in its offshore counterpart, it can be seen that those areas around the coast all the way from Cape Three Point down to the Niger Delta have been experiencing increase in the wind speed during winter. This increase in coastal wind speed can be linked to predominance of the North-west trade winds during this season. This wind originates from the continental Africa and hence expected to be stronger closer to the coast. Since the spatial distribution of wind speed presented earlier (Figures 44 and 45) show higher values during the summer, it can be deduced that the influence

of the predominant wind during the dry season is on the increase thereby driving higher change in the winter wind speed.

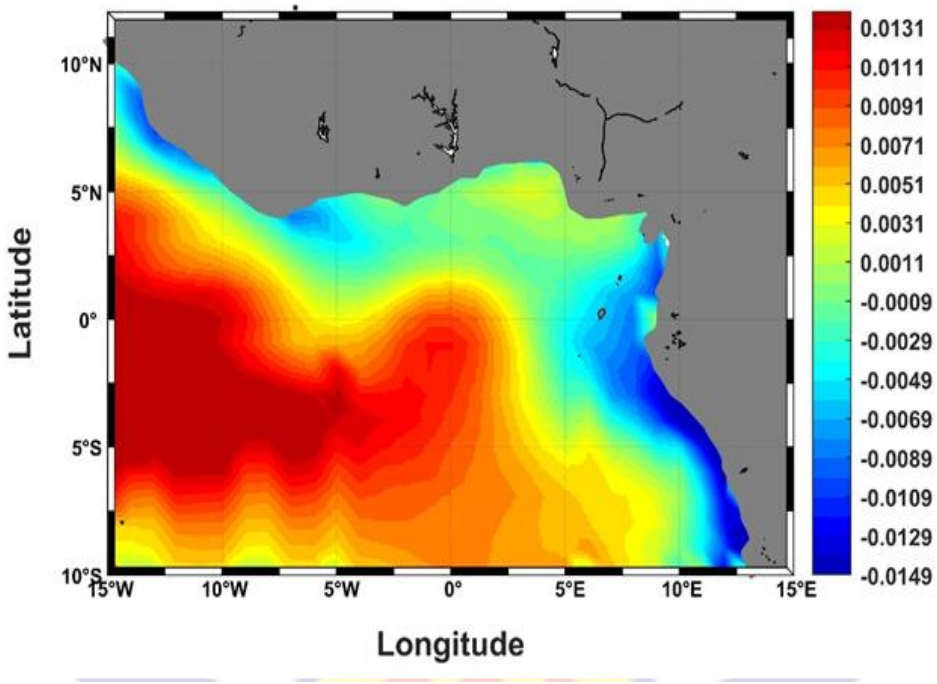

Figure 66: Spatial distribution of winter trends in U10 between 1980-2019.

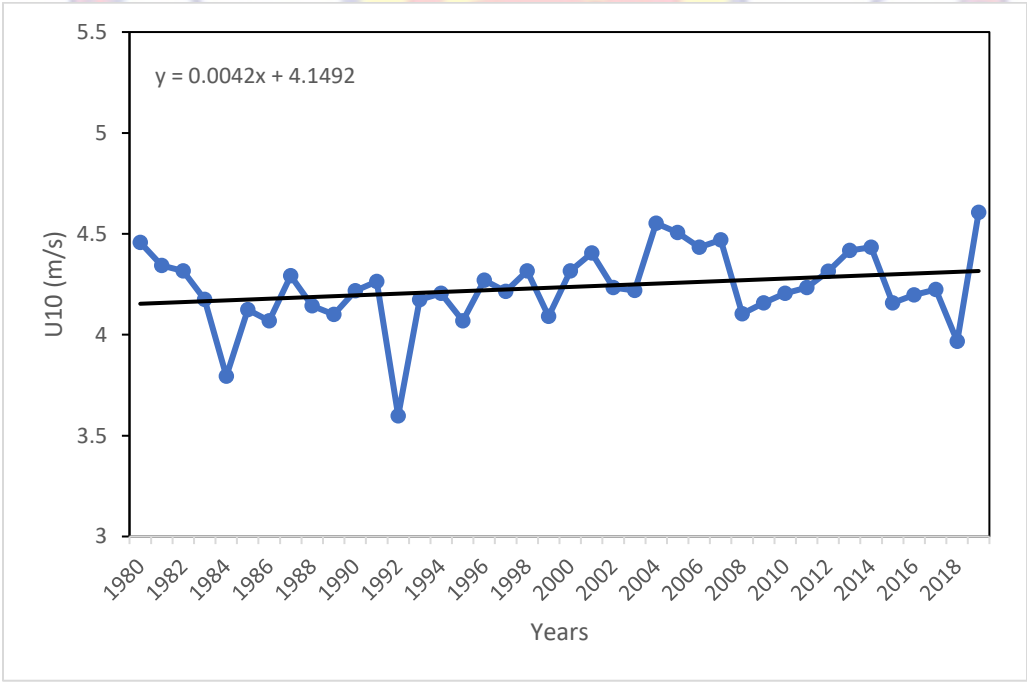

Figure 67: Winter temporal trends in U10 between 1980-2019.

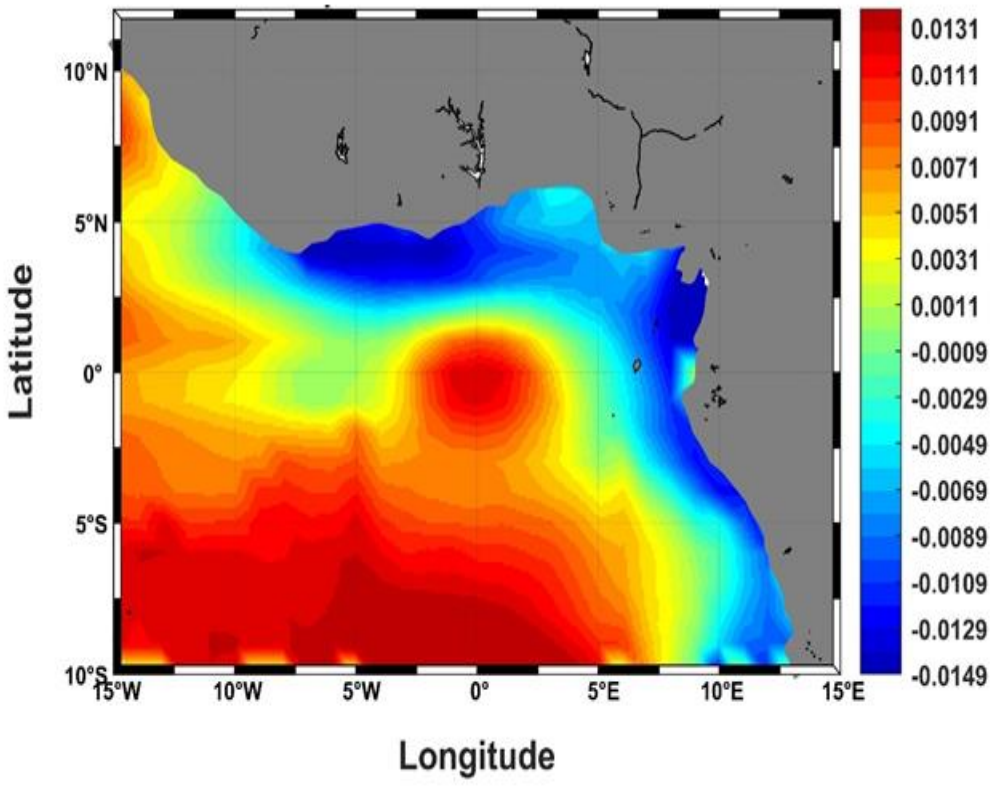

Figure 68: Spatial distribution of summer trends in U10 between 1980-2019.

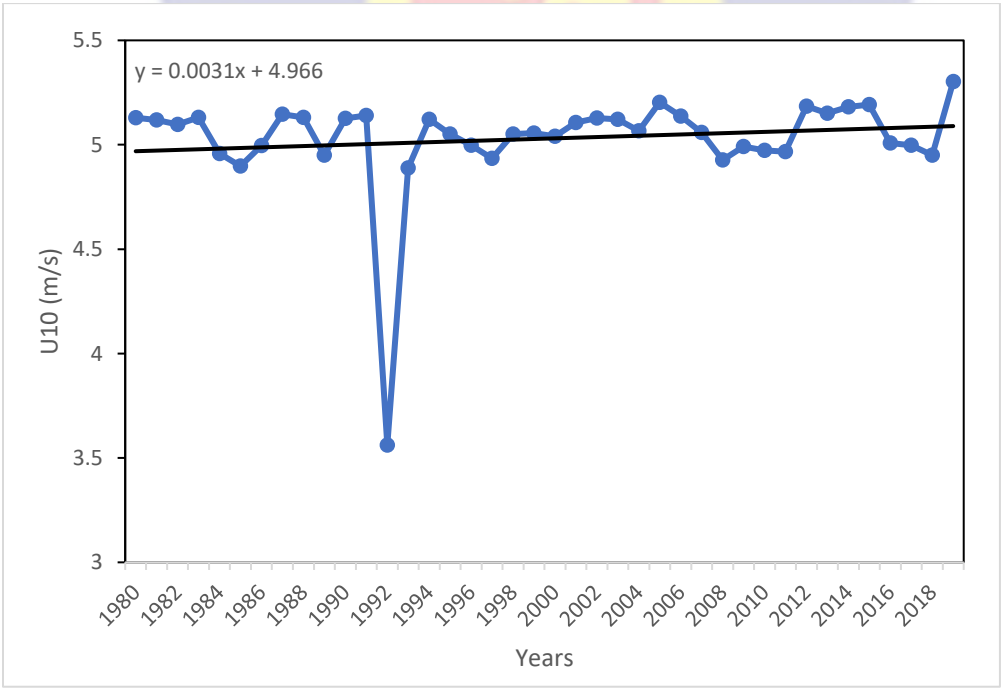

Figure 69: Summer temporal trends in U10 between 1980-2019.

Monthly Analysis

The spatial distribution (Figure 70) and monthly mean (Table 7) of trends confirmed the result shown by the seasonal analysis. All the months except October showed an increasing trend in mean wind speed on average. The observed spatial distribution of trends in October shows weakening of the increasing trend offshore in this month thereby leading to a negative average shown in Table **7**. Higher values of increase up to 5.7 x 10^{-3} m/s per year are seen in winter months with a deviation in January, which is most likely the reason for the unique wave parameters (*Hs* and *Tm*) seen a month later in February.

Table 7: Monthly averages of spatial trends in U10

Month	Average U10 Trend (m/s per year)
January	2.33 x 10^{-3}
February	3.638 x 10^{-3}
March	4.008 x 10^{-3}
April	3.645 x 10^{-3}
May	3.461 x 10^{-3}
June	3.489 x 10^{-3}
July	4.539 x 10^{-3}
August	3.38 x 10^{-3}
September	4.133 x 10^{-3}
October	-1.0 x 10^{-3}
November	5.112 x 10^{-3}
December	5.712 x 10^{-3}

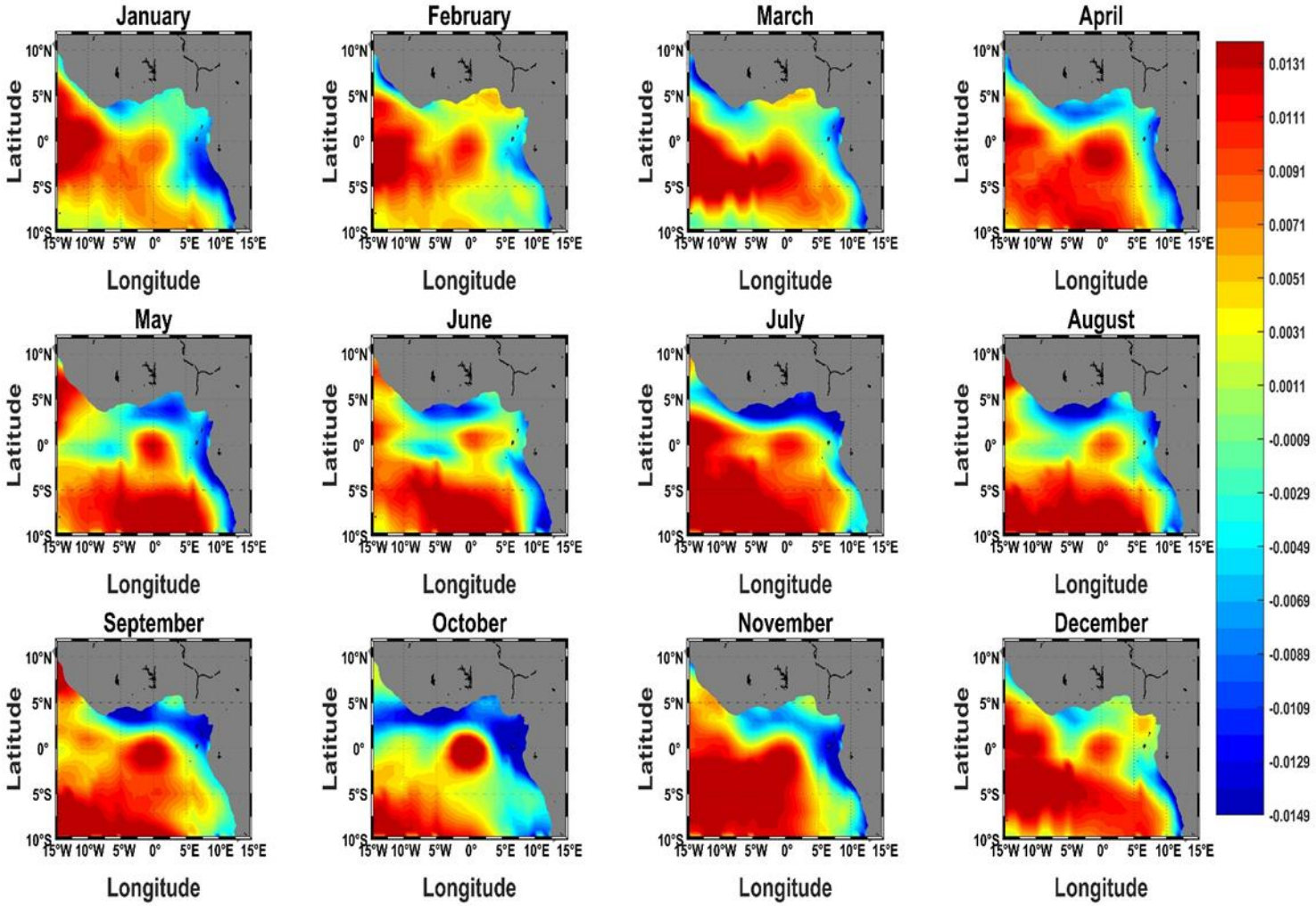

Figure 70: Spatial distribution of monthly trends in U10 between 1980-2019.

Spatial Distribution of 99th Percentile *Hs* or Extreme *Hs*

Annual and Seasonal Analysis

Figures 71 - 73 show the distribution of the 99th percentile of significant wave height in GoG, which can be referred to as the extreme wave heights in the GoG region. The annual average maximum wave height of 2.4290 m shows that the region experiences relatively low and regular waves.

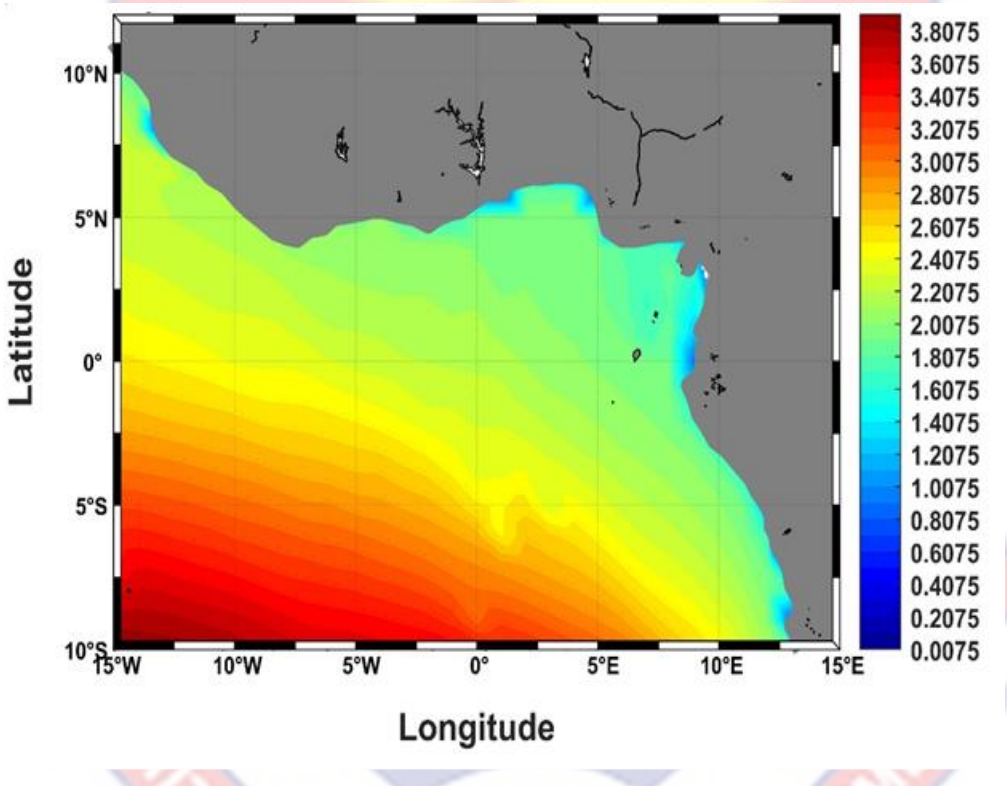

Figure 71: Spatial distribution of annual extreme *Hs* in GoG between 1980-2019.

The seasonal analysis of extreme wave height shows that the extreme values are higher in summer than in winter with average of 1.7763 m for winter and 2.4084 m for summer. Generally, the extremes are higher offshore than nearshore in both seasons. Though values as high as 3.8 m are seen offshore during summer (Figure

73), the winter values are generally low even less than 0.2 m (Figure 72) in some cases.

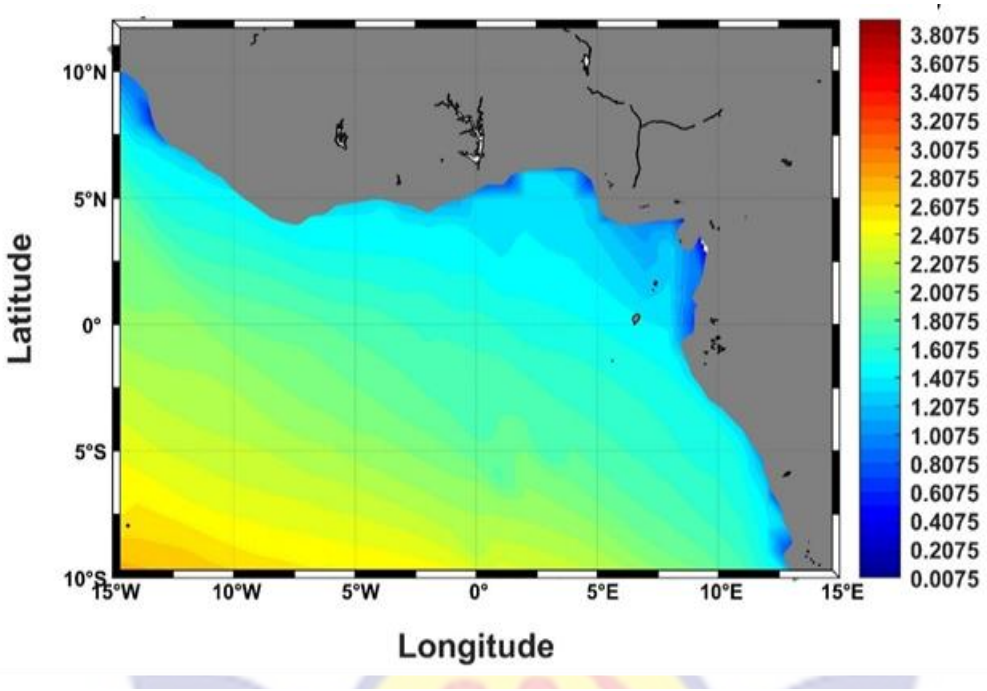

Figure 72: Spatial distribution of winter extreme *Hs* in GoG between 1980-2019.

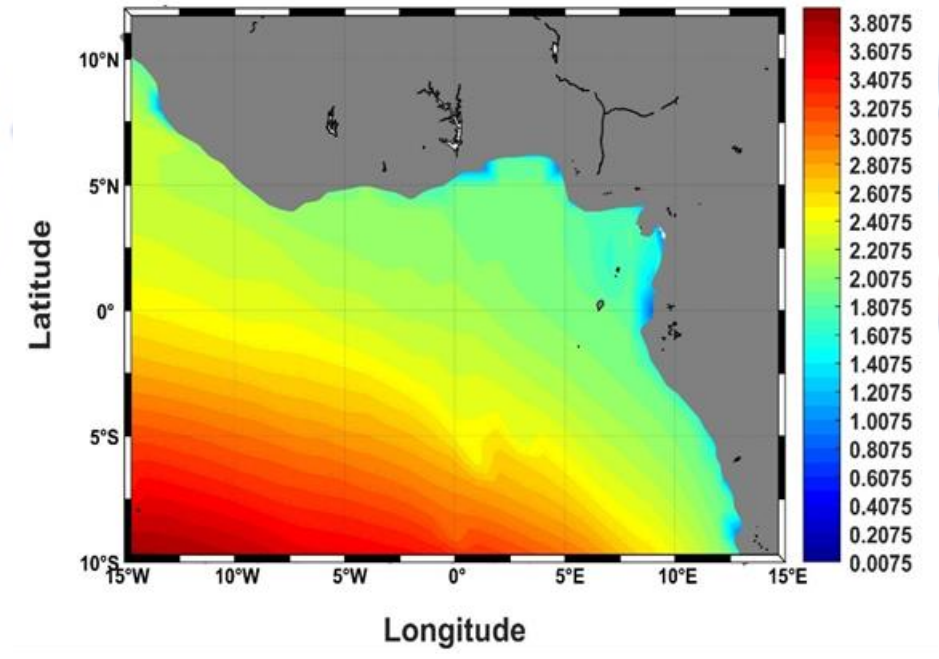

Figure 73: Spatial distribution of summer extreme *Hs* in GoG between 1980-2019.

Spatio-Temporal Distribution of Trend of Extreme *Hs*

Annual and Seasonal Analysis

With regards to the evolution of the extreme wave conditions between the years covered in this study (1980-2019), a trend assessment was done and presented in Figures 74 - 78. From values shown on spatial distribution in Figure 74 and the slope of the regression line in Figure 75, an annual increase of averagely 7.4 x 10^{-3} m per year was experienced in GoG between 1980-2019.

From the seasonal variations of the trends of extreme wave height shown in Figures 76 - 78, it can be observed from the spatial distribution that the average extreme of *Hs* in winter (Figure 76) is lower than summer (Figure 78:) with values of 1.6 x 10^{-3} m per year (Figure 77) and 8.3 x 10^{-3} m per year (Figure 78) respectively.

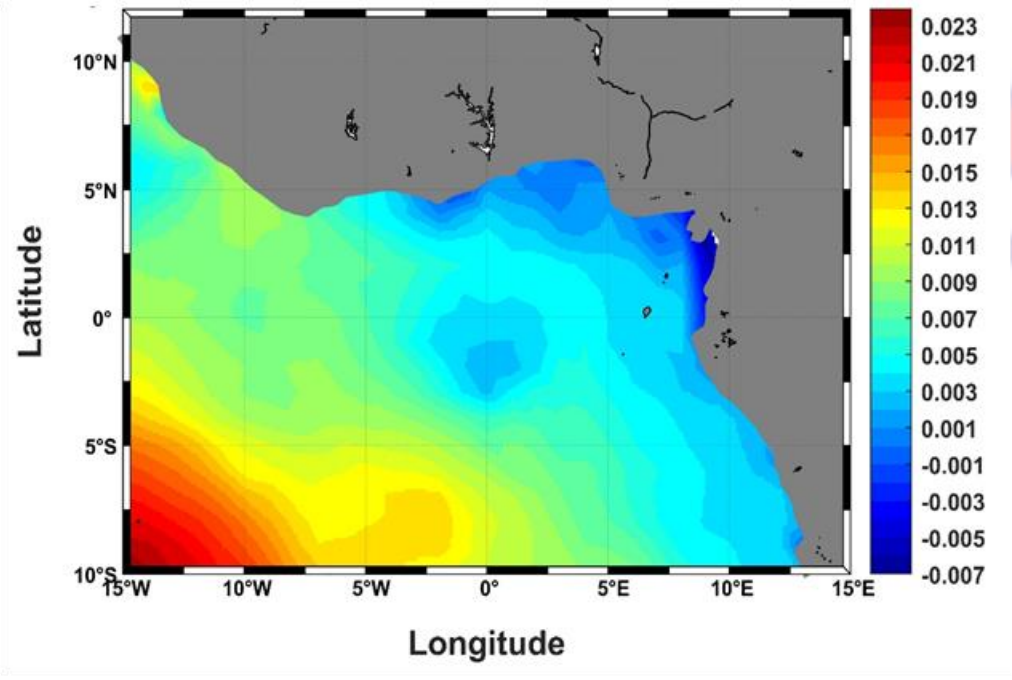

Figure 74: Spatial distribution of annual trend of extreme *Hs* in GoG between 1980-2019.

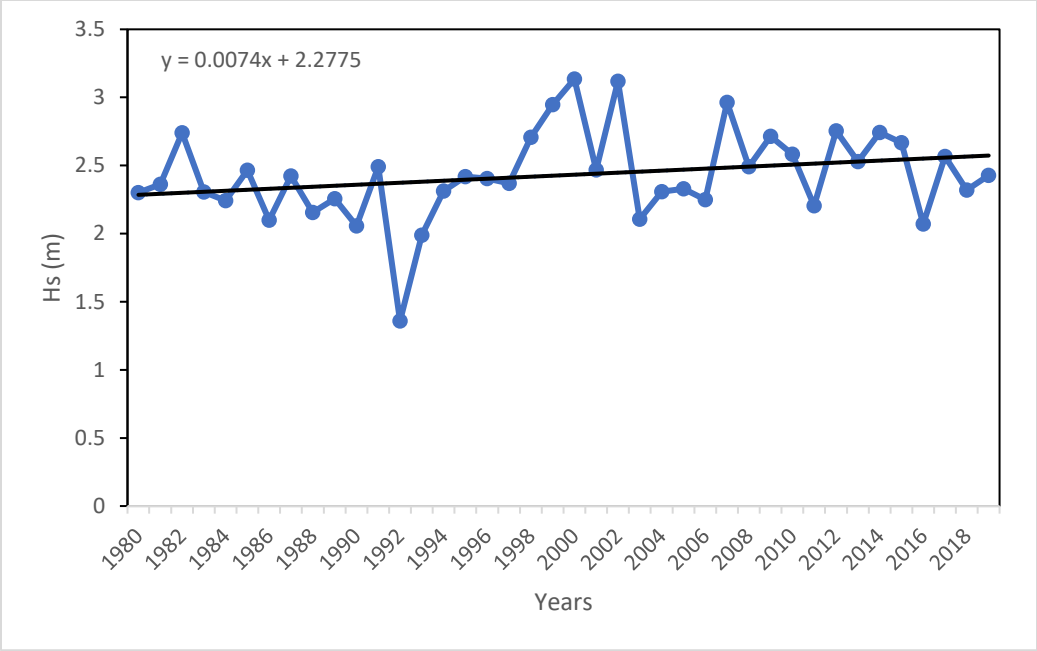

Figure 75: Annual temporal trend of extreme *Hs* in GoG between 1980-2019.

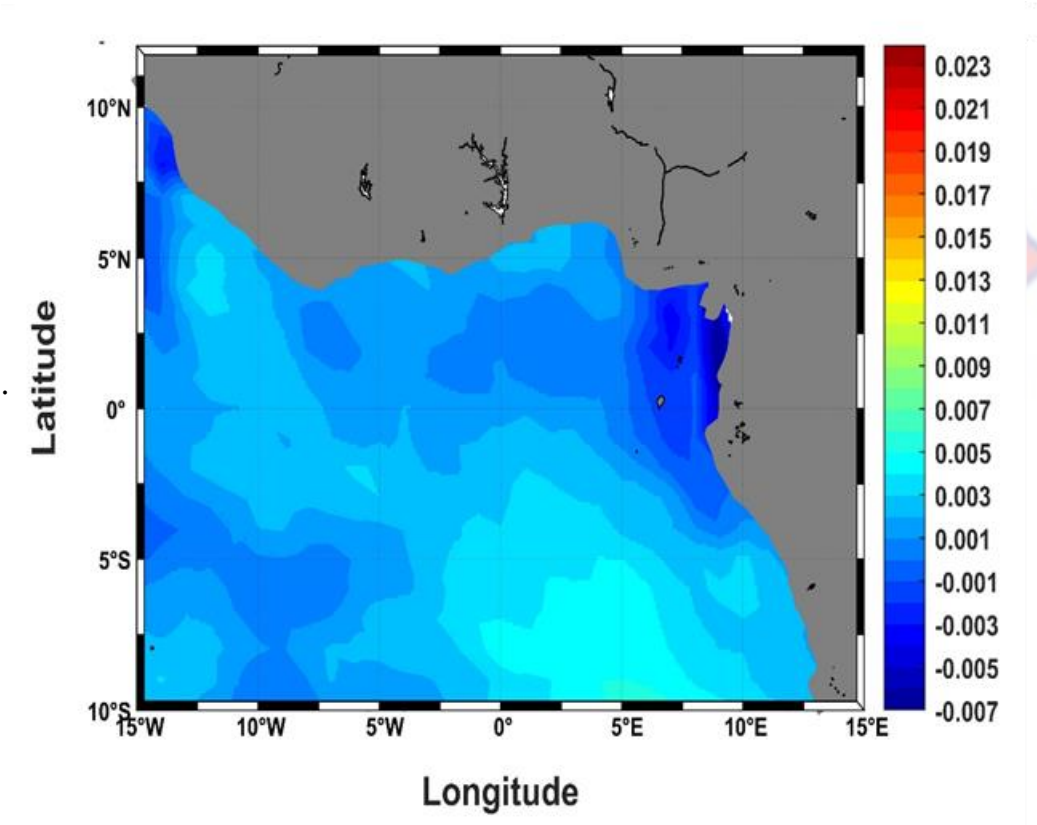

Figure 76: Spatial distribution of winter trend of extreme *Hs* in GoG between 1980-2019.

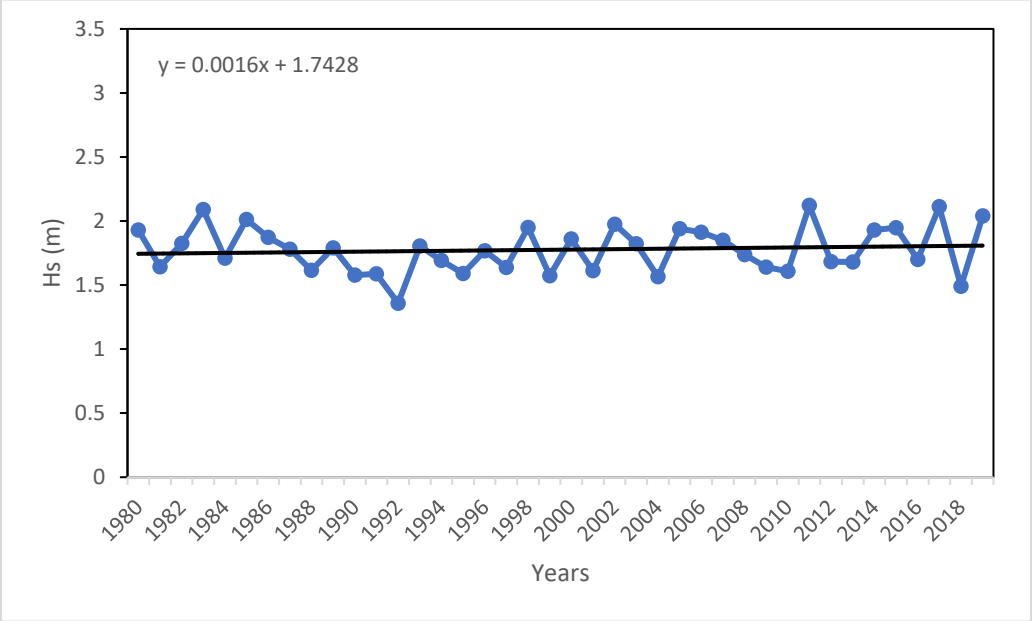

Figure 77: Winter temporal trend of extreme *Hs* in GoG between 1980-2019.

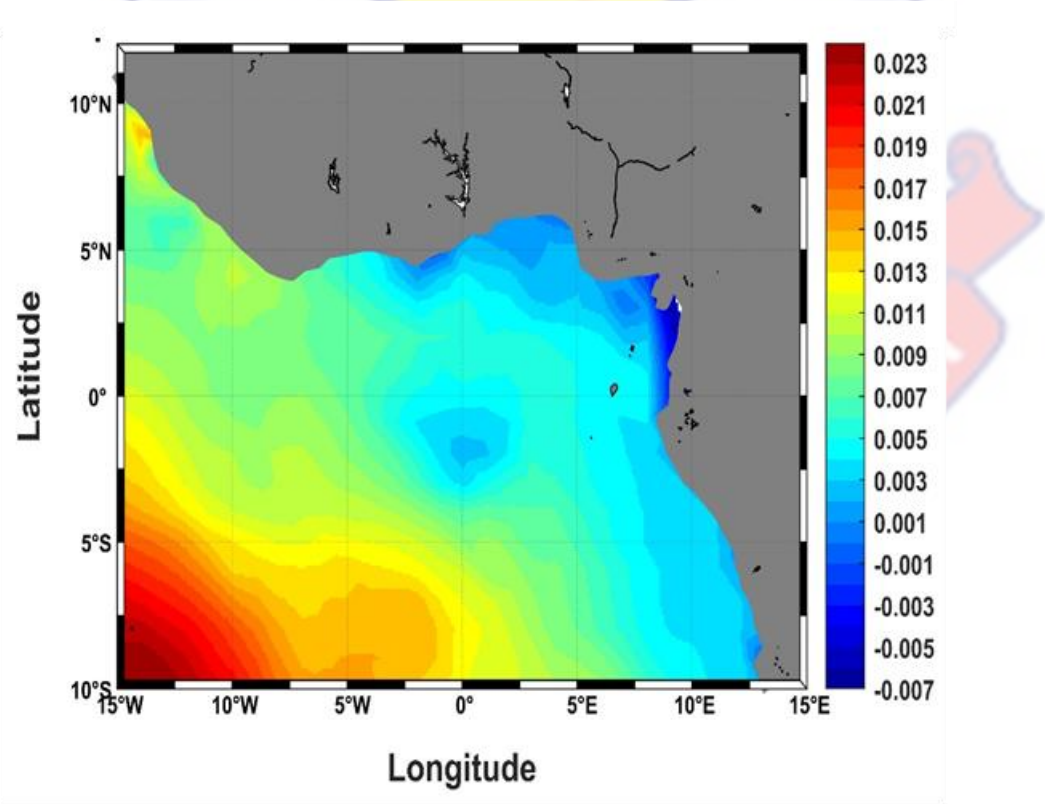

Figure 78: Spatial distribution of summer trend of extreme *Hs* in GoG between 1980-2019.

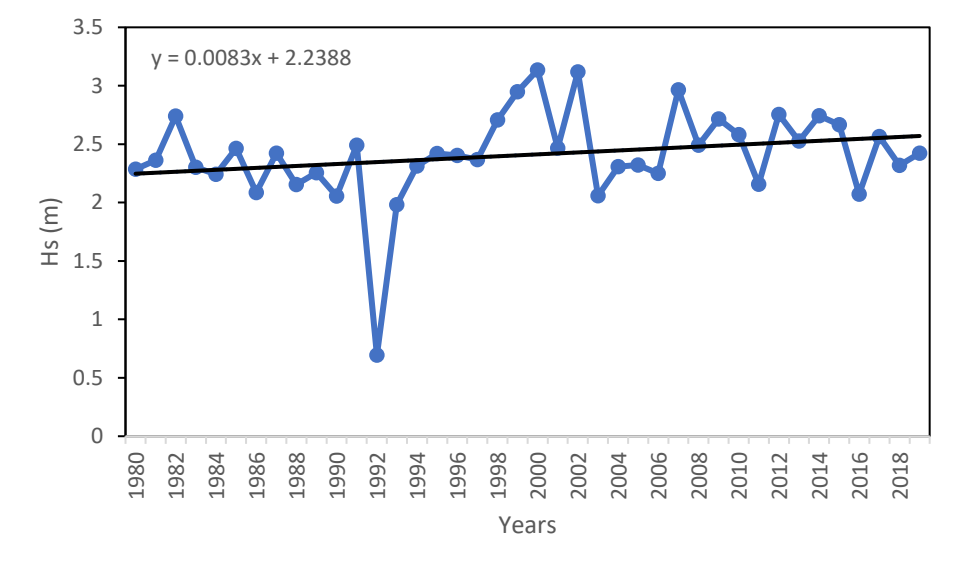

Figure 79: Summer temporal trend of extreme *Hs* in GoG between 1980-2019.

Prediction of Extreme Wave Events

Prediction of extreme wave events for different return periods of 2, 5, 10, 25, 50 and 100 years for this study is done using the Gumbel distribution scheme as used in Young et al. (2012). This relies on the extreme wave conditions (99^{th} percentile) discussed in the last section. This is more or less the maximum significant wave height for each point and period.

These extreme values can be estimated in various ways one of which is the use of statistical quantities like 99^{th} percentile employed in this study. This approach means that the results presented here have the likelihood of being exceeded by only 1% within the years specified by the return period. Therefore, values shown for return periods of 100 years are likely to be exceed only once in every 100 years. As a result of the unavailability of data covering up to 100 years, these extreme wave conditions are usually statistically projected using the available

data relying on probability distribution function such as Gumbel Distribution (Gumbel, 1958) employed in this study.

Annual Analysis

The spatial distribution of the *Hs*, for the various return periods are shown in Figure 80. The average values for 2, 5, 10, 25, 50 and 100 years return periods estimated for this study are 2.2892 m, 2.2892 m, 2.6202 m, 2.6928 m, 3.1128 m, 3.3792 m and 3.5786 m, respectively. This means that before the end of the 2100 century, if the wave climate follows the same trend as seen within the last forty years, waves as high as 3.5 m (Figure *86*) can be expected within some part of the GoG region though higher waves of *Hs* about 6 m can be seen offshore (Figure 83). The bar plot shown in Figure 86 shows the gradual increase of *Hs* projected for the GoG region.

Seasonal Analysis

On a seasonal basis, distributions similar to that seen on the annual basis can be observed in the summer (Figure 82) and winter (Figure 81) though with seasonal variations across the various return periods. It can be confirmed that by the end of the century, *Hs* values higher than 3.5 m should be expected on average in the GoG in both winter (Figure 84) and summer (Figure 85).

These results for return periods as well as the average conditions shown in Figure 86 agree with the findings of Osinowo et al. (2018) for the GoG. Global studies by Rueda et al. (2017) and (Serafin et al., 2019)have also projected similar values of extreme *Hs* for the GoG region before the end of the century.

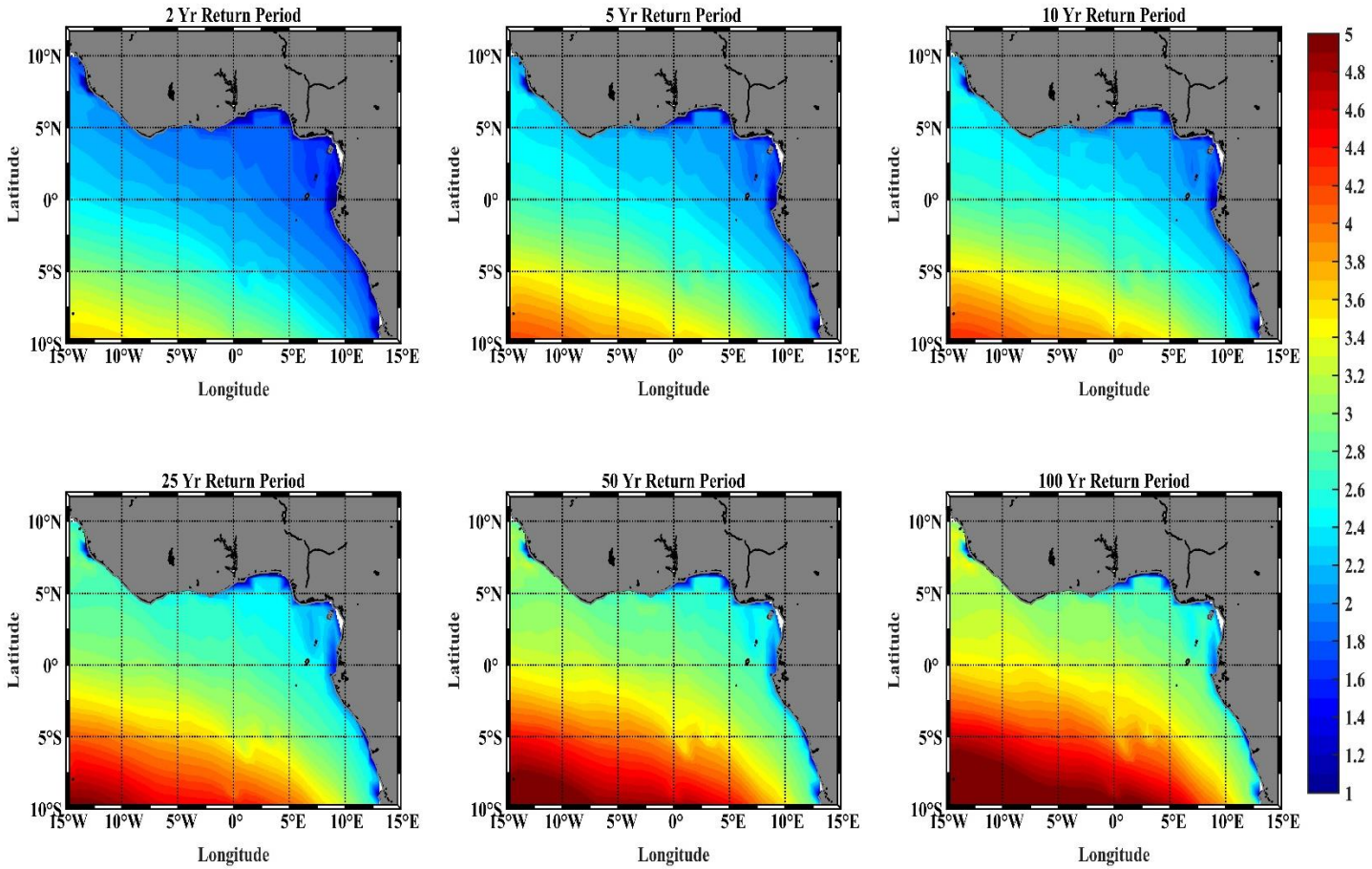

Figure 80: Spatial distribution of annual extreme Hs for various return periods in GoG.

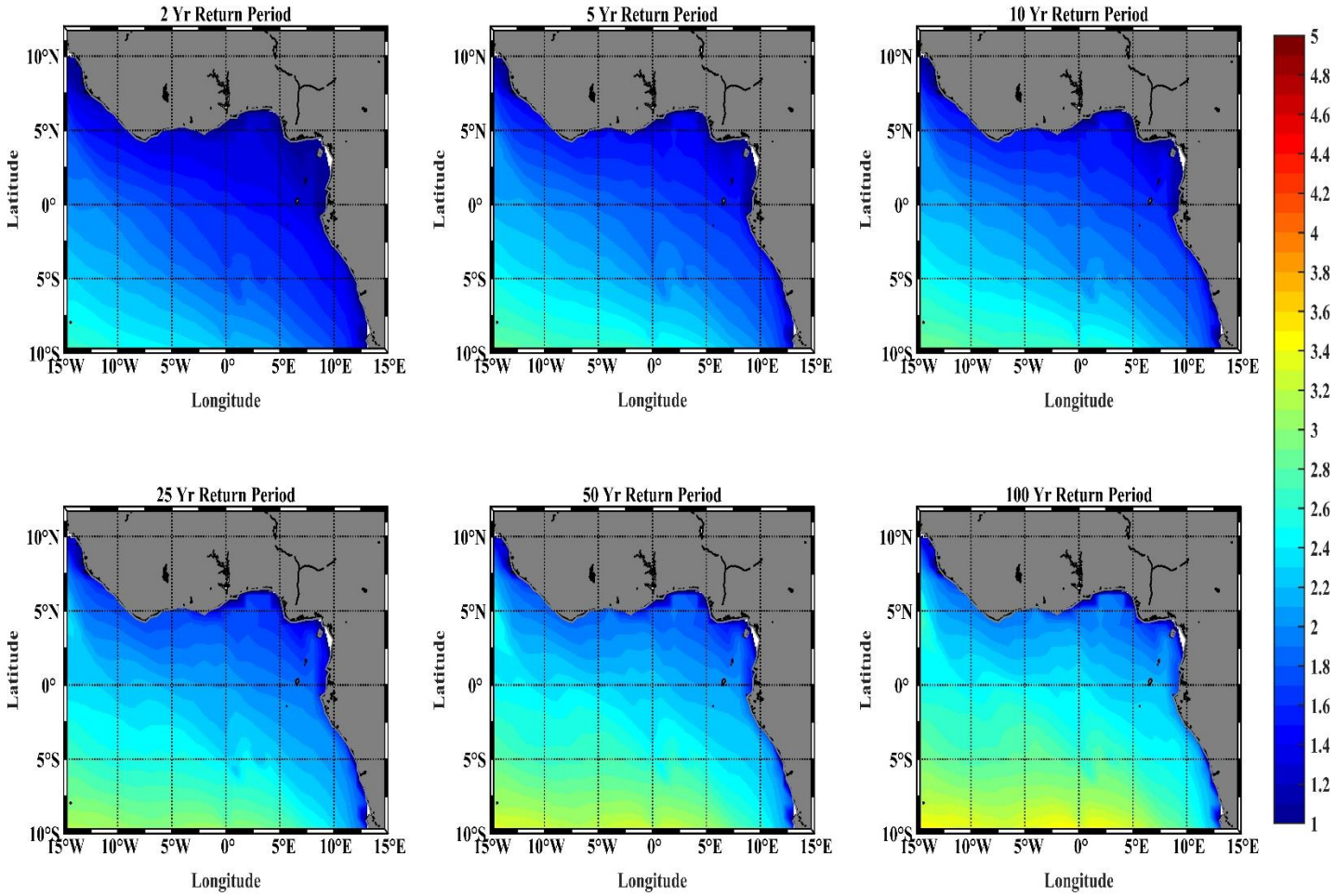

Figure 81: Spatial distribution of winter extreme Hs for various return periods in GoG.

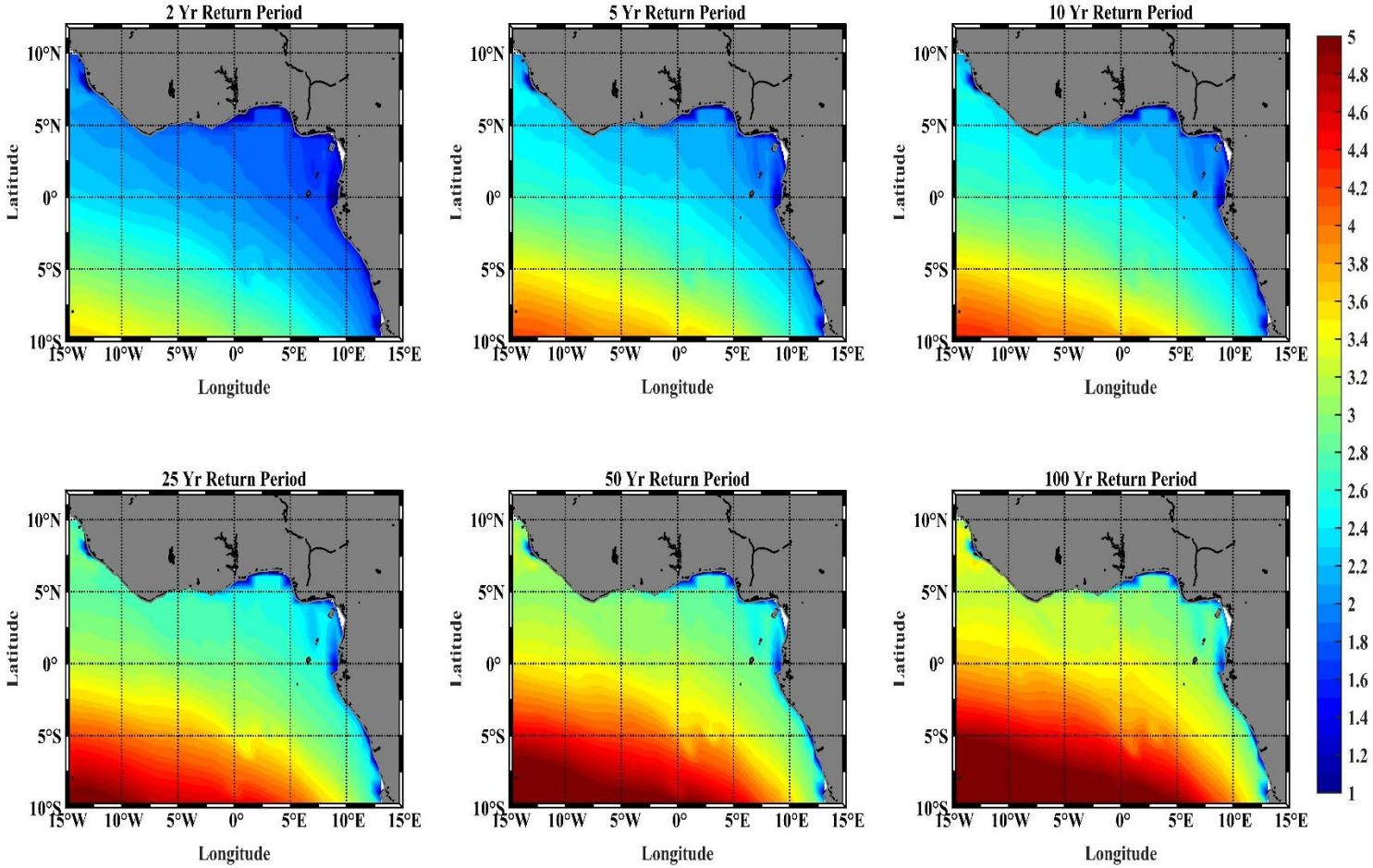

Figure 82: Spatial distribution of summer extreme Hs for variousr return periods in GoG.

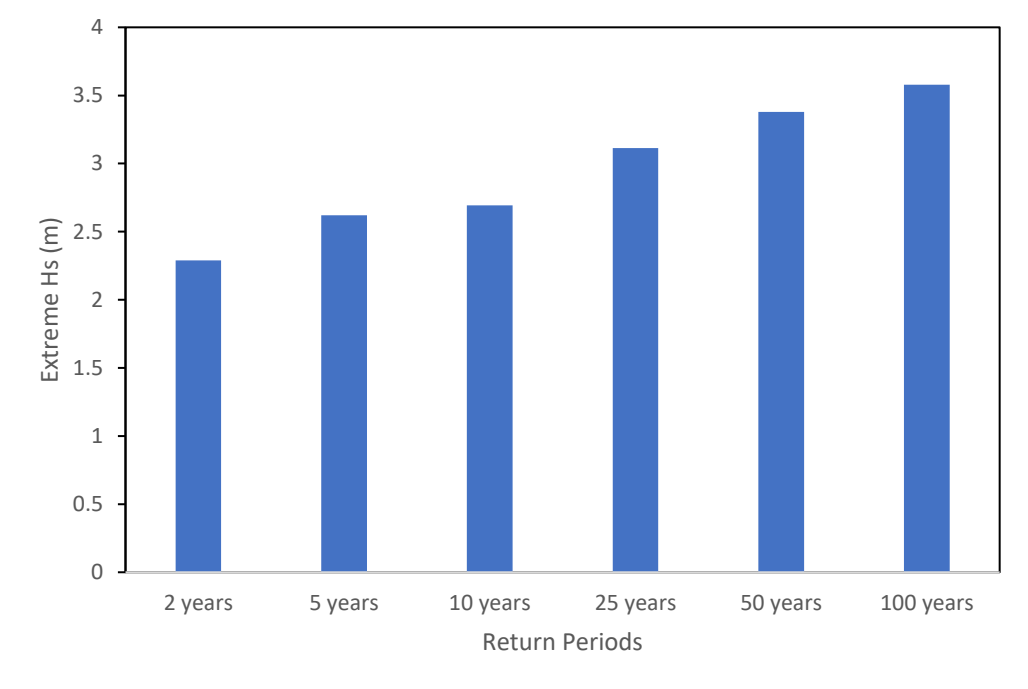

Figure 83: Bar plots of annual extreme *Hs* for various return periods in GoG.

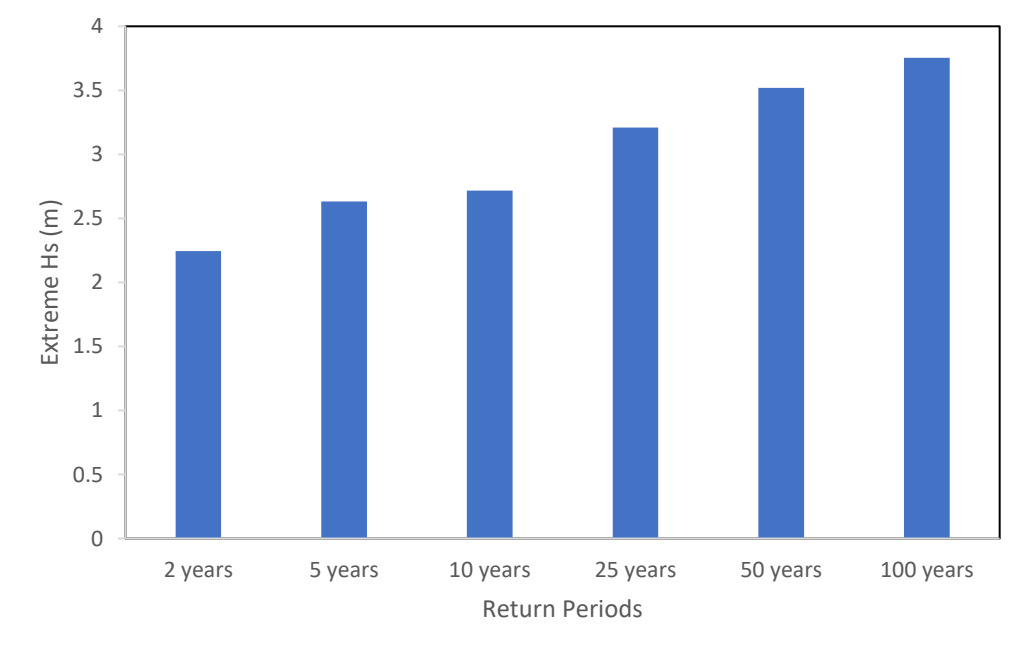

Figure 84: Bar plots of winter extreme *Hs* for various return periods in GoG.

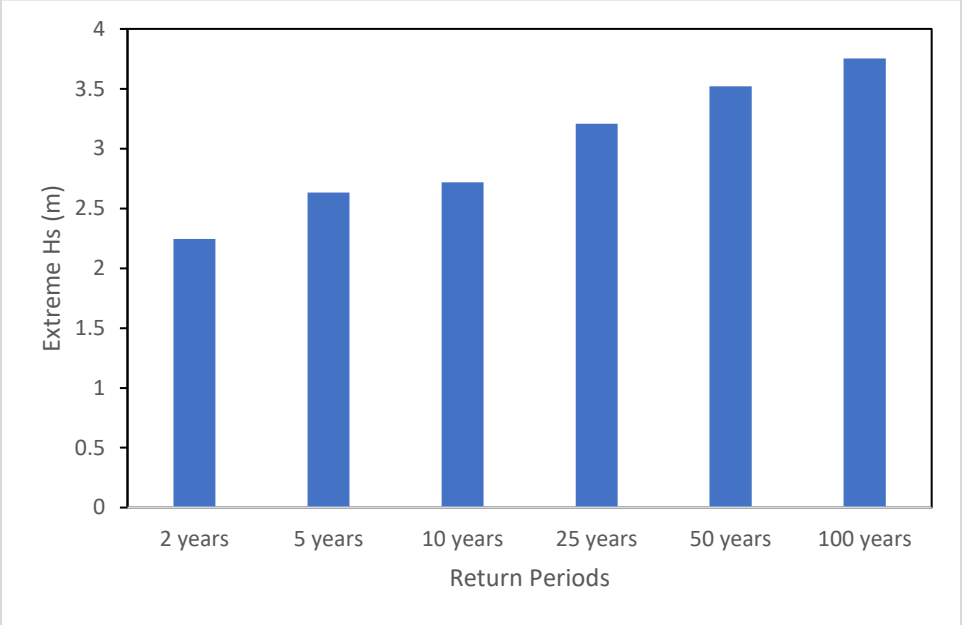

Figure 85: Bar plots of summer extreme *Hs* for various return periods in GoG.

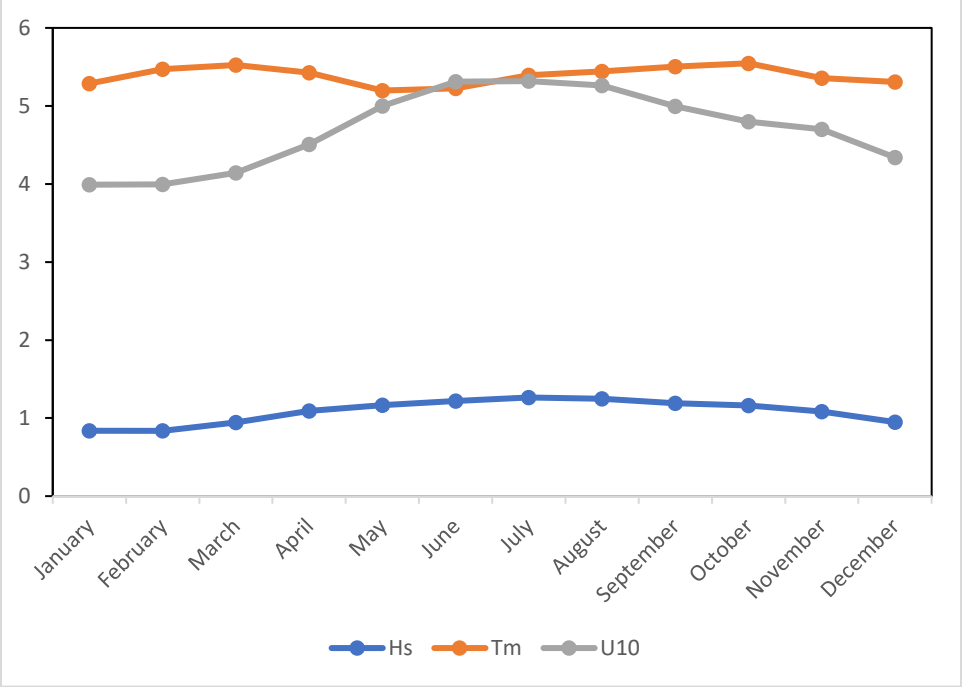

Figure 86: Plots of monthly *Hs*, *Tm* and U10 for GoG between 1980-2019.

Inter-basin Teleconnection and Coastal Structures Influence Assessment

To access the influence of other oceanic phenomena like ENSO and also the impacts of construction of coastal structures like sea defense systems including jetties, groins, ports etc., an equality of mean test using one-way ANOVA was done on yearly and decadal basis. The coast of Ghana was chosen for the assessment of the impacts of coastal structures because it is one of the most recently engineered coasts in West Africa.

Years with major ENSO events were selected to compare with the years before and after the ENSO events for the whole GoG. These major ENSO years are 1982-1983, 1997-1998 and 2014-2016. For the ENSO years 1982-1983, the pre-ENSO and post-ENSO years were chosen to be 1980-1981 and 1984-1985 respectively. Also, for the ENSO years 1997-1998, the pre-ENSO and post-ENSO years were chosen to be 1995-1996 and 1999-2000 respectively. Likewise, for the ENSO years 2014-2016, the pre-ENSO and post-ENSO years were chosen to be 2011-2013 and 2017-2019 respectively.

The one-way ANOVA test carried out for the three ENSO events captured during the period covered by this study showed that there is no significant difference between the years before or years after the ENSO events. These results for both one -way ANOVA and Tukey Honest Significant Difference test done to confirm the results for the three ENSO events are shown by Figures B1-B6 and Tables B1-B3 in Appendix B. These can be interpreted as no significant influence from the ENSO events on the wave climate of the GoG.

The assessment of the influence of coastal structures on the wave conditions in the coast of Ghana can be seen from the results of the comparison of mean test shown in Figures C1-C4 and Tables C1-C2 in Appendix C. It can be observed that the changes in wave height is not periodical during the period 1980-2019. The decadal plots and analysis (Figures C1 and C2 and Table C1) showed that the average *Hs* between 1980-2019 are not significantly different on decadal basis. This statistically unchanging decadal wave height is contradicted by the assessment of the averages on annual basis which showed a contrary result. This is confirmed by the pictorial representation of the Tukey test done on annual basis shown in Figure C4. This can be interpreted by checking for overlaps of the average wave height (shown by the circle) and the range (shown by the two ends of the line) between one year and the others. Years where there are overlaps are interpreted as not significantly different from one another and vice-versa.

This irregular nature of this variation in *Hs* makes it unreliable to assert that these changes are due to either the teleconnection with other ocean basins or construction of coastal structures within the time frame of the study.

The teleconnection between the wave power in North Atlantic and ENSO events found by Reguero et al. (2019) could not be confirmed by the findings in this study. This is most likely due to the fact that the study by Reguero et al. (2019) focused on the European part of the North Atlantic which might have influenced their findings. Nevertheless, the influence of ENSO has been linked to the very low values of *Hs* experienced in 1992 throughout the GoG. This was linked to

weakening of the West African Monsoon as reported by Zheng and Li (2015) and confirmed by Osinowo et al. (2018).

Chapter Summary

The findings in this study have been presented in this chapter with the validation statistics (error metrics) showing that the model adopted, WW3 is a ble to effectively simulate the wave conditions in the GoG. The major findings here include the importance of the influence of the ocean swell originating in the north-western part of the Atlantic Ocean on the wave climate in the GoG. This influence is especially noticed on the wave period through the seasonal variations.

The trend analysis carried out showed that the wave and winds parameters considered in this study have been experiencing changes within the years covered. This change is mostly an increasing trend in most parts of the GoG for *Hs*, *Tm* and U10. It was also seen that this change varies spatially from offshore coastward and east-west.

The statistical forecast done for various return periods showed that the increase of *Hs* will continue through the end of the century with increasing frequency of extreme wave conditions in both dry and wet seasons.

CHAPTER FIVE

SUMMARY, CONCLUSIONS AND RECOMMENDATIONS

Summary

Due to the global impacts of climate change, a need to access the changes in wave condition of the GoG region has been established in this study. This is because wave is one of the most impacted hydrodynamic processes by climate change. As a result of the fact that surface waves are wind-driven and therefore directly influenced by the changes in the atmosphere-ocean interchange, proper understanding of their trends need to be continuously monitored. Despite this susceptibility to climate change impact, studies have not paid much attention to wave climate compared to sea level rise. This gap needs to be filled due to the importance of waves in shaping the coast and its ecosystems. This is especially important in a region like the GoG with very low adaptive and coping capacity to the impacts of climate change as a result of the economic status of the region. Therefore, there is need to closely monitor the evolution of wave conditions based on reliable data. This need motivated the modelling of needed data and assessment of the wave climate in the region on a spatio-temporal scale significant to make scientific conclusion about the trends.

One of the most discussed cause of inadequate studies of the ocean parameters in the GoG is lack of data on spatio-temporal scales to encourage such studies. Waves observation data, for example, is difficult to find in the GoG due to unavailability and when available they are not freely available to researchers. Therefore, the modelling approach was chosen due to relatively lower cost

compared to in-situ observation. Wave models have the ability to reproduce wave conditions for the past, present and future as has been validated in previous studies. WAVEWATCH III, one of the third-generation wave spectral models, was employed in this study due to it open-source nature and ease of use. It has been proven to be effective for wave simulations in previous studies within and outside the GoG.

The WW3 model domain for this study was defined to cover the whole mid-Atlantic Ocean to enable validation against buoys used in this study. The model relied on the ETOPO1 bathymetric data and the ERA5 wind field data for the ocean wave simulation done in this study. The spatial grid was defined as 0.1^{o} x 0.1^{o} whereas the temporal grid was 6-hourly. The three bulk wave parameters *Hs*, *Tm* and *Dm* as well as wind speed was archived for the assessment done in this study. To ascertain the reliability of the model generated data, validations were done against buoy data as well as other wave model databases i.e., ECMWF ERA5 and CMEMS MFWAM. These validations were done using various error metrics including correlation coefficient, root-mean-square error, standard deviation and bias. Most of the analyses including trend, extreme wave projections, one-way ANOVA etc were done using MATLAB functions.

The outcomes of this research have provided very important validated wave conditions data for the Gulf of Guinea (GoG) region of West Africa. Various validation statistics showed very good agreement between WW3 and in-situ observation as well as other wave model databases. It was also shown that the

differences between databases are mostly close to the coast and small islands where the influence of bathymetry is more pronounced.

The assessment of the average wave conditions in the GoG between 1980 and 2019 showed that the region has relatively uniform wave conditions though with some spatial variations. For example, *Hs* and U10 showed similar south to north and west to east increasing pattern in the GoG. The previously reported predominant S-SW wave direction was also seen in this study. The mean wave period showed little spatial variation except for the north western part where the influence of the North-Atlantic Swell is predominant. The seasonal distribution of this parameters also confirmed higher values of *Hs*, *Tm* and U10 in the rainy season (summer) compared to the dry season (winter).

The assessment of the wave climate done with this data shows that the wave conditions in the studied region has been changing between years 1980 and 2019. The annual, seasonal and monthly analysis done for the three wave parameters and one wind parameter showed similar trends of increase basin-wide. The projection for various return periods done based on these data also showed a high likelihood of extreme wave condition in the region before the end of the current century in 2100. However, the one-way ANOVA done to check for likely ENSO and coastal structures influences could not confirm the contributions from these sources to the changing wave climate in the GoG.

Due to continuous influx of people to coastal cities, it is expected that more people will be exposed to the impact of climate change especially those whose livelihood depend on coastal and offshore infrastructures.

Conclusion

From the various validation results shown in the result and discussion chapter, it can be concluded that WW3 is an effective model for simulating wave condition in the Gulf of Guinea. It also showed that the higher the spatio-temporal resolution of a model, the better it is able to efficiently replicate in-situ ocean surface wave data. Therefore, future studies should take advantage of the data assimilation option in WW3 when more in-situ observation are available for the GoG.

This study confirms the global changes projected for wave conditions through the positive trends showed by the *Hs*, *Tm* and U10. This increase in the average conditions of wave also resulted in the increase frequency of the extreme wave conditions. This increase in extreme wave conditions is expected to lead to more severe erosion on the coast and more frequent storm surge due to the projected increase in the wind speed in the region. The increasing trend observed in U10 both offshore and close to the coast suggests that both winds seas generated close to the coast as well as ocean swells generated offshore will experience more increase in the future leading to more severe impacts of climate change on wave conditions and consequently on coastal areas in the GoG.

The influence of the North Atlantic swell in the GoG which is not usually emphasized was seen in this study. This influence was captured in this study because of the regional scale of the study area. This allowed for a larger view of the wave conditions from different parts thereby giving a clearer picture of various sources of wave which were not captured in previous local scale studies. Hence,

the need to properly account for this minor but impactful swell source in coastal and offshore projects planning in the GoG region. This is important because, as seen in the trend results for *Tm*, this influence has been on the increase especially in winter. This may lead to future higher values of *Hs* in the GoG contrary to what is currently experienced. The North Atlantic Swell is generated from a source closer to the GoG compared to the currently predominant South-Western Atlantic Swell source. This suggests a future likelihood of bigger waves in the GoG owing to the increasing trend of both wave sources. Therefore, this research has provided the knowledge on the past trends in various wave parameters and the likely future changes in the GoG region.

Due to the all-year-round changes seen in the wave and wind parameters assessed in this study, it is difficult to draw conclusion regarding the influence of ENSO and coastal structures. However, they are both contributing factors to the changes observed rather than the major reason for the variabilities in the wave conditions in the GoG. For example, the low *Hs* in 1992 and the high *Hs* in the following years confirmed the influence of ENSO (El Nino and La Nina, respectively) in the GoG region. However, the frequency and time-lag between ENSO events and their effects on the wave conditions in the GoG could not be confirmed. This is because no regular pattern was found in the cycles of these ENSO influence. Also, the equality of mean test done on decadal basis showed no significant difference between the decades considered. This could have suggested the influence of coastal structures had there been a significant change because a

decade is enough time for the effect of coastal structures on wave climate to be captured, if it exists.

Recommendations

The increase in the frequency and severity of extreme wave conditions projected for the GoG in this study requires that more attention should be placed on planning and management of coastal structures. This requires that proper feasibility study and environmental impact assessment be done before governments in the region put up coastal defence systems to increases efficiency and reduce their negative impacts on neighbouring countries or communities.

This recommendation is most urgent in the countries such as Cote d'Iviore in the western part of the GoG. This is because several reports have been made of increasing frequency and severity of storm surges in this part within the last few years.

Recommendation for Further Research

The statistical projection done for the future wave conditions in the GoG needs to be confirmed by carrying out further study to cover the future time-slice. This future scenario should be done using dynamical approach of wave modelling under the different climate change Representative Concentration Pathway (RCP) scenarios.

Another very important further research needed is the application of the data derived from this study to assess the region-wide sediment budget. This will give a better picture of the evolution of sediment transport in the region during the time covered.

REFERENCES

AIT, S. T., Weesakul, S., Dastgheib, A., & Ranasinghe, R. (2014). *Climate Change Driven Variations in Future Longshore Sediment Transport Rates along the Coast of Vietnam*.

Alexander, M. A., Bladé, I., Newman, M., Lanzante, J. R., Lau, N.-C., & Scott, J. D. (2002). The atmospheric bridge: The influence of ENSO teleconnections on air–sea interaction over the global oceans. *Journal of Climate*, *15*(16), 2205–2231.

Allersma, E., & Tilmans, W. M. K. (1993). Coastal conditions in West Africa-A review. *Ocean and Coastal Management*, *19*(3), 199–240. https://doi.org/10.1016/0964-5691(93)90043-X

Almar, R., Kestenare, E., Reyns, J., Jouanno, J., Anthony, E. J., Laibi, R., Hemer, M., Du Penhoat, Y., & Ranasinghe, R. (2015). Response of the Bight of Benin (Gulf of Guinea, West Africa) coastline to anthropogenic and natural forcing, Part1: Wave climate variability and impacts on the longshore sediment transport. *Continental Shelf Research*, *110*, 48–59. https://doi.org/10.1016/j.csr.2015.09.020

Alves, B., Angnuureng, D. B., Morand, P., & Almar, R. (2020). A review on coastal erosion and flooding risks and best management practices in West Africa: what has been done and should be done. *Journal of Coastal Conservation*, *24*(3), 38. https://doi.org/10.1007/s11852-020-00755-7

Alves, J.-H. G. M. (2006). Numerical modeling of ocean swell contributions to the global wind-wave climate. *Ocean Modelling*, *11*(1–2), 98–122.

Anthony, E. J., Almar, R., Besset, M., Reyns, J., Laibi, R., Ranasinghe, R., Abessolo Ondoa, G., & Vacchi, M. (2019). Response of the Bight of Benin (Gulf of Guinea, West Africa) coastline to anthropogenic and natural forcing, Part 2: Sources and patterns of sediment supply, sediment cells, and recent shoreline change. *Continental Shelf Research*, *173*(December 2018), 93–103. https://doi.org/10.1016/j.csr.2018.12.006

Anthony, Edward J., & Blivi, A. B. (1999). Morphosedimentary evolution of a delta-sourced, drift-aligned sand barrier–lagoon complex, western Bight of Benin. *Marine Geology*, *158*(1–4), 161–176. https://doi.org/10.1016/S0025-3227(98)00170-4

Ardhuin, F., Chapron, B., & Collard, F. (2009). Observation of swell dissipation across oceans. *Geophysical Research Letters*, *36*(6).

Barnett, T. P. (1968). On the generation, dissipation, and prediction of ocean wind waves. *Journal of Geophysical Research*, *73*(2), 513–529.

Bird, E. C. F. (1985). *Coastline changes. A global review*.

Booij, N., Ris, R. C., & Holthuijsen, L. H. (1999). A third-generation wave model for coastal regions: 1. Model description and validation. *Journal of Geophysical Research: Oceans*, *104*(C4), 7649–7666. https://doi.org/10.1029/98JC02622

Bouws, E, Draper, L., Shearman, E., Laing, A., Feit, D., Mass, W., Eide, L., Francis, P., Carter, D., & Battjes, J. (1998). *Guide to Wave analysis and forecasting. No. 702*.

Bouws, Eda, Draper, L., Shearman, E. D. R., Laing, A. K., Feit, D., Mass, W., Eide, L. I., Francis, P., Carter, D. J. T., & Battjes, J. A. (1998). Guide to Wave analysis and forecasting. WMO-No. 702. *World Meteorological Organization*.

Brink, K. H., & Robinson, A. R. (2005). *The Global Coastal Ocean-Regional Studies and Syntheses* (Vol. 11). Harvard University Press.

Caires, S., Sterl, A., Bidlot, J. R., Graham, N., & Swail, V. (2004). Intercomparison of different wind–wave reanalyses. *Journal of Climate*, *17*(10), 1893–1913.

Casale, R. (2004). *Natural disasters and sustainable development*. Springer Science & Business Media.

Cavaleri, L, Fox-Kemper, B., & Hemer, M. (2012). Wind waves in the coupled climate system. *Bulletin of the American Meteorological Society*, *93*(11), 1651–1661.

Cavaleri, Luigi, & Rizzoli, P. M. (1981). Wind wave prediction in shallow water: Theory and applications. *Journal of Geophysical Research: Oceans*, *86*(C11), 10961–10973.

Chawla, A., & Tolman, H. L. (2007). Automated grid generation for WAVEWATCH III. *Technical Bulletin*, *254*.

Chowdhury, P., & Behera, M. R. (2017). Effect of long-term wave climate variability on longshore sediment transport along regional coastlines. *Progress in Oceanography*, *156*, 145–153.

Chowdhury, P., & Behera, M. R. (2019). Evaluation of CMIP5 and CORDEX derived wave climate in Indian Ocean. *Climate Dynamics*, *52*(7), 4463–4482.

Chowdhury, P., Behera, M. R., & Reeve, D. E. (2019). Wave climate projections along the Indian coast. *International Journal of Climatology*, *39*(11), 4531–4542.

Chune, S. L., Aouf, L., Bruno, L., & Dalphinet, A. (2019). *Global High Resolution Production Centre GLOBAL_REANALYSIS_WAV_001_032*.

Coëtlogon, G. de, Janicot, S., & Lazar, A. (2010). Intraseasonal variability of the ocean—atmosphere coupling in the Gulf of Guinea during boreal spring and summer. *Quarterly Journal of the Royal Meteorological Society*, *136*(S1), 426–441.

Cowell, P. J., Stive, M. J. F., Niedoroda, A. W., de Vriend, H. J., Swift, D. J. P., Kaminsky, G. M., & Capobianco, M. (2003). The coastal-tract (part 1): a conceptual approach to aggregated modeling of low-order coastal change. *Journal of Coastal Research*, 812–827.

Croitoru, L., Miranda, J. J., & Sarraf, M. (2019). *The cost of coastal zone degradation in west Africa: Benin, Cote d'ivoire, Senegal and Togo*. World Bank.

Crowley, T. J. (2000). Causes of climate change over the past 1000 years. *Science*, *289*(5477), 270–277.

Dastgheib, A., Reyns, J., Thammasittirong, S., Weesakul, S., Thatcher, M., & Ranasinghe, R. (2016). Variations in the wave climate and sediment transport due to climate change along the coast of Vietnam. *Journal of Marine Science and Engineering*, *4*(4), 86.

DNV, G. L. (2017). Recommended practice DNVGL-RP-C205 environmental conditions and environmental loads. *Høvik: DNV GL AS*.

EPA. (2015). Climate Impacts on Coastal areas. *Unitesd States Environmental Protection Agency*, 2–9. http://www3.epa.gov/climatechange/impacts/coasts.html#impactssea

Ewing, J. A. (1971). A numerical wave prediction method for the North Atlantic Ocean. *Deutsche Hydrografische Zeitschrift*, *24*(6), 241–261.

Faye, I. (2010). *Dynamique du trait de côte sur les littoraux sableux de la Mauritanie à la Guinée-Bissau (Afrique de l'Ouest): Approches régionale et locale par photo-interprétation, traitement d'images et analyse de cartes anciennes*.

Faye, I. B. (2010). *Coastline Dynamics on Sandy Littorals from Mauritania to Guinea-Bissau (West Africa): Regional and Local Approach through Photo-Interpretation, Image Processing and Ancient Maps Analysis*. Ph. D. dissertation, 314p.

Field, C. B., Barros, V. R., Dokken, D. J., Mach, K. J., Mastrandrea, M. D., Bilir, T. E., Chatterjee, M., Ebi, K. L., Estrada, Y. O., & Genova, R. C. (2014). IPCC 2014: Summary for policymakers in Climate Change 2014: Impacts, Adaptation, and Vulnerability. Part A: Global and Sectoral Aspects. Contribution of Working Group II to the Fifth Assessment Report of the Intergovernmental Panel on Climate Change. *Contrib. Work. Gr. II to Fifth Assess. Rep. Intergov. Panel Clim. Chang*, 1–32.

Folley, M. (2017). The wave energy resource. *Handbook of Ocean Wave Energy*, *7*, 43–80.

Forristall, G. Z., Ewans, K., Olagnon, M., & Prevosto, M. (2013). The West Africa Swell Project (WASP). *Proceedings of the International Conference on Offshore Mechanics and Arctic Engineering - OMAE*, *2 B*(June). https://doi.org/10.1115/OMAE2013-11264

Fowler, A. M., & Hennessy, K. J. (1995). Potential impacts of global warming on the frequency and magnitude of heavy precipitation. *Natural Hazards*, *11*(3), 283–303.

Fredsøe, J., & Deigaard, R. (1992). *Mechanics of coastal sediment transport* (Vol. 3). World Scientific.

Fyfe, J. C. (2003). Extratropical Southern Hemisphere cyclones: Harbingers of climate change? *Journal of Climate*, *16*(17), 2802–2805.

Garrison, T. (2009). Oceanography: an invitation to marine science. Cengage Learning. *Inc.(Belmont)*.

Garrison, T. S. (2012). *Oceanography: an invitation to marine science*. Cengage Learning.

Germain, J., & Armengol, C. (1999). Gulf of Guinea: a deep offshore opportunity. *The Journal of Energy and Development*, *25*(1), 87–95.

Giardino, A., Di Leo, M., Bragantini, G., De Vroeg, H., Tonnon, P. K., Huisman, B., & De Bel, M. (2015). An integrated sediment management scheme for the coastal area of Batumi (Georgia). *12th International Conference on the Mediterranean Coastal Environment, MEDCOAST 2015*, *2*(1), 703–714.

Giardino, A., Schrijvershof, R., Nederhoff, C. M., De Vroeg, H., Brière, C., Tonnon, P.-K. K., Caires, S., Walstra, D. J., Sosa, J., Van Verseveld, W., Schellekens, J., & Sloff, C. J. (2018). A quantitative assessment of human interventions and climate change on the West African sediment budget. *Ocean and Coastal Management*, *156*(February), 249–265. https://doi.org/10.1016/j.ocecoaman.2017.11.008

Goda, Y. (2010). *Random seas and design of maritime structures*. World scientific.

Grigorieva, V., & Gulev, S. (2008). Extreme waves in visual wave observations by VOS. *Rogue Waves 2008 Workshop, IFREMER, Brest, France*, 13–15.

Grigorieva, V., & Gulev, S. (2006). Extreme wind waves worldwide from the VOS data and their changes over the last 50 years. *Proceedings of 9th International Workshop on Wave Hindcasting and Forecasting, September Victoria, British Columbia, Canada*, 24–29.

Group, S. (1985). Sea Wave Modelling Project (SWAMP). *An Intercomparison Study of Wind Wave Prediction Models, Part, 1*, 3–153.

Group, T. W. (1988). The WAM model—A third generation ocean wave prediction model. *Journal of Physical Oceanography*, *18*(12), 1775–1810.

Guedes Soares, C., & Henriques, A. C. (1996). *Statistical uncertainty in long-term distributions of significant wave height*.

Guerrera, F., Martín-Martín, M., Tramontana, M., Nimon, B., & Essotina Kpémoua, K. (2021). Shoreline Changes and Coastal Erosion: The Case Study of the Coast of Togo (Bight of Benin, West Africa Margin). *Geosciences*, *11*(2), 40.

Gulev, S. K., & Grigorieva, V. (2004). Last century changes in ocean wind wave height from global visual wave data. *Geophysical Research Letters*, *31*(24).

Gulev, S. K., Grigorieva, V., Sterl, A., & Woolf, D. (2003). Assessment of the reliability of wave observations from voluntary observing ships: Insights from the validation of a global wind wave climatology based on voluntary observing ship data. *Journal of Geophysical Research: Oceans*, *108*(C7).

Gumbel, E. J. (1958). *Statistics of extremes*. Columbia university press.

Hanson, J. L., Tracy, B. A., Tolman, H. L., & Scott, R. D. (2009). Pacific hindcast performance of three numerical wave models. *Journal of Atmospheric and Oceanic Technology*, *26*(8), 1614–1633.

Hasselmann, K, Sell, W., Ross, D. B., & Müller, P. (1976). A parametric wave prediction model. *Journal of Physical Oceanography*, *6*(2), 200–228.

Hasselmann, Klaus, Barnett, T. P., Bouws, E., Carlson, H., Cartwright, D. E., Enke, K., Ewing, J. A., Gienapp, H., Hasselmann, D. E., & Kruseman, P. (1973). Measurements of wind-wave growth and swell decay during the Joint North Sea Wave Project (JONSWAP). *Ergänzungsheft 8-12*.

Hasselmann, S., Hasselmann, K., Bauer, E., Janssen, P., Komen, G. J., Bertolli, L., Lionello, P., Guillaume, A., Cardone, V. J., & Greenwood, J. A. (1988). WAMDI group. *The WAM Model—a Third Generation Ocean Wave Prediction Model. J. Phys. Oceanogr*, *18*, 1775–1810.

Hastenrath, S. (2012). *Climate and Circulation of the Tropics* (Vol. 8). Springer Science & Business Media.

Hemer, M A, Wang, X. L., Church, J. A., & Swail, V. R. (2010). Coordinating global ocean wave climate projections. *Bulletin of the American Meteorological Society*, *91*(4), 451–454.

Hemer, Mark A., Fan, Y., Mori, N., Semedo, A., & Wang, X. L. (2013). Projected changes in wave climate from a multi-model ensemble. *Nature Climate*

Change, *3*(5), 471–476. https://doi.org/10.1038/nclimate1791

Hemer, Mark A, Church, J. A., & Hunter, J. R. (2010). Variability and trends in the directional wave climate of the Southern Hemisphere. *International Journal of Climatology: A Journal of the Royal Meteorological Society*, *30*(4), 475–491.

Hemer, Mark A, & Trenham, C. E. (2016). Evaluation of a CMIP5 derived dynamical global wind wave climate model ensemble. *Ocean Modelling*, *103*, 190–203.

Herbich, J. B., & Walters, T. (1987). *WAVE CLIMATEWave climate BT - Climatology* (p. 922). Springer US. https://doi.org/10.1007/0-387-30749-4_195

Hersbach, H. (2016). The ERA5 Atmospheric Reanalysis. *AGU Fall Meeting Abstracts*, *2016*, NG33D-01.

Hersbach, H., Bell, B., Berrisford, P., Hirahara, S., Horányi, A., Muñoz-Sabater, J., Nicolas, J., Peubey, C., Radu, R., & Schepers, D. (2020). The ERA5 global reanalysis. *Quarterly Journal of the Royal Meteorological Society*, *146*(730), 1999–2049.

Hisaki, Y. (2018). Wave hindcast in the North Pacific area considering the propagation of surface disturbances. *Progress in Oceanography*, *165*, 332–347.

Hoegh-Guldberg, O., & Bruno, J. F. (2010). The impact of climate change on the world's marine ecosystems. *Science*, *328*(5985), 1523–1528.

Holthuijsen, L. H. (2010). *Waves in oceanic and coastal waters*. Cambridge university press.

Houghton, E. (1996). *Climate change 1995: The science of climate change: contribution of working group I to the second assessment report of the Intergovernmental Panel on Climate Change* (Vol. 2). Cambridge University Press.

Ipcc Iii, W. G. (2001). Third assessment report. *Summary for Policymakers.-2001*.

Izaguirre, C., Méndez, F. J., Menéndez, M., & Losada, I. J. (2011). Global extreme wave height variability based on satellite data. *Geophysical Research Letters*, *38*(10).

Izaguirre, C., Mendez, F. J., Menendez, M., Luceño, A., & Losada, I. J. (2010). Extreme wave climate variability in southern Europe using satellite data. *Journal of Geophysical Research: Oceans*, *115*(C4).

Jin, F.-F., Boucharel, J., & Lin, I.-I. (2014). Eastern Pacific tropical cyclones intensified by El Niño delivery of subsurface ocean heat. *Nature*, *516*(7529),

82–85.

Kamphuis, J. W. (2020). *Introduction to coastal engineering and management* (Vol. 48). World Scientific.

Laïbi, R. A., Anthony, E. J., Almar, R., Castelle, B., Senechal, N., & Kestenare, E. (2014). Longshore drift cell development on the human-impacted Bight of Benin sand barrier coast, West Africa. *Journal of Coastal Research*, *70*(70), 78–83. https://doi.org/10.2112/SI70-014.1

Mangor, K., Drønen, N. K., Kærgaard, K. H., & Kristensen, S. E. (2004). *Shoreline management guidelines*.

Margottini, C. (2004). Natural Disasters and Sustainable Development: From Theory to Practice in Italy? In *Natural Disasters and Sustainable Development* (pp. 249–270). Springer.

Massel, S. R. (2017). *Ocean surface waves: their physics and prediction* (Vol. 45). World scientific.

Masselink, G., Austin, M., Scott, T., Poate, T., & Russell, P. (2014). Role of wave forcing, storms and NAO in outer bar dynamics on a high-energy, macro-tidal beach. *Geomorphology*, *226*, 76–93.

Mathiesen, M., Goda, Y., Hawkes, P. J., Mansard, E., Martín, M. J., Peltier, E., Thompson, E. F., & Van Vledder, G. (1994). Recommended practice for extreme wave analysis. *Journal of Hydraulic Research*, *32*(6), 803–814.

McGranahan, G., Balk, D., & Anderson, B. (2007). The rising tide: assessing the risks of climate change and human settlements in low elevation coastal zones. *Environment and Urbanization*, *19*(1), 17–37.

Mendes, D., Souza, E. P., Trigo, I. F., & Miranda, P. M. A. (2007). On precursors of South American cyclogenesis. *Tellus A: Dynamic Meteorology and Oceanography*, *59*(1), 114–121.

Mentaschi, L., Vousdoukas, M. I., Voukouvalas, E., Dosio, A., & Feyen, L. (2017). Global changes of extreme coastal wave energy fluxes triggered by intensified teleconnection patterns. *Geophysical Research Letters*, *44*(5), 2416–2426.

Merrifield, M. A., Thompson, P. R., & Lander, M. (2012). Multidecadal sea level anomalies and trends in the western tropical Pacific. *Geophysical Research Letters*, *39*(13).

Mitsuyasu, H. (1969). On the growth of the spectrum of wind-generated waves, Part II. *Rept. Res. Inst. Appl. Mech., Kyushu Univ.*, *17*, 235–243.

Morim, J., Trenham, C., Hemer, M., Wang, X. L., Mori, N., Casas-Prat, M., Semedo, A., Shimura, T., Timmermans, B., & Camus, P. (2020). A global

ensemble of ocean wave climate projections from CMIP5-driven models. *Scientific Data*, *7*(1), 1–10.

Munk, W. H. (1944). Proposed uniform procedure for observing waves and interpreting instrument records. *Scripps Institution of Oceanography, Wave Project Rep*, *26*, 22.

Munk, W. H. (1951). *Origin and generation of waves*. Scripps Institution of Oceanography La Jolla Calif.

Ndour, A., Laïbi, R. A., Sadio, M., Degbe, C. G. E., Diaw, A. T., Oyédé, L. M., Anthony, E. J., Dussouillez, P., & Sambou, H. (2018). Management strategies for coastal erosion problems in west Africa: Analysis, issues, and constraints drawn from the examples of Senegal and Benin. *Ocean & Coastal Management*, *156*, 92–106.

Ondoa, G. A., Almar, R., Kestenare, E., Bahini, A., Houngue, G. H., Jouanno, J., Du Penhoat, Y., Castelle, B., Melet, A., Meyssignac, B., Anthony, E. J., Laibi, R., Alory, G., & Ranasinghe, R. (2016). Potential of video cameras in assessing event and seasonal coastline behaviour: Grand Popo, Benin (Gulf of Guinea). *Journal of Coastal Research*, *1*(75), 442–446. https://doi.org/10.2112/SI75-089.1

Osinowo, A., Lin, X., Zhao, D., & Wang, Z. (2016). Long-term variability of extreme significant wave height in the South China Sea. *Advances in Meteorology*, *2016*.

Osinowo, A A, Okogbue, E. C., Eresanya, E. O., & Akande, O. S. (2018). Extreme significant wave height climate in the Gulf of Guinea. *African Journal of Marine Science*, *40*(4), 407–421.

Osinowo, Adekunle Ayodotun, Balogun, I. A., & Eresanya, E. O. (2018). Assessment of wave energy resource in the mid-Atlantic based on 37-year numerical hindcast data. *Modeling Earth Systems and Environment*, *4*(3), 935–959.

Ostdiek, V. J., & Bord, D. J. (2012). *Inquiry into physics*. Cengage Learning.

Pachauri, R. K., Allen, M. R., Barros, V. R., Broome, J., Cramer, W., Christ, R., Church, J. A., Clarke, L., Dahe, Q., & Dasgupta, P. (2014). *Climate change 2014: synthesis report. Contribution of Working Groups I, II and III to the fifth assessment report of the Intergovernmental Panel on Climate Change*. Ipcc.

Parry, M. L., Canziani, O. F., Palutikof, J. P., Van Der Linden, P. J., & Hanson, C. E. (2007). IPCC, 2007: climate change 2007: impacts, adaptation and vulnerability. Contribution of working group II to the fourth assessment report of the intergovernmental panel on climate change. *Cambridge Uni-Versity Press, Cambridge, UK*.

Philippart, C. J. M., Anadon, R., Danovaro, R., Dippner, J. W., Drinkwater, K. F., Hawkins, S. J., Oguz, T., O'Sullivan, G., & Reid, P. C. (2007). Impacts of climate change on the European marine and coastal environment: ecosystems approach. ESF Marine Board Position Paper, 9. European Science Foundation, Marine Board: Strasbourg, France. *European Science Foundation, Marine Board, Strasbourg, France*.

Phillips, O. M. (1957). On the generation of waves by turbulent wind. *Journal of Fluid Mechanics*, *2*(5), 417–445.

Prevosto, M., Ewans, K., Forristall, G. Z., & Olagnon, M. (2013). Swell genesis, modelling and measurements in West Africa. *Proceedings of the International Conference on Offshore Mechanics and Arctic Engineering - OMAE*, *2 B*(June). https://doi.org/10.1115/OMAE2013-11201

Programme., U. N. E. (2008). *UNEP climate change strategy*. Author Nairobi.

Ranasinghe, R. (2016). Assessing climate change impacts on open sandy coasts: A review. *Earth-Science Reviews*, *160*, 320–332.

Ranasinghe, R., Duong, T. M., Uhlenbrook, S., Roelvink, D., & Stive, M. (2013). Climate-change impact assessment for inlet-interrupted coastlines. *Nature Climate Change*, *3*(1), 83–87.

Ranasinghe, R., & Stive, M. J. F. (2009). *Rising seas and retreating coastlines*. Springer Netherlands.

Rascle, N., & Ardhuin, F. (2013). A global wave parameter database for geophysical applications. Part 2: Model validation with improved source term parameterization. *Ocean Modelling*, *70*, 174–188.

Rascle, N., Ardhuin, F., Queffeulou, P., & Croizé-Fillon, D. (2008). A global wave parameter database for geophysical applications. Part 1: Wave-current–turbulence interaction parameters for the open ocean based on traditional parameterizations. *Ocean Modelling*, *25*(3–4), 154–171.

Reguero, B. G., Losada, I. J., & Méndez, F. J. (2019). A recent increase in global wave power as a consequence of oceanic warming. *Nature Communications*, *10*(1), 1–14.

Rueda, A., Vitousek, S., Camus, P., Tomás, A., Espejo, A., Losada, I. J., Barnard, P. L., Erikson, L. H., Ruggiero, P., & Reguero, B. G. (2017). A global classification of coastal flood hazard climates associated with large-scale oceanographic forcing. *Scientific Reports*, *7*(1), 1–8.

Sadio, M., Anthony, E. J., Diaw, A. T., Dussouillez, P., Fleury, J. T., Kane, A., Almar, R., & Kestenare, E. (2017). Shoreline changes on the wave-influenced Senegal River delta, West Africa: The roles of natural processes and human interventions. *Water (Switzerland)*, *9*(5).

https://doi.org/10.3390/w9050357

Schwartz, M. (2006). *Encyclopedia of coastal science*. Springer Science & Business Media.

Semedo, A., Saetra, Ø., Rutgersson, A., Kahma, K. K., & Pettersson, H. (2009). Wave-induced wind in the marine boundary layer. *Journal of the Atmospheric Sciences*, *66*(8), 2256–2271.

Semedo, A., SušElj, K., Rutgersson, A., & Sterl, A. (2011). A global view on the wind sea and swell climate and variability from ERA-40. *Journal of Climate*, *24*(5), 1461–1479. https://doi.org/10.1175/2010JCLI3718.1

Semedo, A., Weisse, R., Behrens, A., Sterl, A., Bengtsson, L., & Günther, H. (2012). Projection of global wave climate change toward the end of the twenty-first century. *Journal of Climate*, *26*(21), 8269–8288.

Serafin, K. A., Ruggiero, P., Barnard, P. L., & Stockdon, H. F. (2019). The influence of shelf bathymetry and beach topography on extreme total water levels: Linking large-scale changes of the wave climate to local coastal hazards. *Coastal Engineering*, *150*, 1–17.

Sharma, N., Anderson, S. P., Brickley, P., Nobre, C., & Cadwallader, M. L. (2009). Quantifying the seasonal and interannual variability of the formation and migration pattern of North Brazil Current Rings. *OCEANS 2009*, 1–7.

Short, A. D. (2012). Coastal processes and beaches. *Nature Education Knowledge*, *3*(10), 15.

Sitarz, J. A. (1960). Côtes africaines: Etude des profils d'équilibre de plage. *Trav. Centre d'Etude et de Recherche En Océanographie*, *3*(4), 4362.

Snelgrove, P. V. R. (1999). Getting to the bottom of marine biodiversity: sedimentary habitats: ocean bottoms are the most widespread habitat on earth and support high biodiversity and key ecosystem services. *BioScience*, *49*(2), 129–138.

Soares, C. G., & Scotto, M. (2001). Modelling uncertainty in long-term predictions of significant wave height. *Ocean Engineering*, *28*(3), 329–342.

Sullivan, P. P., Edson, J. B., Hristov, T., & McWilliams, J. C. (2008). Large-eddy simulations and observations of atmospheric marine boundary layers above nonequilibrium surface waves. *Journal of the Atmospheric Sciences*, *65*(4), 1225–1245.

Taylor, K. E. (2001). Summarizing multiple aspects of model performance in a single diagram. *Journal of Geophysical Research: Atmospheres*, *106*(D7), 7183–7192.

Thammasittirong, S., Dastgheib, A., Weesakul, S., & Ranasinghe, R. (2014).

Climate Change Driven Variations in Future Longshore Sediment Transport Rates along the Coast of Vietnam Rev.4. March.

Tolman, H L. (n.d.). the WAVEWATCH III® Development Group (2014). *User Manual and System Documentation of WAVEWATCH III® Version*, *4*.

Tolman, H L. (2010). Practical wind wave modeling. In *Water Waves: Theory and Experiment* (pp. 79–92). World Scientific.

Tolman, Hendrik L. (1989). *The numerical model WAVEWATCH: a third generation model for hindcasting of wind waves on tides in shelf seas*. Faculty of Civil Engineering, Delft University of Technology.

Tolman, Hendrik L. (1991). A third-generation model for wind waves on slowly varying, unsteady, and inhomogeneous depths and currents. *Journal of Physical Oceanography*, *21*(6), 782–797.

Tolman, Hendrik L. (1992). Effects of numerics on the physics in a third-generation wind-wave model. *Journal of Physical Oceanography*, *22*(10), 1095–1111.

Tolman, Hendrik L. (2008). A mosaic approach to wind wave modeling. *Ocean Modelling*, *25*(1–2), 35–47.

Tolman, Hendrik L. (2009). User manual and system documentation of WAVEWATCH III R version 4.07. *Technical Note, MMAB Contribution*, *276*, 220.

Tolman, Hendrik L, Balasubramaniyan, B., Burroughs, L. D., Chalikov, D. V, Chao, Y. Y., Chen, H. S., & Gerald, V. M. (2002). Development and implementation of wind-generated ocean surface wave Modelsat NCEP. *Weather and Forecasting*, *17*(2), 311–333.

Toualy, E., Aman, A., Koffi, P., Marin, F., & Wango, T. E. (2015). Ocean swell variability along the northern coast of the Gulf of Guinea. *African Journal of Marine Science*, *37*(3), 353–361. https://doi.org/10.2989/1814232X.2015.1074940

Tracy, B., Devaliere, E., Hanson, J., Nicolini, T., & Tolman, H. (2007). Wind Sea and Swell Delineation for Numerical Wave Modeling. *10th International Workshop on Wave Hindcasting and Forecasting Coastal Hazard Symposium*, P12. papers2://publication/uuid/BDC84DF4-52C0-4FB7-AC88-5FBEDCE68D4F

Ukwe, C. N., & Ibe, C. A. (2010). A regional collaborative approach in transboundary pollution management in the guinea current region of western Africa. *Ocean & Coastal Management*, *53*(9), 493–506.

Vanem, E. (2015). Uncertainties in extreme value modelling of wave data in a climate change perspective. *Journal of Ocean Engineering and Marine*

Energy, *1*(4), 339–359.

Wang, X. L., Feng, Y., & Swail, V. R. (2014). Changes in global ocean wave heights as projected using multimodel CMIP5 simulations. *Geophysical Research Letters*, *41*(3), 1026–1034.

Wang, X. L., & Swail, V. R. (2001). Changes of extreme wave heights in Northern Hemisphere oceans and related atmospheric circulation regimes. *Journal of Climate*, *14*(10), 2204–2221.

Wang, X. L., & Swail, V. R. (2002). Trends of Atlantic wave extremes as simulated in a 40-yr wave hindcast using kinematically reanalyzed wind fields. *Journal of Climate*, *15*(9), 1020–1035.

Wang, X. L., & Swail, V. R. (2006). Climate change signal and uncertainty in projections of ocean wave heights. *Climate Dynamics*, *26*(2–3), 109–126.

Wang, X. L., Swail, V. R., Zwiers, F. W., Zhang, X., & Feng, Y. (2009). Detection of external influence on trends of atmospheric storminess and northern oceans wave heights. *Climate Dynamics*, *32*(2–3), 189–203.

Wang, X. L., Zwiers, F. W., & Swail, V. R. (2004). North Atlantic ocean wave climate change scenarios for the twenty-first century. *Journal of Climate*, *17*(12), 2368–2383.

Wellens-Mensah, J., Armah, A. K., Amlalo, D. S., & Tetteh, K. (2002). Ghana national report phase 1: integrated problem analysis. *GEF MSP Sub-Saharan Africa Project (GF/6010-0016): Development and Protection of the Coastal and Marine Environment in Sub-Saharan Africa. Accra, Ghana*.

Wessel, P., & Smith, W. H. F. (1996). A global, self-consistent, hierarchical, high-resolution shoreline database. *Journal of Geophysical Research: Solid Earth*, *101*(B4), 8741–8743.

Wiafe, G., & Nyadjro, E. S. (2015). Satellite observations of upwelling in the Gulf of Guinea. *IEEE Geoscience and Remote Sensing Letters*, *12*(5), 1066–1070.

Wiegel, R. L. (2013). *Oceanographical engineering*. Courier Corporation.

Wigley, G. Y. (2007). Schellnhuber, HJ, W. Cramer, N. Nakicenivic, T. *Meteorologische Zeitschrift*, *16*(4), 461–463.

Wilks, D. S. (2011). *Statistical methods in the atmospheric sciences* (Vol. 100). Academic press.

Woolf, D. K., Challenor, P. G., & Cotton, P. D. (2002). Variability and predictability of the North Atlantic wave climate. *Journal of Geophysical Research: Oceans*, *107*(C10), 1–9.

Wright, L. D., & Short, A. D. (1984). Morphodynamic variability of surf zones and beaches: a synthesis. *Marine Geology*, *56*(1–4), 93–118.

WW3DG, 2019, WW3DG, User Manual and System Documentation of WAVEWATCH III Version 6.07, the W. I. D. G. T. N. 316, (2019), N., Url:, & Https://github.com/NOAA-EMC/WW3/wiki/files/manual.pdf. (2019). *User manual and system documentation of WAVEWATCH III*. *333*.

Yang, X.-Y., Huang, R. X., & Wang, D. X. (2007). Decadal changes of wind stress over the Southern Ocean associated with Antarctic ozone depletion. *Journal of Climate*, *20*(14), 3395–3410.

Young, I. R., Vinoth, J., Zieger, S., & Babanin, A. V. (2012). Investigation of trends in extreme value wave height and wind speed. *Journal of Geophysical Research: Oceans*, *117*(C11).

Young, I. R., Zieger, S., & Babanin, A. V. (2011). Global trends in wind speed and wave height. *Science*, *332*(6028), 451–455.

Zacharioudaki, A., & Reeve, D. E. (2011). Shoreline evolution under climate change wave scenarios. *Climatic Change*, *108*(1), 73–105.

Zhang, K., Douglas, B. C., & Leatherman, S. P. (2004). Global warming and coastal erosion. *Climatic Change*, *64*(1–2), 41.

Zheng, C. W., & Li, C. Y. (2015). Variation of the wave energy and significant wave height in the China Sea and adjacent waters. *Renewable and Sustainable Energy Reviews*, *43*, 381–387.

APPENDICES

APPENDIX A: MONTHLY SIGNIFICANT WAVE HEIGHT BETWEEN 1980-2019 FOR GULF OF GUINEA

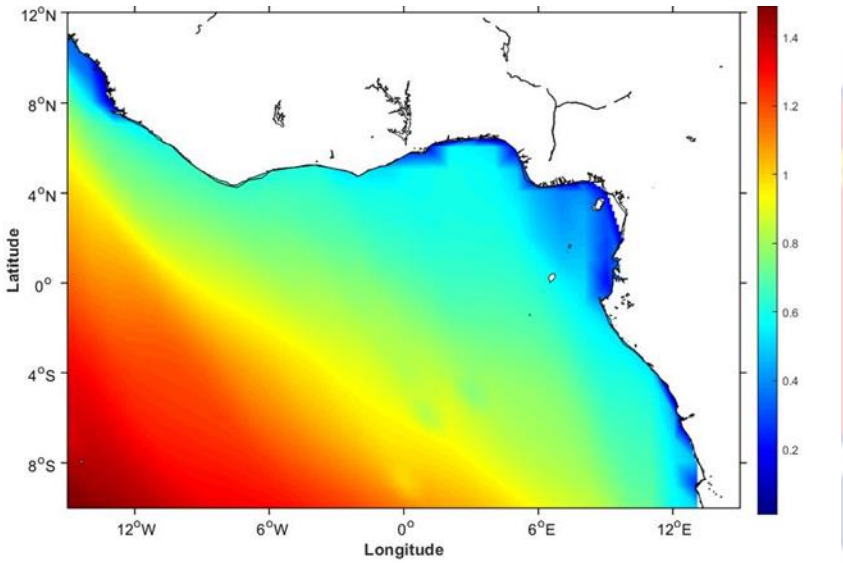

Figure A1: Regional spatial distribution of the mean *Hs* in GoG between 1980-2019 for January.

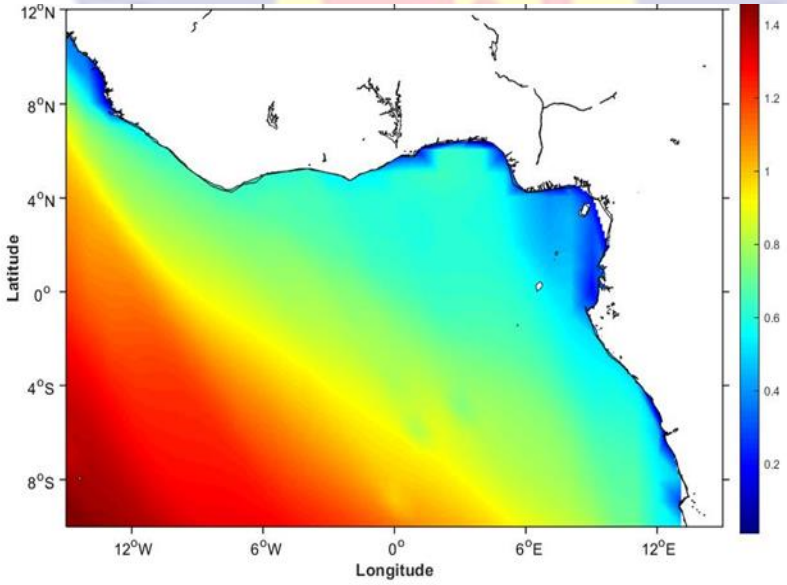

Figure A2: Regional spatial distribution of the mean *Hs* in GoG between 1980-2019 for February.

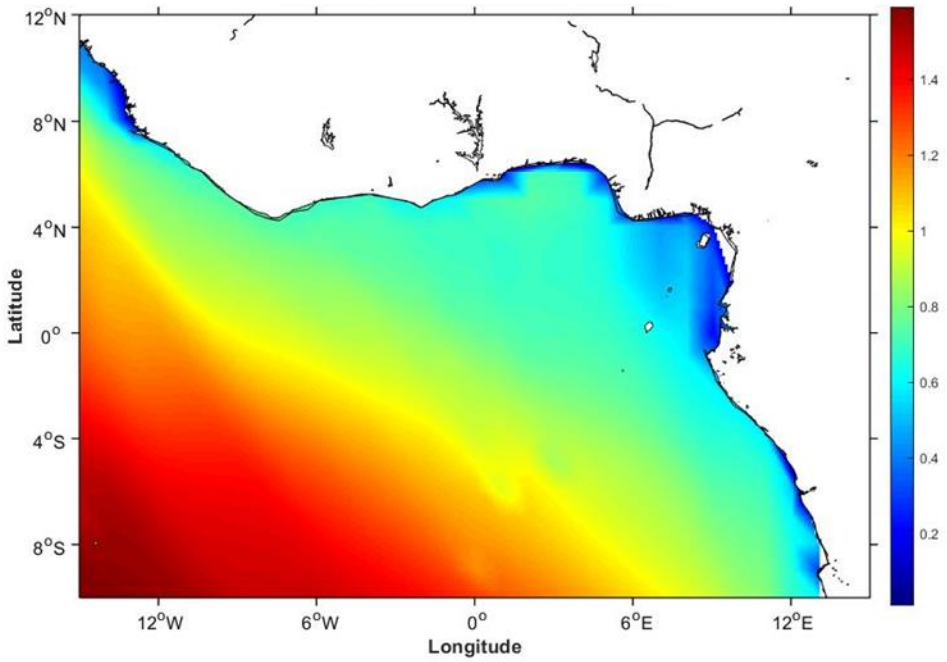

Figure A3: Regional spatial distribution of the mean *Hs* in GoG between 1980-2019 for March.

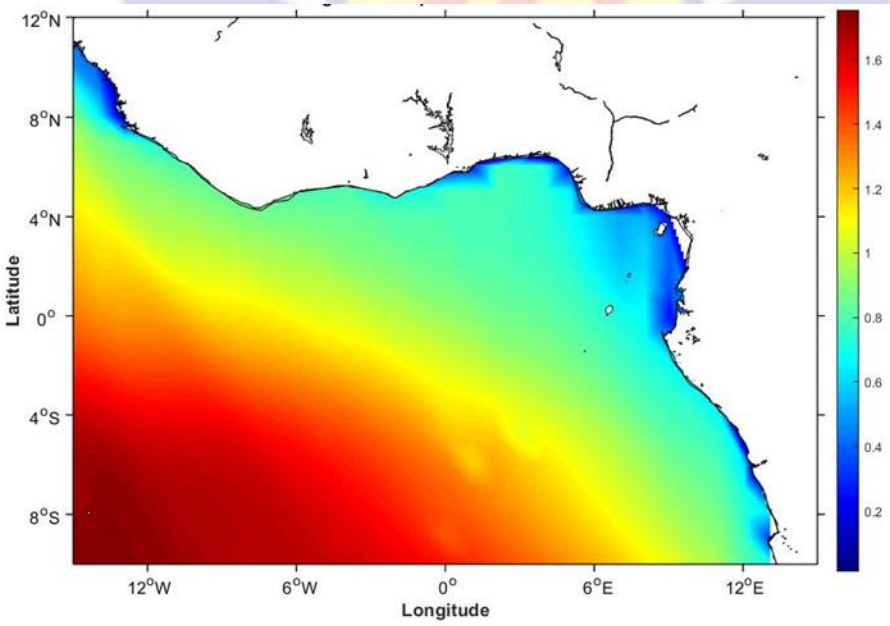

Figure A4: Regional spatial distribution of the mean *Hs* in GoG between 1980-2019 for April.

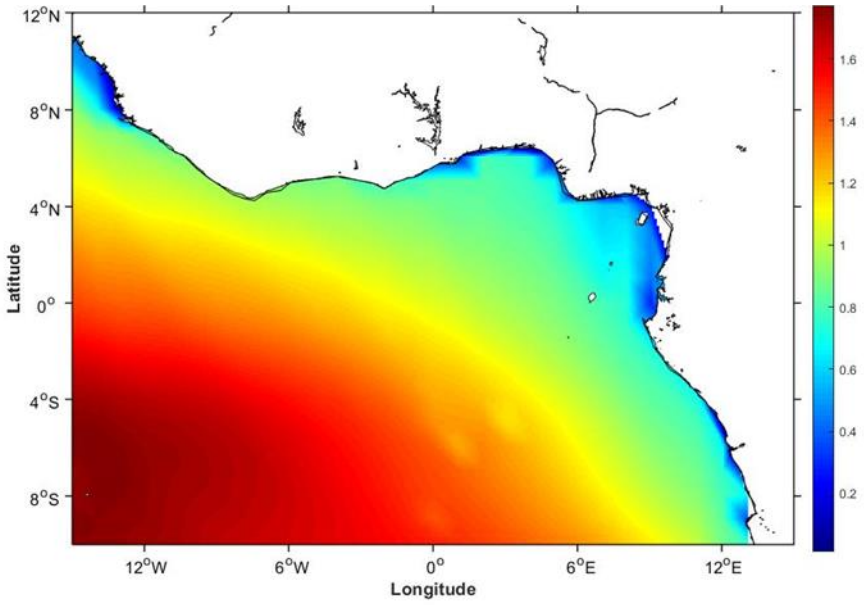

Figure A5: Regional spatial distribution of the mean *Hs* in GoG between 1980-2019 for May.

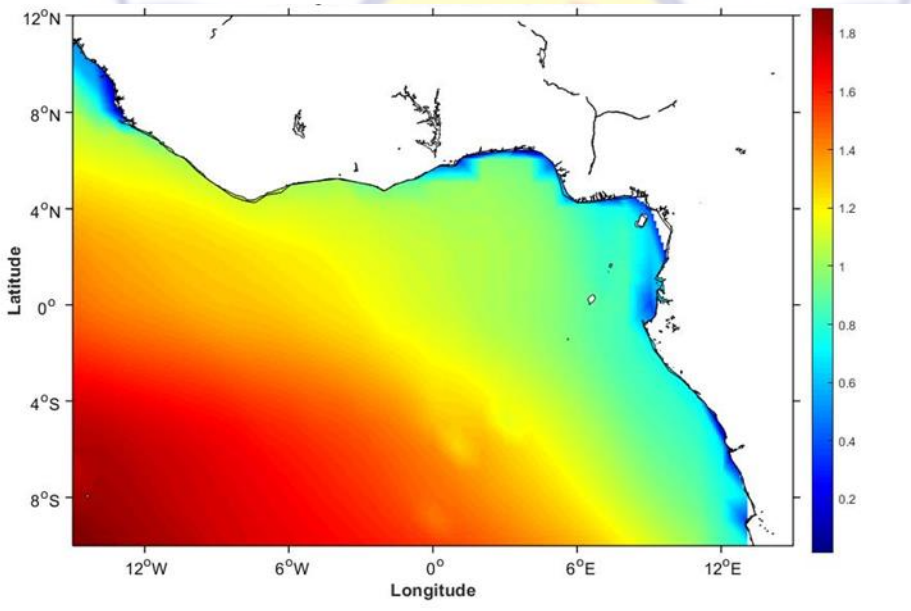

Figure A6: Regional spatial distribution of the mean *Hs* in GoG between 1980-2019 for June.

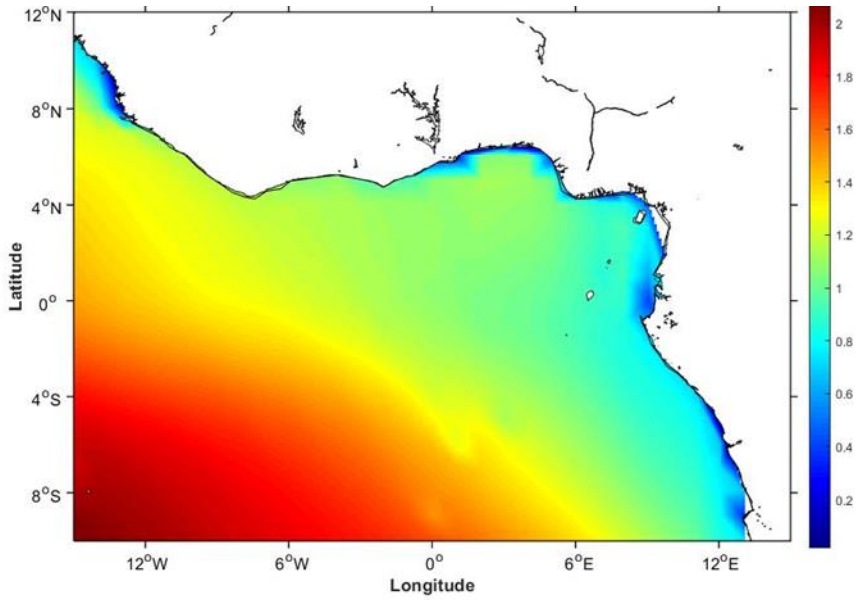

Figure A7: Regional spatial distribution of the mean *Hs* in GoG between 1980-2019 for July.

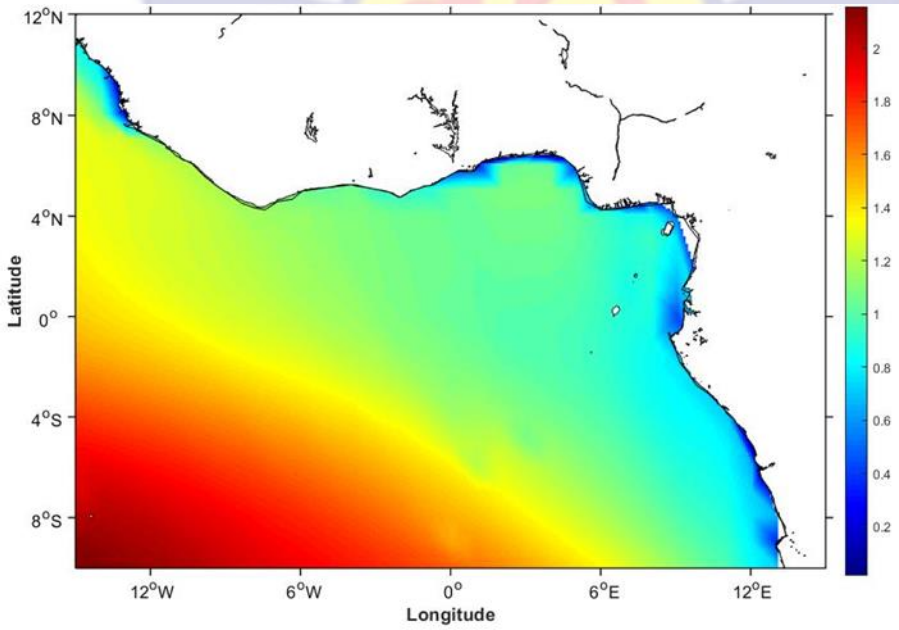

Figure A8: Regional spatial distribution of the mean *Hs* in GoG between 1980-2019 for August.

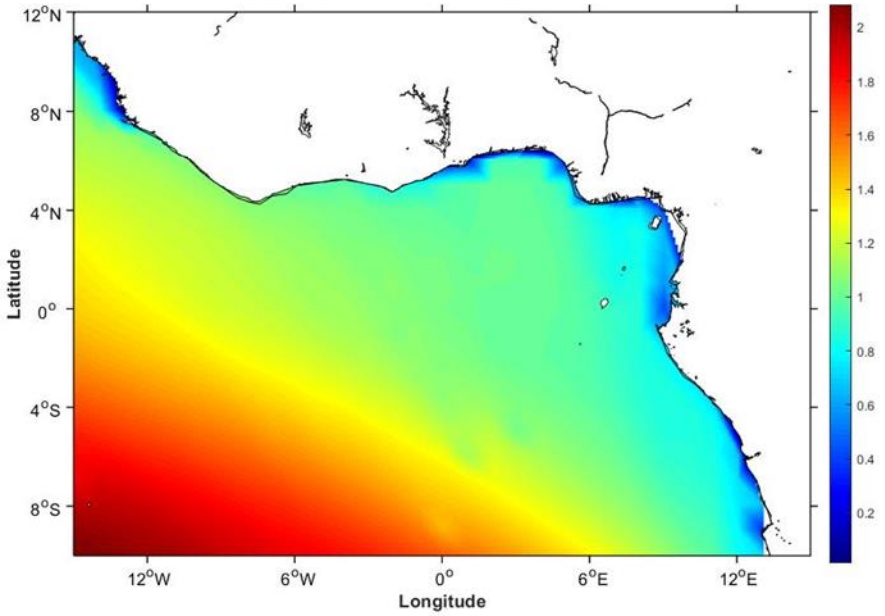

Figure A9: Regional spatial distribution of the mean *Hs* in GoG between 1980-2019 for September.

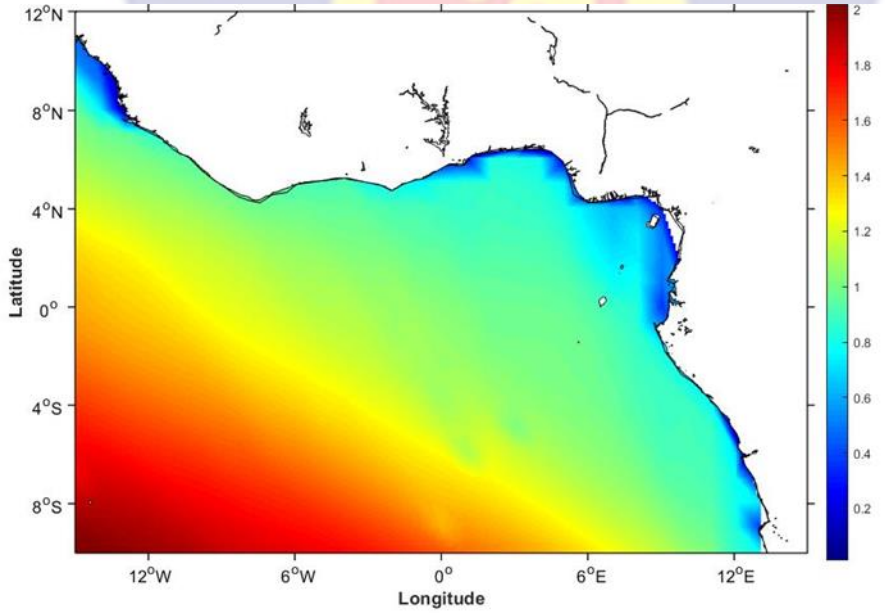

Figure A10: Regional spatial distribution of the mean *Hs* in GoG between 1980-2019 for October.

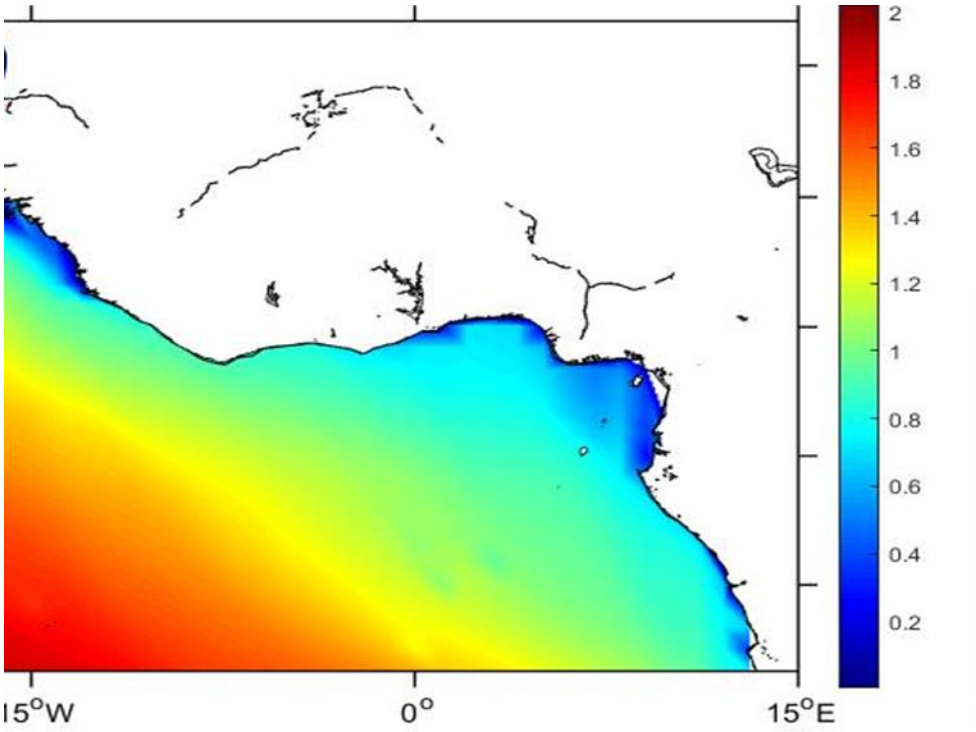

Figure A11: Regional spatial distribution of the mean *Hs* in GoG between 1980-2019 for November.

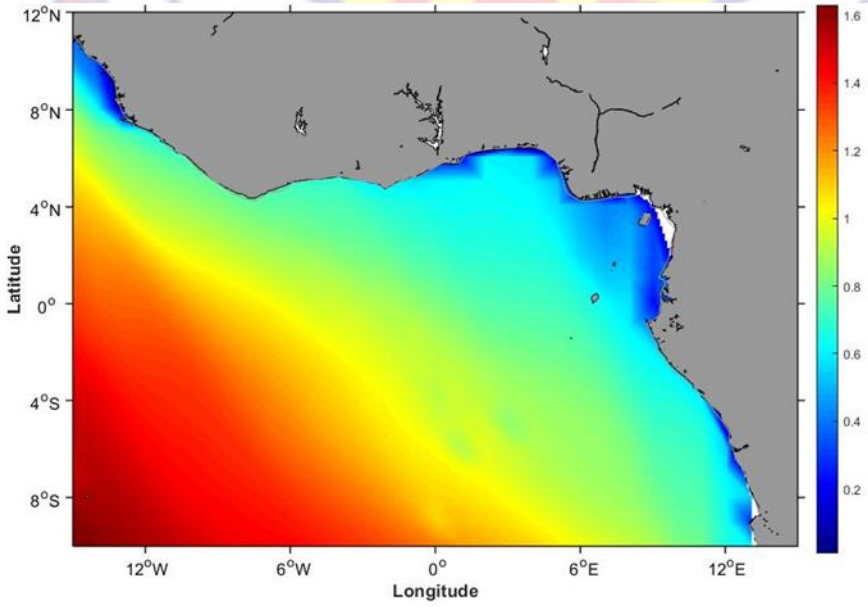

Figure A12: Regional spatial distribution of the mean *Hs* in GoG between 1980-2019 for December.

APPENDIX B: STATISTICAL TESTS RESULTS FOR ENSO EVENTS

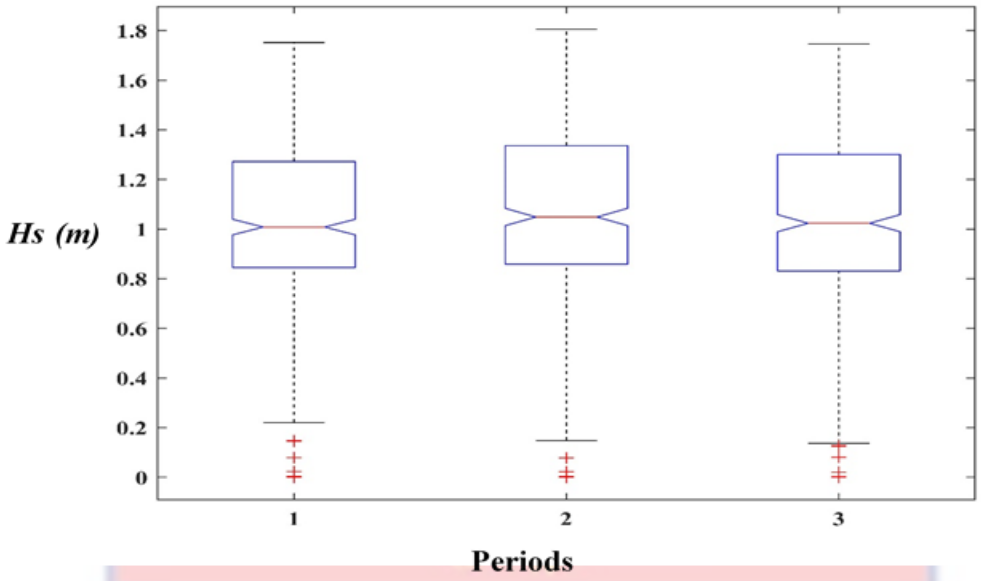

Figure B1: Box plots showing the average and range of *Hs* for 1980-1981, 1982-1983 and 1984-1985 represented by periods 1, 2 and 3 respectively on the x axis.

Table B1: Results of one-way ANOVA for the case in Figure B1

ANOVA Table

Source	SS	df	MS	F	Prob>F
Columns	0.413	2	0.20675	1.77	0.1713
Error	160.099	1368	0.11703		
Total	160.513	1370			

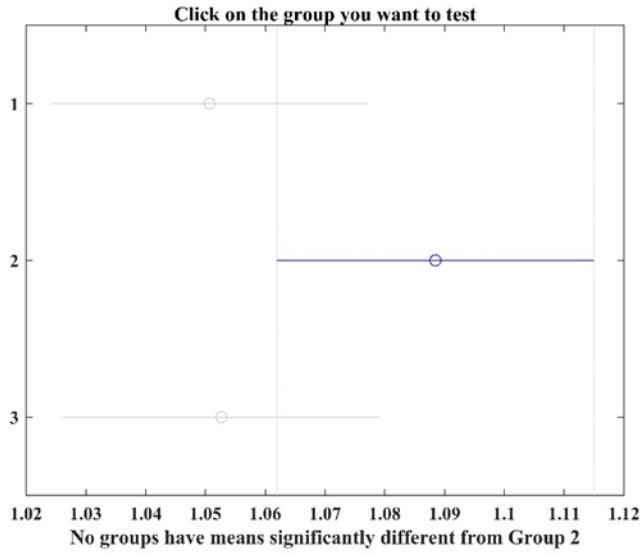

Figure B2: Tukey test to confirm the results shown in Table B1.

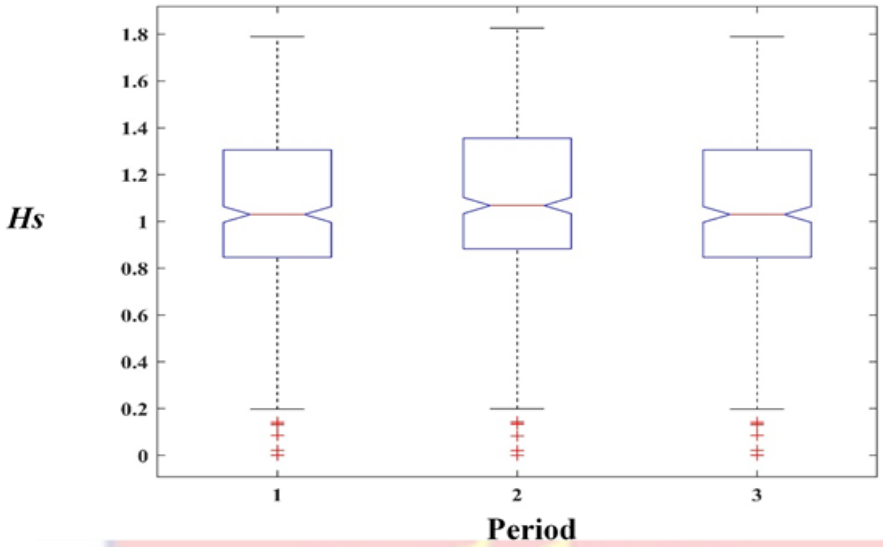

Figure B3: Box plots showing the average and range of *Hs* for 1995-1996, 1997-1998 and 1999-2000 represented by periods 1, 2 and 3 respectively on the x axis.

Table B2: Results of one-way ANOVA for the case in Figure B3

ANOVA Table

Source	SS	df	MS	F	Prob>F
Columns	0.411	2	0.20563	1.65	0.1931
Error	170.869	1368	0.1249		
Total	171.281	1370			

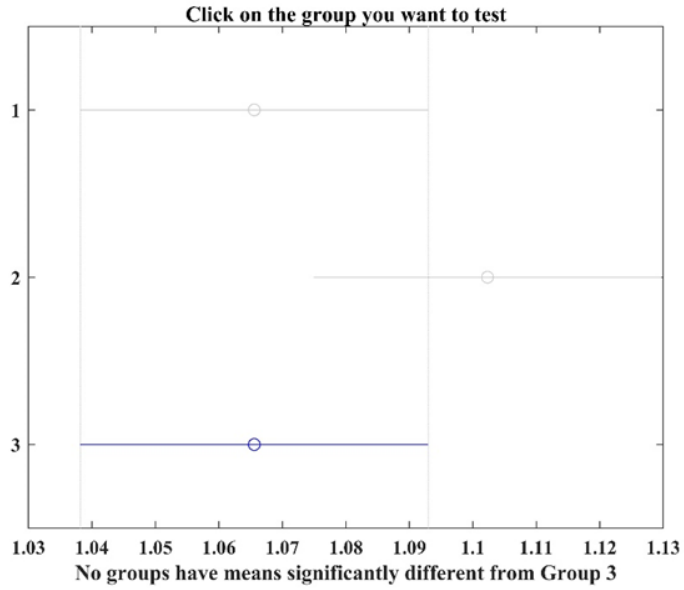

Figure B4: Tukey test to confirm the results shown in Table B2.

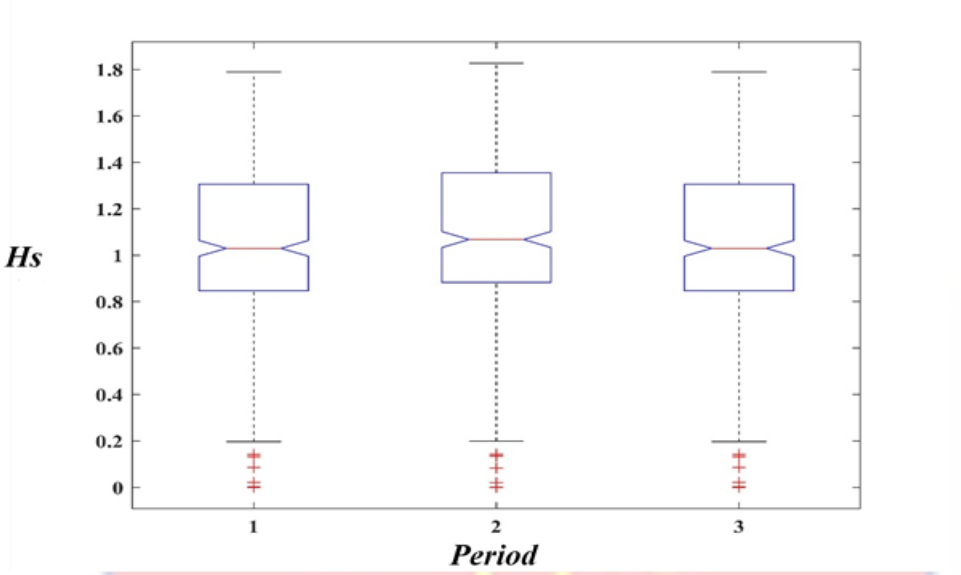

Figure B5: Box plots showing the average and range of *Hs* for 2011-2013, 2014-2016 and 2017-2019 represented by periods 1, 2 and 3 respectively on the x axis

Table B3: Results of one-way ANOVA for the case in Figure B5.

ANOVA Table

Source	SS	df	MS	F	Prob>F
Columns	0.411	2	0.20563	1.65	0.1931
Error	170.869	1368	0.1249		
Total	171.281	1370			

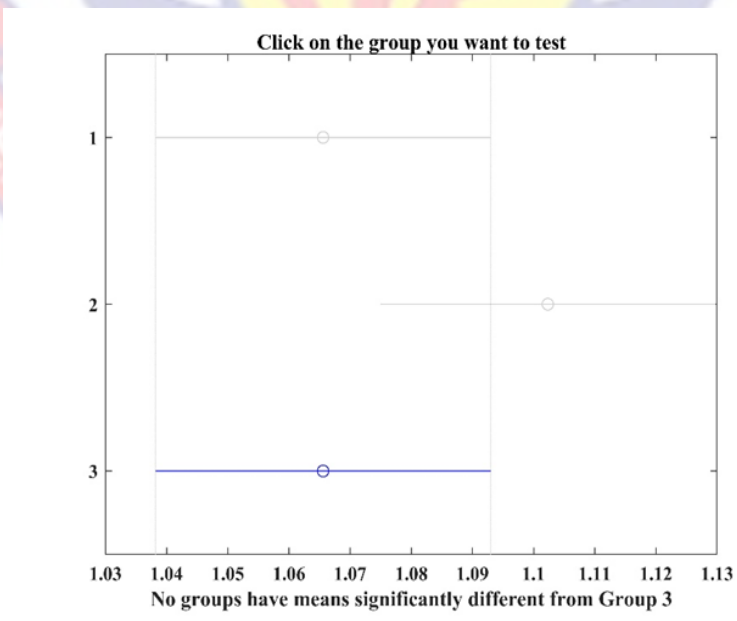

Figure B6: Tukey test to confirm the results shown in Table B3.

APPENDIX C: STATISTICAL TESTS RESULTS FOR COASTAL STRUCTURE INFLUENCES

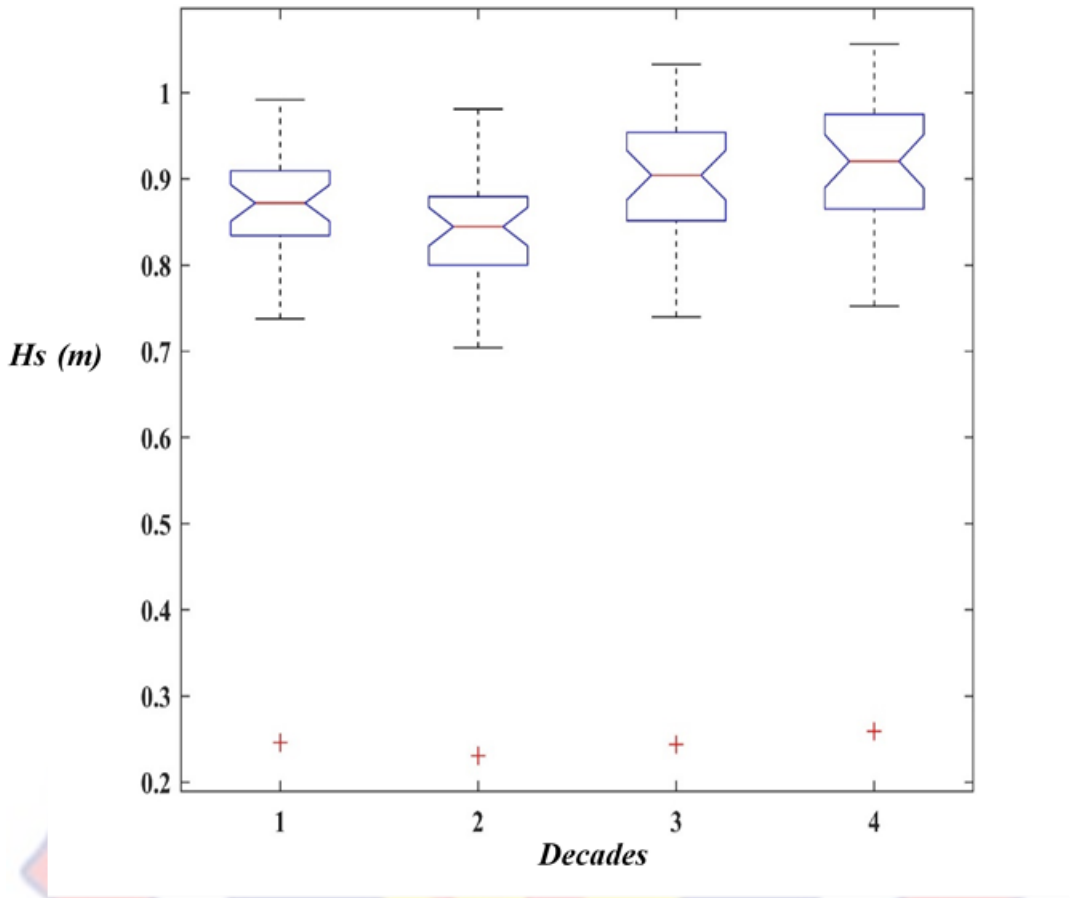

Figure C1: Box plots showing the average and range of *Hs* for 1980-1989, 1990-1999, 2000-2009 and 2010-2019 represented by decades 1, 2, 3 and 4 respectively on the x axis.

Table C1: Results of one-way ANOVA for the case in Figure C1.

ANOVA Table

Source	SS	df	MS	F	Prob>F
Columns	0.09869	3	0.0329	1.88	0.1364
Error	2.09833	120	0.01749		
Total	2.19702	123			

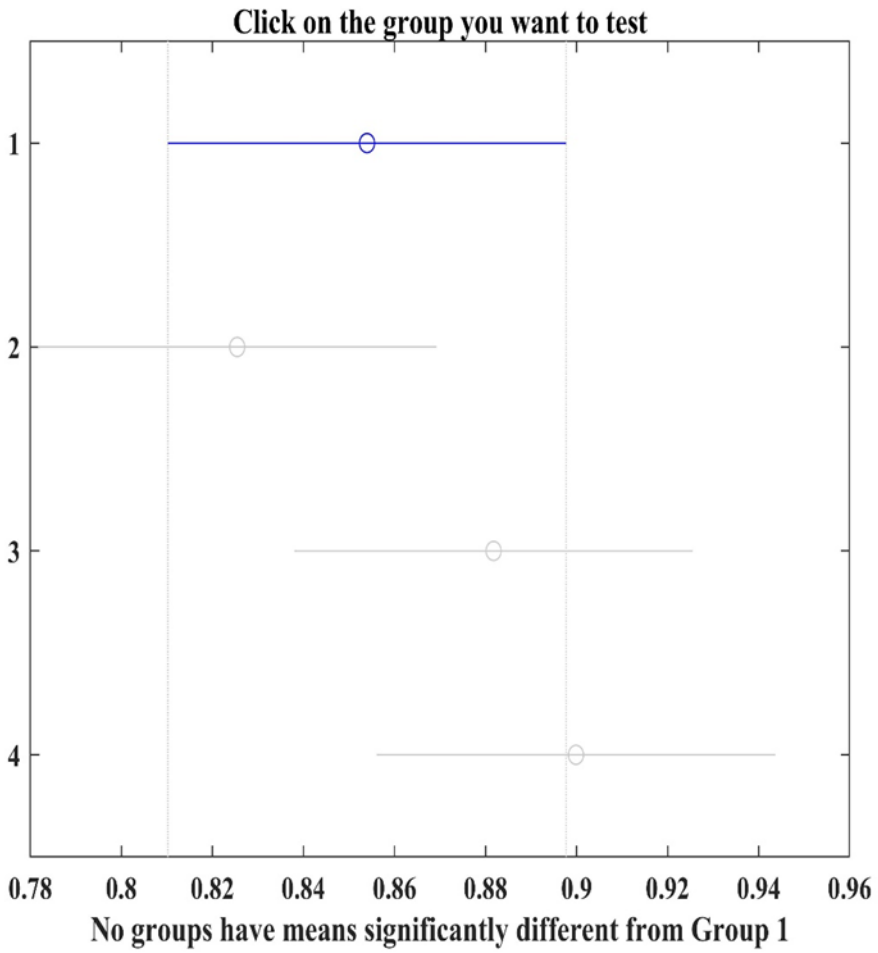

Figure C2: Tukey test to confirm the results shown in Table C1.

Table C2: Results of one-way ANOVA for the case in Figure C3.

ANOVA Table

Source	SS	df	MS	F	Prob>F
Groups	341.6	39	8.75894	116.3	0
Error	4398.11	58400	0.07531		
Total	4739.71	58439			

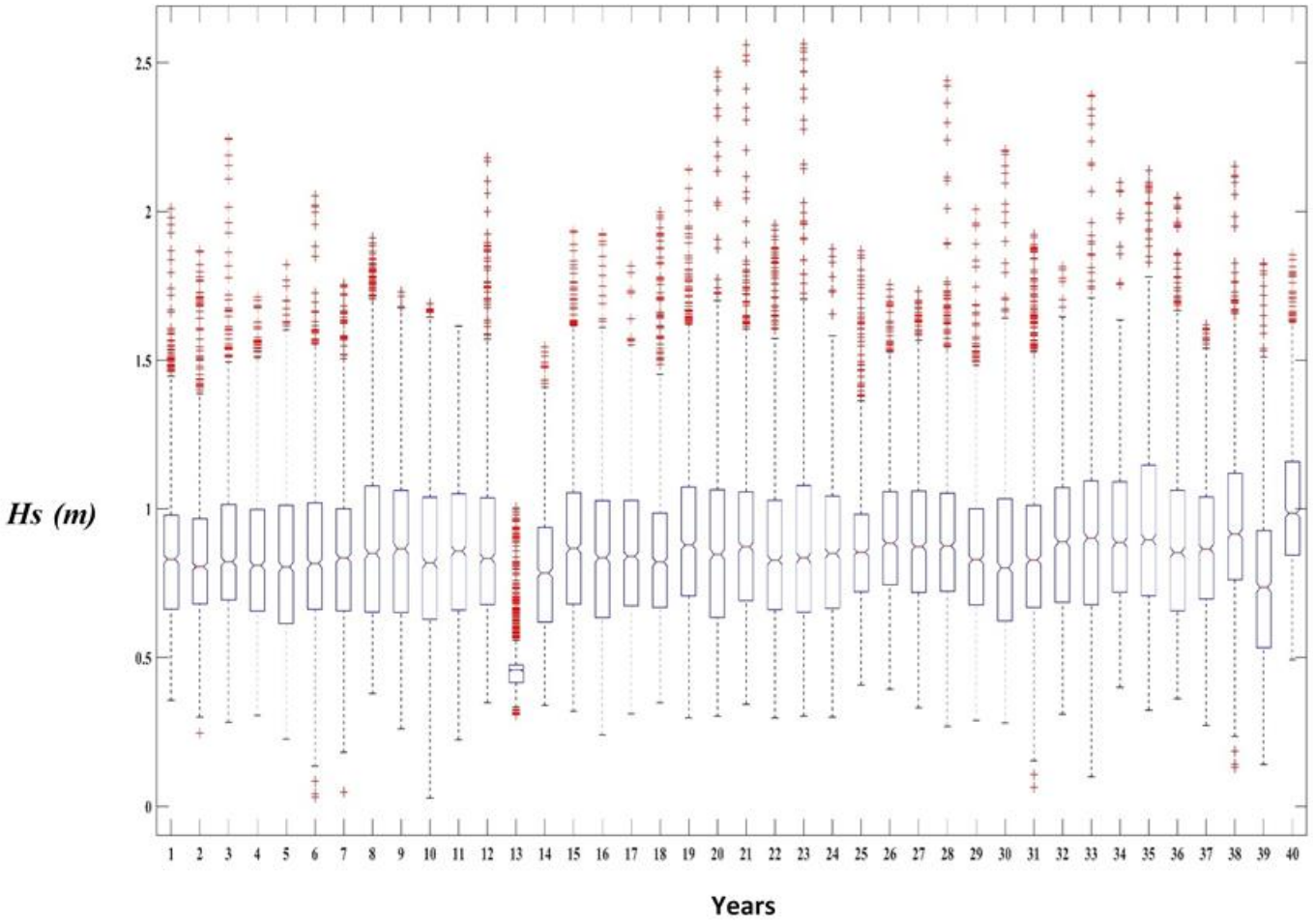

Figure C3: Box plots showing the average and range of *Hs* for 1980-2019 represented by years 1-40 respectively on the x axis

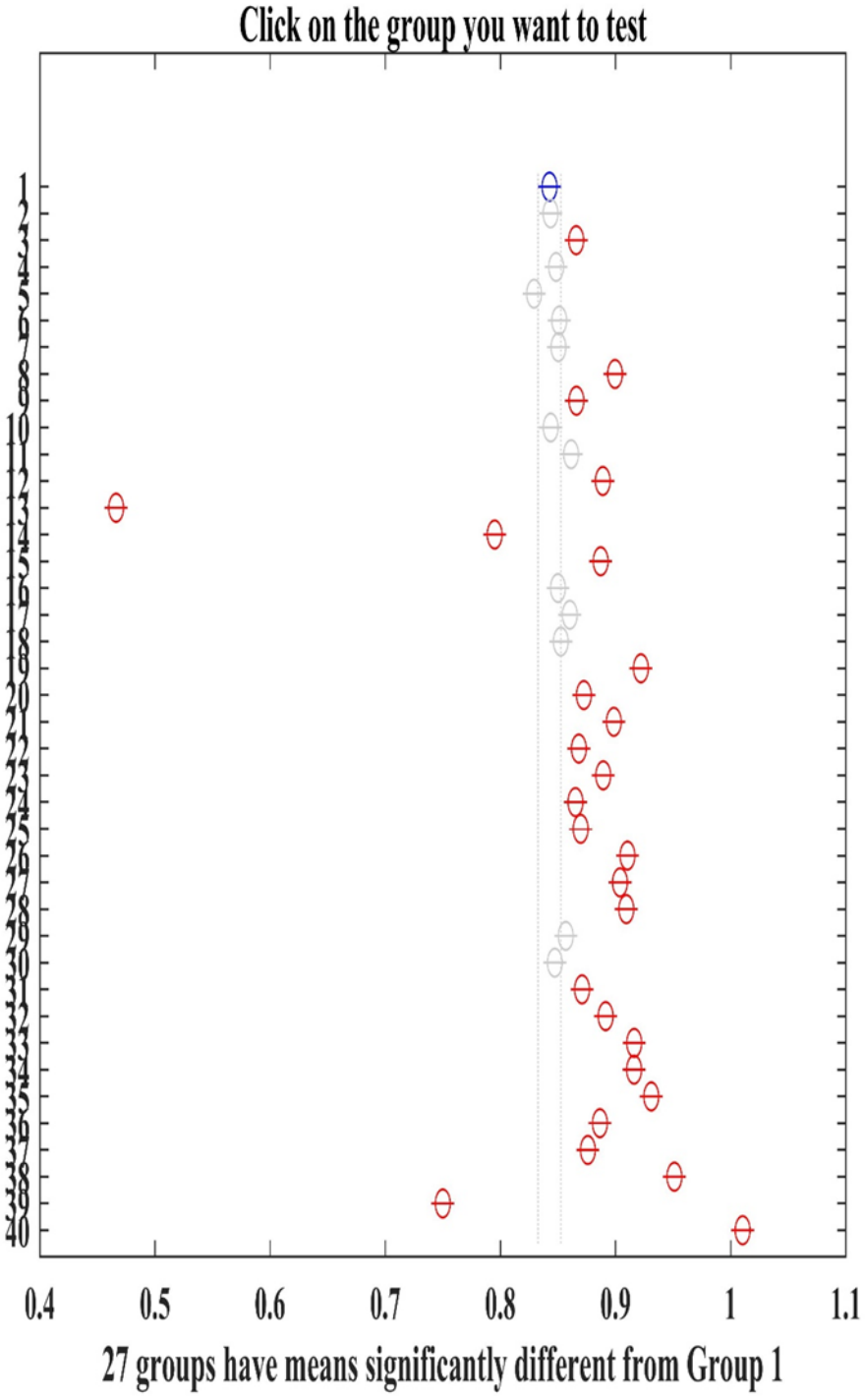

Figure C4: Tukey test to confirm the results shown in Table C2.